Wang, P., Prell, W.L., Blum, P., et al., 2000
Proceedings of the Ocean Drilling Program, Initial Reports Volume 184

5. Site 1144[1]

Shipboard Scientific Party[2]

BACKGROUND AND OBJECTIVES

The primary objectives of Site 1144 (proposed site SCS-1) on the northern margin of the South China Sea (SCS) were to (1) recover a continuous sequence of high-sedimentation-rate hemipelagic sediments that will allow reconstruction of the paleomonsoon history on millennial, centennial, or higher resolution time scales over the last million years; (2) compare these records with orbital-scale and higher frequency records from ice cores, other nearby marginal seas, and terrestrial deposits; and (3) establish a high-resolution record of faunal, isotopic, and sea-surface temperature (SST) changes associated with variability in the winter monsoon.

Site 1144 (SCS-1) is located at 20°3.18′N, 117°25.14′E, at a water depth of ~2037 m, which is above the sill depth of the Bashi Strait (2600 m) (see Figs. **F2,** p. 46, and **F9,** p. 53, both in the "Leg 184 Summary" chapter). The location of Site 1144 is distinguished by extremely high sedimentation rates. The Holocene deposits in the nearby core SONNE95-17940 have sedimentation rates of ~700 m/m.y., whereas glacial sediments accumulate at ~400 m/m.y. Similarly, nearby core MD 97-2-146 reaches only to the marine oxygen isotope Stage (MIS) 4/5 boundary at 38 m, indicating a sedimentation rate of ~500 m/m.y. (C. Huang, pers. comm., 1997). These high sedimentation rates have allowed reconstruction of centennial-scale summer monsoon variability in the Holocene and millennial-scale dry/humid cyclicity in the uppermost Pleistocene (Wang et al., 1995; Sun, 1996), indicating the great potential of this site to deliver high-resolution records of the Quaternary climate. The target penetration of 450 m was expected to recover Quaternary sediments (~1 m.y.). We planned a standard drilling program at Site 1144: Hole 1144A was to be cored to refusal using the advanced hydraulic piston corer (APC), deepened with the extended core barrel (XCB) to 450 meters below seafloor (mbsf), and wireline logged (using

[1]Examples of how to reference the whole or part of this volume.
[2]Shipboard Scientific Party addresses.

Ms 184IR-105

the triple combination tool, the geological high-resolution magnetic tool (GHMT), and the Formation MicroScanner (FMS)–sonic tool suite). Holes 1144B and 1144C were to be APC cored to refusal. However, Hole 1144B was deepened with the XCB to 450 mbsf (see "Operations," p. 3).

Site 1144 is located on a thick sediment drift at the intersection of seismic Lines SO95-20 (common depth point [CDP] 3482, 04:02) and SO95-10 (CDP 9600, 04:20) (Figs. F5, p. 17, F16A, p. 31, and F16B, p. 32, all in the "Seismic Stratigraphy" chapter). The drift nature of the sediment is indicated by high sedimentation rates, the geometry/morphology of the deposit, and its surface and internal structure (Figs. F7, p. 20, and F8, p. 21, both in the "Seismic Stratigraphy" chapter). The *JOIDES Resolution* 3.5-kHz depth recorder data and the *Sonne* PARASOUND data (Sarnthein et al., 1994) show that the surface near Site 1144 is irregular although locally smoothed by sediment accumulation in lower areas (Fig. F5, p. 17, in the "Seismic Stratigraphy" chapter). Parabolic hills on the order of 50–100 m in height were observed near the site. The *JOIDES Resolution* data show that Site 1144 is located near the crest of a large hill with a thick, uniform sediment drape. The sediment thickness above a prominent basinward dipping reflector is ~0.75 s, or ~650 m. The seismic structure of the sediment column is characterized by an upper reflector series (0–0.5 s) that has distinct, closely spaced reflectors and a lower, more diffuse zone (0.5–0.7 s) with less-distinct reflectors. The northwest-southeast dip line (SO95-10) reveals a wedge of sediment ranging from ~1725 to ~2400 m in water depth. Internal reflectors indicate that the beds thin and pinch out with increasing water depth toward the toe of the deposit. The strike line (SO95-20) reveals wavy reflectors, suggesting possible drift-type transport or redeposition of suspended sediments. The conforming nature of the draped sediments and the lack of horizontally filled depressions imply that they are not bottom-transported, gravity-driven deposits.

Site 1144 is located near the center of the deposit, where reflectors are relatively uniform and evenly structured in both lines. We expected that the 450-mbsf penetration at Site 1144 would recover only the upper reflector series.

The high accumulation rate sediments at Site 1144 should offer an unprecedented opportunity to reconstruct late Quaternary monsoonal variations on centennial to orbital scales. Studies of the past 40 k.y. (Wang et al., 1999; Pflaumann and Jian, 1999; Pelejero et al., 1999; Sun and Li, 1999) have used a number of monsoonal and paleoclimate proxies, including the composition of planktonic faunas (tropical/subtropical nature and SST), the $\delta^{18}O$ of mixed-layer-dwelling foraminifers (salinity and SST), biomarker $U_{37}^{k'}$ (SST and productivity), pollen and charcoal (vegetation and aridity), clay content (fluvial/eolian source), and grain size (fluvial/eolian transport). These proxies have been used to infer that the summer monsoon rainfall was weaker and the winter monsoon eolian transport was stronger during the past glacial interval and, conversely, that the summer monsoon rainfall was stronger and the winter monsoon eolian transport weaker during the Holocene interglacial interval (Wang et al., 1999; Sun and Li, 1999). Superimposed on these glacial–interglacial-scale changes are short-term (10^2–10^3 yr) increases in monsoonal intensity that can be correlated with the first 10 Dansgaard-Oeschger Events in the GISP2 ice core (Wang et. al., 1999). Similarly, four periods of reduced summer monsoon precipitation and

increased winter monsoon winds are observed and correlative with Heinrich Events 1–4.

On the basis of a broad $\delta^{18}O$ minimum and a fluvial clay maximum, the summer monsoon is thought to have reached its Holocene maximum in the South China Sea at ~10 ka. Similar timing is observed in the Arabian Sea (Prell, 1984; Sirocko et al., 1993).

We expected the multi-APC holes at Site 1144 to provide a high-quality spliced record that will enable sample intervals as small as 20 yr and thus enable centennial- to millennial-scale studies of the East Asian monsoon history.

OPERATIONS

Site Survey

Several of the proposed sites on the continental slope of China were selected on the basis of a single seismic line. Final approval of these sites by the Pollution Prevention and Safety Panel (PPSP) was contingent upon the *JOIDES Resolution* acquiring crossing seismic lines. A single-channel survey was designed to cover all such proposed sites that we were likely to drill: SCS-4, SCS-5C, and SCS-5E. At 1100 hr on 12 March, the vessel slowed to deploy the seismic equipment. Two seismic cross tracks a few nautical miles in length were acquired at each of the three proposed sites (see **"Site 1146 (SCS-4)," p. 7**, and **"Sites 1147 and 1148 (SCS-5C)," p. 8**, both in the "Seismic Stratigraphy" chapter). The survey was finished by 1200 hr on 13 March, with a total distance surveyed of 133 nmi and an average speed of 5.5 kt. After the seismic equipment was retrieved, the vessel continued at full speed to proposed site SCS-1.

Site 1144 (Proposed Site SCS-1)

The beacon was dropped on GPS coordinates for proposed site SCS-1 at 1745 hr on 13 March. The corrected precision depth recorder depth referenced to the dual elevator stool was 2051.4 m.

Hole 1144A

Hole 1144A was spudded with the APC at 2245 hr on 13 March. The seafloor depth was inferred to be 2047.0 m from the recovery of the first core. Piston coring advanced to 234.9 mbsf with an excellent average recovery of 104.4%. The high recovery percentage was in part a result of the gas expansion of many of the cores. APC refusal was encountered when the core barrel for Core 25H could not be pulled free of the sediment with an overpull of 120,000 lb. The core barrel had to be drilled over to free it from the sediment. The cores were oriented starting with Core 3H. During piston coring, heat-flow measurements were obtained at 26, 64, 102, and 149 mbsf. A low temperature gradient of 24°C/km was calculated from these data (see **"Physical Properties," p. 19**). The hole was deepened with the XCB to a depth of 452.6 mbsf. The XCB average recovery was 102.6%; the average recovery for this hole was an exceptional 103.6% (Tables **T1, T2** [both also in **ASCII format**]). Only moderate amounts of biogenic methane were measured in the cores (see **"Organic Geochemistry," p. 13**).

T1. Site 1144 coring summary, **p. 74.**

T2. Site 1144 coring summary by section, **p. 76.**

After the hole was flushed with a 30-bbl mud treatment, the bore was displaced with an additional 115 bbl of sepiolite. During the pipe trip to the logging depth of 87 mbsf, the driller did not observe any increased weight resulting from restriction in the size of the hole. Logging began at 1145 hr on 15 March. Three successful wireline logging runs were completed with all three tool suites (triple combo, FMS-sonic, and GHMT) covering the open hole from 452 to 87 mbsf. Hole conditions were good with some washouts detected in the lower portion. No problems with the swelling clays were encountered at Site 1144. At 0615 hr on 16 March, the logging equipment was disassembled and the drill string pulled back. The bit cleared the seafloor at 0655 hr on 16 March.

Hole 1144B

The vessel was offset 20 m east of Hole 1144A. Hole 1144B was spudded with the APC at 0800 hr on 16 March. The seafloor depth inferred from recovery was 2049.8 m. Piston coring advanced to 199.6 mbsf with an average recovery of 98.3%. The cores were oriented starting with Core 3H. Time saved at the previous hole and during wireline logging permitted us to deepen Hole 1144B with the XCB to provide a stratigraphic overlap with Hole 1144A. The hole was deepened to 452.0 mbsf by 1930 hr on 17 March. Once again, the XCB did well with an average recovery of 100.0%. The recovery for the entire hole was 98.6% (Tables T1, T2). The bit was pulled clear of the seafloor at 2115 hr on 17 March.

Hole 1144C

Hole 1144C was spudded with the APC at 2230 hr on 17 March and advanced to a depth of 198.7 mbsf, which was considered the target depth for this hole. The average recovery for the hole was 99.9%; all cores were oriented starting with Core 3H. The interval from 37.2 to 42.2 mbsf was washed ahead without coring to obtain a proper stratigraphic overlap with Hole 1144B.

The total recovery for Site 1144 was 1113.3 m, 100.9% of the cored interval (Tables T1, T2). After the bit cleared the seafloor at 1245 hr on 18 March, the drilling crew temporarily interrupted the pipe trip to perform the routine maintenance of slipping and cutting 115 ft of drilling line. The bit was at the rotary table by 1630 hr. Both primary and backup beacons were recovered. The drilling equipment, hydrophones, and thrusters were secured for the short voyage to the next site. The vessel was under way at 1645 hr on 18 March.

COMPOSITE SECTION

We built a continuous meters composite depth (mcd) scale and a splice (as defined in "Composite Section," p. 3, in the "Explanatory Notes" chapter) that range from the top of Core 184-1144C-1H to the bottom of Section 184-1144A-23H-7. The splice and the continuous portion of the mcd scale extend from 0.0 to 235.41 mcd. Splice construction below this interval was precluded by incomplete core recovery and alignment of core gaps. As described below, however, we were able to construct a discontinuous ("floating") mcd scale (see "Composite Section," p. 3, in the "Explanatory Notes" chapter) for cores below 235 mcd.

The mcd scale and the splice are based on the stratigraphic correlation of whole-core multisensor track (MST) and split-core color spectral reflectance (CSR) data (lightness, L*) collected at 4- to 8-cm intervals (see **"Physical Properties,"** p. 19, for details). From the MST, we used magnetic susceptibility (MS), gamma-ray attenuation (GRA) bulk density, and natural gamma radiation (NGR) data. These data and the splice constructed from them are presented on the mcd scale in Figures **F1, F2, F3,** and **F4** (also as Synergy Software KaleidaGraph plots and Microsoft Excel data files [see the **"Supplementary Materials"** contents list]; the spliced records are also available in **ASCII format**). The depth offsets that comprise the mcd scale are given in Table **T3** (also in **ASCII format**). The splice tie points (Table **T4,** also in **ASCII format**) should be used as a guide for detailed postcruise sampling.

Magnetic susceptibility was the most useful stratigraphic tool for correlation. Color spectral reflectance and NGR were helpful in intervals where MS structure was ambiguous or the signal amplitude low. Failure of the NGR recorder on the MST resulted in the loss of NGR data over much of Hole 1144B. Gamma-ray attenuation was the least useful for correlation because intracore squeezing and stretching (resulting from the coring process as well as gas expansion) degraded the signal significantly. We constructed the mcd scale by assuming that the uppermost sediment (the "mudline") in Core 184-1144B-1H was the sediment/water interface. However, based on a preliminary comparison of the MS structure in this core with that from core MD97-2146 (collected during the IMAGES III cruise in the same general vicinity but in water 300 m shallower), we suspect that the upper 2 m of the sedimentary section was not recovered at Site 1144.

Core 184-1144C-1H, the "anchor" in the composite depth scale, is the only core with depths that are the same on the mbsf and mcd scales. From this anchor we worked downhole, correlating the stratigraphy on a core-by-core basis. Stratigraphic misalignment was evident in the cores with the highest gas (and thus void) content, such as those in the upper 50 mcd of the section. The core-splitting process, which involves pulling a cutting wire lengthwise along the section, can dislodge sediments and reposition voids, thus offsetting the split-core CSR and whole-core MST data (see **"Composite Section,"** p. 3, in the "Explanatory Notes" chapter). Thus, stratigraphic correlations based on CSR may differ slightly from those based on MST data. Fortunately, many of the voids were removed on the catwalk by drilling gas-escape holes in the liner and manually pushing together sedimentary intervals within the core liner.

Correlation of the intervals spanning 18 to 40 mcd, 122 to 150 mcd, and 180 to 196 mcd were especially challenging because of low amplitude in the MS signal. Here we relied more on CSR and NGR data to construct stratigraphic ties, although alternative correlations are possible. In the splice, we chose to append successive cores from Hole 1144B at two locations (Table **T4**), rather than to incorporate short intervals from other holes. Independent verification of stratigraphic continuity across these ties is required.

Although the cores below 235 mcd could not be tied directly to the composite depth scale (and thus the splice), they could be correlated with each other. We placed the cores in a relative, or discontinuous, composite depth scale. This "floating" scale is not tied to the overlying mcd scale (and thus back to the mudline). Instead, the positions of the cores are adjusted such that correlative features match. At other Leg 184 sites, we chose a single hole (keeping core offsets within it constant be-

F1. Magnetic susceptibility data and splice, **p. 27.**

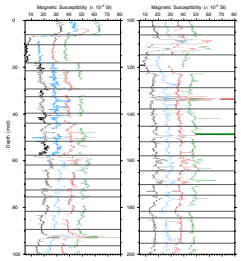

F2. Smoothed/correlated NGR data and splice, **p. 30.**

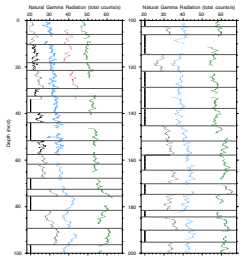

F3. GRA data and splice, **p. 33.**

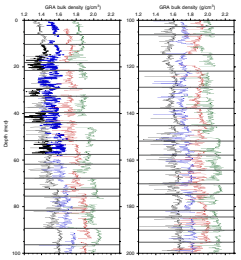

F4. Smoothed/correlated L* values from the CSR data and splice, **p. 36.**

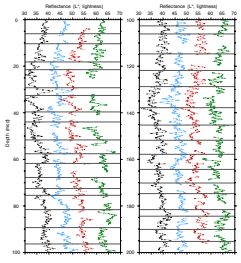

T3. Composite depths for Site 1144, **p. 77.**

T4. Site 1144 splice tie points, **p. 78.**

low the splice) and mapped cores from the other holes to the chosen hole. This approach was not possible at Site 1144 because of inadequate core quality in the lower section.

LITHOSTRATIGRAPHY

Lithologic Unit

Unit 1 (0–519.19 mcd)

Interval: Cores 184-1144A-1H through 48X; Cores 184-1144B-1H through 49X; Cores 184-1144C-1H through 21H
Depth: 0–452.6 mbsf (Hole 1144A); 0–452 mbsf (Hole 1144B); 0–203.7 mbsf (Hole 1144C)
Age: Pleistocene

Only one lithologic unit was recognized at Site 1144 (Fig. F5). The sediments represent continuous hemipelagic sedimentation of fine-grained, clay-sized terrigenous material, quartz silt, and calcareous nannofossils. APC coring at Site 1144 failed to recover the oxidized sediment layer from the seafloor (see "Composite Section," p. 4). Despite the relative homogeneity, we propose a three-part subdivision of the unit based on the abundance of "iron sulfides," pyrite, and siliceous biota, as noted in core description and smear-slide analysis.

The dominant lithology throughout the recovered section at Site 1144 is clay with quartz silt and nannofossils. Other lithologies include clay with quartz silt and sponge spicules, clay with quartz silt and diatoms, clay with silt, silty clay, and clay. These minor lithologies comprise only ~5%–10% of the total sediment recovered. Irregularly shaped white pockets, typically a few millimeters in diameter, are randomly distributed in the structureless clay, sometimes quite densely. These are filled with sponge spicules and particles of recrystallized authigenic and/or biogenic silica.

Subordinate lithologies, such as ash layers and green clay layers, are rare throughout, comprising <1% of the total section. Green clay layers, which are abundant at Site 1143 in the southern South China Sea (see "Lithostratigraphy," p. 8, in the "Site 1143" chapter), are seldom recognized at Site 1144 (13 layers in Hole 1144A, seven layers in Hole 1144B, and four layers in Hole 1144C). In addition to well-defined green layers, a large number of rather indistinct green clay layers and patches are noted over these same intervals in the three holes at Site 1144. The same relationship of discrete and indistinct layers was also noted for the green clay at Site 1143 (see "Lithostratigraphy," p. 8, in the "Site 1143" chapter). A single fine sand interval, ~1 mm thick, occurs at 189.39–189.40 mcd in Hole 1144B, but otherwise coarse clastic material is limited to silt-sized material disseminated in the sediment, normally dominated in composition by quartz, feldspar, and, locally, pyrite. Volcanic glass shards and altered igneous rock fragments are minor but frequent components of the silt fraction.

In general, the sediments at Site 1144 were only slightly disturbed by the coring process but were often extremely disturbed over discrete intervals. Disturbance is seen as porous, soupy sediment and as spaces between core segments. These gaps are caused by gas, mainly methane and some hydrogen sulfide in the top three cores (see "Organic Geochemistry," p. 13).

F5. Site 1144 recovery and lithology, p. 39.

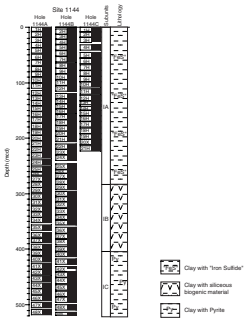

Bulk X-ray diffraction of one sample per core in Hole 1144A revealed that the mineralogy follows the overall visual homogeneity of the sediment (Fig. F6). A decrease in the quartz content occurs below about 277 mcd, but this may simply reflect the trend toward an increase of finer grained material for the older sediments at this site. Analysis of color indices measured with the spectrophotometer, qualitatively compared with the clay content as determined by smear-slide analysis, indicates that lower values of the L* parameter and higher values of the a* parameter (toward red) correlate with higher percentages of clay.

F6. Hole 1144A bulk mineralogy, p. 40.

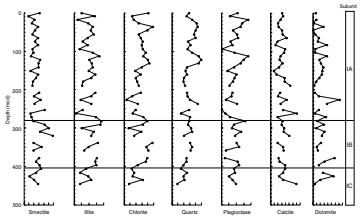

Subunit IA (0–283.43 mcd)

Interval: Cores 184-1144A-1H through 26X; Cores 184-1144B-1H through 28X; Cores 184-1144C-1H through 21H
Depth: 0–241.3 mbsf (Hole 1144A); 0–253.5 mbsf (Hole 1144B); 0–203.7 mbsf (Hole 1144C)
Age: Pleistocene

Subunit IA is distinguished from the rest of the section by the common presence of fine-grained "iron sulfide" (its actual mineralogy to be determined), which is seen as a mild to intense black mottling of the cut core face, whereas pyrite is rare. Opaque material is also noted in smear slides, both in the mottled and normal clay lithologies throughout the upper 283.43 mcd of the drilled section (Fig. F7).

F7. Abundance of "FeS" and pyrite, nannofossil content, and total siliceous organisms, p. 41.

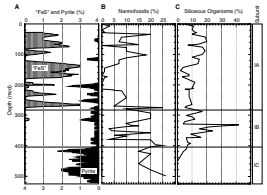

Subunit IB (283.43–404.07 mcd)

Interval: Cores 184-1144A-27X through 38X; Cores 184-1144B-29X through 39X
Depth: 241.3–356.7 mbsf (Hole 1144A); 253.5–359.7 mbsf (Hole 1144B)
Age: Pleistocene

Subunit IB is distinguished from the overlying subunit by a sudden drop in black "iron sulfide" mottling, coinciding closely with a significant increase in the proportion of nannofossils (Fig. F7). Pyrite is observed in modest quantities, usually as a replacement of burrow fills (Fig. F7). This subunit contains the highest proportion of siliceous biogenic debris, principally diatoms and sponge spicules (Fig. F7), noted over the drilled section.

Subunit IC (404.07–519.19 mcd)

Interval: Cores 184-1144A-39X through 48X; Cores 184-1144B-40X through 49X
Depth: 356.7–452.6 mbsf (Hole 1144A); 359.7–452.0 mbsf (Hole 1144B)
Age: Pleistocene

The basal subunit is distinguished on the basis of the high proportion of pyrite, usually present in burrows. Like Subunit IB, the proportion of nannofossils observed in smear slides remains high, and fine-grained "iron sulfides" are present only in minute amounts, whereas siliceous organisms decrease in concentration (Fig. F7).

Discussion

"Iron sulfide" mottling in the sediments in Subunit IA contrasts with an increase in pyrite in Subunit IC and implies changes in sedimentary

and early diagenetic environments. Pyrite is an authigenic mineral that usually forms early during diagenesis and burial of fine marine sediments and is usually found just a few centimeters below the seafloor. The pyrite concretions found at Site 1144 show enrichment in iron and sulfur as a result of local biological activity. In contrast, the "iron sulfide" mottles reflect relative enrichment in iron but a relative deficiency in sulfur, as shown by sulfur analyses of the interstitial water at Site 1144 (see **"Inorganic Geochemistry,"** p. 17). The abundance of "iron sulfides" in Subunit IA was likely caused by high organic carbon flux.

The clayey sediment at Site 1144 is completely homogenized by bioturbation. Carbonate content (i.e., nannofossils, foraminifers, and other forms of calcite, biogenic and/or nonbiogenic) varies between 5% and 45%, based on smear-slide observation. In comparison, coulometric analysis of carbonate content ranges from 10 to 20 wt% (see **"Organic Geochemistry,"** p. 13). The mismatch reflects the difficulty in estimating carbonate fractions accurately using smear slides as well as the sampling resolution of the chemical analyses, which consider much higher volumes, spaced regularly through the core, whereas the smear slides reflect mineralogic composition of small volumes at specified levels.

Diffuse mottling occurs throughout the sedimentary section. Yellowish olive and brownish olive-gray clay patches, up to 5 cm across, are locally present in moderate amounts but are much reduced compared to the sediments observed at Sites 1143. The patchy appearance is presumed to reflect bioturbation.

Layers of foraminifer ooze with small amounts of pyrite are noted. These layers form a very small proportion of the total section, <0.1%, and are typically <1 cm thick (e.g., 500.00–500.01 mcd; interval 184-1144A-47X-3, 147–148 cm). Sharp bases and normal grading are often, but not always, associated with these intervals. These beds probably represent deposition from turbidity currents.

Volcanic Ash Layers

Volcanic ash layers, ranging from <1 to 6 cm thick, are observed at Site 1144. Eight ash layers are observed in Hole 1144A, six in Hole 1144B, and two in Hole 1144C (Table **T5**). The ash layers are composed of angular glass shards and volcanic minerals. The thicker ash layers are often light colored, suggesting a composition dominated by high-silica glass as well as small amounts of quartz (<5%). Most of these ash layers have relatively sharp lower boundaries with bioturbated tops. Bioturbation may also result in mixed and/or homogenized sediments of volcanic ash and silty clay. A comparison between Holes 1144A, 1144B, and 1144C reveals that many ashes were seen in only one of the holes. However, one correlative ash layer occurs at 176.07–176.03, 175.05–176.11, and 176.01–176.07 mcd in Holes 1144A, 1144B, and 1144C, respectively. Lack of interhole correlation between the other ash layers may be caused by dispersion of the layers by bioturbation (Fig. **F8**) or by current redistribution, so that only patches of the thin layers are preserved (Fig. **F8**).

T5. Volcanic ash layers, **p. 79.**

F8. Site 1144 identified volcanic ash layers, **p. 42.**

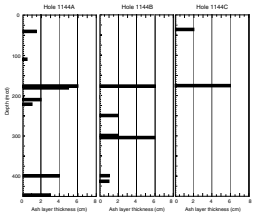

Fossils

Nannofossils are abundant throughout Site 1144. Among other microfossils, foraminifers are always recognized in smear slides but are often invisible on the cut core face. A few intervals have common to

abundant foraminifers, such as a 1-cm-thick layer at 179.45–179.46 mcd at Section 184-1144A-18H-5, 39 cm, as well as an interval of three to four layers between 456.47 and 456.57 mcd (interval 184-1144A-47X-3, 147 cm, to 47X-4, 10 cm), and a 10-cm-thick interval comprising pockets of foraminifers at 456.47–456.57 mcd (interval 184-1144B-44X-4, 29–39 cm). Sponge spicules, often present as millimeter-scale and irregularly shaped white pockets, are rare to common in all sections of the three holes; these may be interpreted as burrow fills, as representing small (or parts of) individual sponges, or as the result of redepositional processes (Martini and Locker, 1990).

Macrofossils are rare; however, ~1-cm-long gastropods, ~1-cm-long scaphopods, and up to ~1-cm-long pteropods are observed. Wood debris is uncommon but is observed at several intervals in all three holes; individual pieces are as long as 4 cm. Fragments of echinoderms are found only in the shallower intervals of the recovered section.

BIOSTRATIGRAPHY

Calcareous Nannofossils

Calcareous nannofossil biostratigraphy for Site 1144 was done mainly on core-catcher samples from Hole 1144A and supplemented by selected core-catcher samples from Holes 1144B and 1144C (Tables **T6, T7;** Fig. **F9**). Sediments recovered at Site 1144 yield abundant nannofossils that are generally well preserved above 387.8 mcd but are slightly to moderately dissolved below that level.

A middle to upper Pleistocene calcareous nannofossil assemblage was recognized, which is characterized by abundant *Emiliania huxleyi, Gephyrocapsa caribbeanica, Gephyrocapsa oceanica,* and *Pseudoemiliania lacunosa* (Table **T7**). *Florisphaera profunda* was less abundant (<20%) in comparison to the Pleistocene nannofossil assemblage at Site 1143 (>50%). This probably reflects the greater overall productivity at Site 1144 (i.e., less light penetration to the thermocline where *F. profunda* resides).

Five nannofossil datums were determined, as given in Table **T6** and Fig. **F9.** Because of the frequent occurrences of reworked Miocene to lower Pleistocene nannofossils, the two late Pleistocene biostratigraphic markers, *P. lacunosa* and *Reticulofenestra asanoi,* are almost continuously present in Pleistocene sediments (Table **T7;** Fig. **F10**). This leads to difficulties in determining the levels of their last occurrences. To obtain better biostratigraphic control, the relative abundances of *P. lacunosa* and *R. asanoi* were determined by counting nannofossils. The abundance of *P. lacunosa* shows two distinct intervals: above 288.7 mcd, its abundance is lower than 20 specimens/10 fields of view; below this level, its abundance increases significantly. Also, observations of other reworked fossils show no distinct increase in reworking below this level (Fig. **F10A**). This suggests that the increase in *P. lacunosa* below 288.7 mcd is not a result of reworking and places the last occurrence (LO) of *P. lacunosa* at this level. A significant increase in the abundance of *R. asanoi* was noted at 417.0 mcd (Fig. **F10B**). Furthermore, various gradational morphological changes between *P. lacunosa* and *R. asanoi* were observed below 422.7 mcd. These morphological changes occur only within the interval of *R. asanoi* (1.16 to 0.90 Ma) in the Northeast Atlantic (Su, 1996). This evidence allows us to assign the LO of *R. asanoi* at 422.7 mcd. The interval from 505.3 to 518.5 mcd is assigned to the *Gephyro-*

T6. Summary of biohorizons, **p. 80.**

T7. Calcareous nannofossil checklist, **p. 81.**

F9. Age-depth plot, **p. 43.**

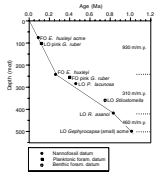

F10. Relative abundance variations, **p. 44.**

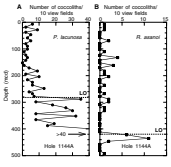

capsa (small) acme zone based on the disappearance of large and medium *Gephyrocapsa* spp., which indicates an age range of 1.01–1.20 Ma.

Planktonic Foraminifers

Planktonic foraminifers were also examined in all core-catcher samples from Hole 1144A and selected core-catcher samples from Holes 1144B and 1144C. The very soft sediments at this site allowed the clay to be easily removed from these samples by soaking them in a dilute Calgon and hydrogen peroxide solution and washing through a 150-µm sieve. Site 1144 yielded a moderate abundance of well-preserved planktonic foraminifers. This preservation was documented by infrequent test breakage (fragmentation <8%; see Fig. **F11**), little to no evidence of dissolution or diagenetic alteration, and the observation of numerous clear tests.

The planktonic foraminiferal biostratigraphy for Site 1144 is based on Hole 1144A (see Table **T8** for details). Because *Globorotalia truncatulinoides* is present continuously down the full length of this hole (518.5 mcd), this interval is assigned to Zone N22 (Blow, 1969). The complete absence of *Globigerinoides fistulosus* constrains the age of the sediments in Hole 1144A to younger than 1.77 Ma. Within Zone N22, we used the LO (0.12 Ma; Thompson et al., 1979) and first occurrence (FO) (0.40 Ma; Li, 1997) of pink *Globigerinoides ruber* as two biostratigraphic control points (Table **T6**).

As shown by previous studies in the South China Sea and Pacific Ocean (Wang et al., 1995; Le and Shackleton, 1992), the ratio between tropical species *Globorotalia menardii* and temperate species *Globorotalia inflata,* the relative abundance of *Pulleniatina obliquiloculata,* and the planktonic foraminiferal fragmentation increased during the interglacial stages, whereas the ratio between pteropods and planktonic foraminifers increased during the deglacial and glacial stages (Wang et al., 1997) (Fig. **F11C, F11D, F11E, F11F**). On the basis of planktonic foraminiferal and calcareous nannofossil events (Table **T6**), we can tentatively recognize glacial–interglacial MISs 1–9 from changes in the above-mentioned four indicators (Fig. **F11**). However, we cannot identify any glacial–interglacial cycles before MIS 9 (below ~250 mcd); sample resolution is very low because of the decreased sedimentation rate (Fig. **F9;** Table **T6**).

Benthic Foraminifers

The benthic foraminifers observed at Site 1144 comprised ~4% of the total foraminiferal fauna. The relative abundance of benthic foraminifers, indicative of high organic carbon flux (e.g., *Globobulimina* spp., *Chilostomella ovoidea,* and *Uvigerina peregrina*), is very high above ~240 mcd and then decreases downhole (Fig. **F11**). This trend corresponds well to the changes in the group abundance of siliceous microfossils such as radiolarians and diatoms (Fig. **F11**) and organic carbon content in Hole 1144A, indicating that productivity decreases downhole. In particular, Hole 1144A can be divided into three sections based on the changes in productivity and sedimentation rate. For the upper section, 0 to ~240 mcd, the high productivity corresponds to a high sedimentation rate. The middle section, between ~240 and ~420 mcd, has a low sedimentation rate with a moderate productivity. However, the low productivity in the lower section, below 420 mcd, corresponds to a high sedimentation rate rather than a low one (Fig. **F11**).

F11. Downhole biostratigraphic changes, **p. 45.**

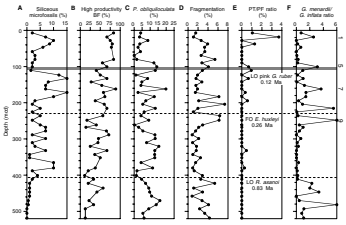

T8. Planktonic foraminifer checklist, **p. 82.**

One useful genus of benthic foraminifer, *Stilostomella,* was observed at 365.5 mcd (Sample 184-1144A-35X-CC). This genus has several species that disappeared from the global ocean at different latitudes during the time interval of 1.0–0.6 Ma. For the latitude of this site, we used 0.75 Ma as the LO of *Stilostomella* (for the northern South China Sea) (Schönfeld, 1996).

Summary

At Site 1144, both planktonic foraminifers and calcareous nannofossils are abundant and well preserved, whereas the nannofossils are occasionally to commonly reworked. Benthic foraminifers are generally few in number.

An age-depth plot shows that biohorizons from the three fossil groups generally agree with each other (Fig. **F9**). The maximum ages of Holes 1144A, 1144B, and 1144C are >1.01 Ma, >1.01 Ma, and <0.26 Ma, respectively. The sedimentation rates at Site 1144, calculated based on biostratigraphic data (Table **T6;** Fig. **F9**), are 930 m/m.y. after 0.26 Ma, 750 m/m.y. before 0.83 Ma, and 310 m/m.y. in between.

PALEOMAGNETISM

Shipboard paleomagnetic measurements for Holes 1144A, 1144B, and 1144C consisted of long-core measurements of the natural remanent magnetization (NRM) at intervals of 4–8 cm before and after alternating field (AF) demagnetization, usually up to 20 mT (see **"Paleomagnetism,"** p. 12, in the "Explanatory Notes" chapter). Measurements were carried out on the archive halves of all APC and XCB cores for Hole 1144A. In addition, discrete samples were collected from the working halves of Hole 1144A (APC and XCB cores) at a spacing of one sample per section (1.5 m). Some of these samples were subjected to progressive AF demagnetization up to 70 mT. Only the archive halves of APC cores from Holes 1144B and 1144C were measured. Cores 184-1144A-3H through 25H, 184-1144B-3H through 22H, and 184-1144C-3H through 21H were oriented using the Tensor tool.

Hole 1144A

The nonmagnetic cutting shoe was used with a standard core barrel on every second core, starting with Core 184-1144A-5H. Long-core measurements were carried out at 4-cm intervals with AF demagnetization steps at 10 and 20 mT for Cores 184-1144A-1H through 5H, then at 8-cm intervals with one step of demagnetization at 20 mT down to Core 184-1144A-47X.

The intensity of magnetization after demagnetization at 20 mT is on the order of 10^{-3} A/m down to ~430 mcd. A progressive increase of about two orders of magnitude is present below this depth. This trend, as well as other short-term characteristics, correlates with changes in magnetic susceptibility measured by the multisensor track (Fig. **F12;** see **"Physical Properties,"** p. 19). This change in the concentration of magnetic minerals is evidence that major changes occurred in the source of this material and/or in the mechanisms of transport to the site.

The direction of the NRM (after demagnetization at 20 mT and correction using the Tensor tool data) is shown in Figure **F13.** Above 260

F12. Intensity of magnetization and low-field magnetic susceptibility, Hole 1144A, **p. 46.**

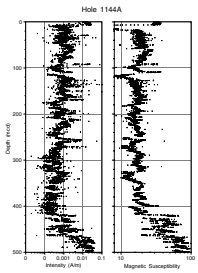

F13. Declination and inclination for Hole 1144A, 0–500 mcd, **p. 47.**

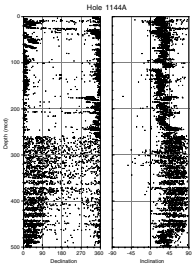

mcd (APC cores) the declination oscillates around 0°, and the inclination is about the value expected for a geocentered dipole field at this latitude (38°). The amplitude of the fluctuations in declination and inclination is consistent with the secular variation of the geomagnetic field. In Core 184-1144A-3H at 24 mcd, we observed a clear swing of the declination to reverse direction and then back to normal, with very high correlative values of inclination (Fig. F14). Although no negative inclinations were observed, we tentatively suggest that this represents a (partial) record of the Laschamp Event. High inclinations indicate that excursional virtual geomagnetic poles are close to the site, which is not inconsistent with the hypothesis of transitional preferred longitudinal bands during polarity reversals. We did not observe any other directional change—in particular, a change that could be associated with the Blake Event (~110 ka) was not found. No significant difference in the direction of magnetization was noted between the nonmagnetic cutting shoe used on odd cores and the standard cutting shoe used on even cores.

Below 260 mcd (XCB cores), the declinations reveal a tendency to lie between 0° and 90° with a large scatter. Inclinations are also scattered and are significantly steeper than expected at the site latitude. This high value reflects a large overprint in all XCB cores directed along the z-axis. This overprint was not removed after demagnetization at 20 mT; therefore, the direction of the primary magnetization could not be retrieved from long-core analyses.

We have attempted to obtain at least the magnetic polarity from discrete samples from the bottom of Hole 1144A (Cores 184-1144A-45X through 48X). Alternating field demagnetization of these samples to 70 mT, however, yielded somewhat ambiguous results: a few samples changed to negative polarity upon demagnetization, whereas others did not show evidence for reverse directions (Fig. F15A, F15B). Often the direction became erratic after the 45-mT step, possibly indicating some acquisition of anhysteretic magnetization in the demagnetizing coils. Therefore, the presence of reverse directions (suggested by some reverse discrete samples) needs additional postcruise confirmation.

F14. Enlarged view of the declination and inclination for Hole 1144A, 0–50 mcd, p. 48.

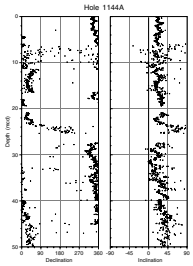

F15. AF demagnetization to 70 mT of Samples 184-1144A-45X-4, 86 cm, and 47X-2, 86 cm, p. 49.

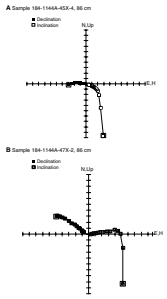

Holes 1144B and 1144C

Only long-core measurements were made on cores from Holes 1144B and 1144C, with readings spaced by 8 cm and one demagnetization step at 20 mT. Only normal polarities were observed.

Normalized Magnetization

Normalized magnetization is obtained by dividing the measured magnetization by a suitable normalizer to compensate for changes in the concentration of remanence-carrying grains (usually anhysteretic remanent magnetization, isothermal remanent magnetization, or, less frequently, magnetic susceptibility). Under restrictive conditions of uniformity of magnetic mineralogy (magnetite with uniform granulometry in the pseudosingle domain state), normalized magnetization may represent a proxy for changes of the geomagnetic field intensity. Although all these restricting hypotheses remain to be proven true for Site 1144 by shore-based studies, we have tentatively divided the intensity after demagnetization at 20 mT by magnetic susceptibility. The results, shown in Figure F16 for the three holes, are still contaminated by high-frequency peaks. Nevertheless, some similarities are observed between

F16. Preliminary normalized intensity, p. 50.

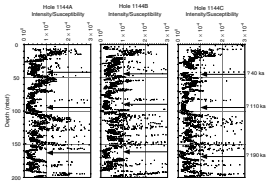

the smoothed records from the three holes, particularly between Holes 1144A and 1144B. Identification of the lows in the Hole 1144A record with known lows in the geomagnetic field intensity (Lehman et al., 1996; Guyodo and Valet, 1996) leads to the age assignment indicated in Figure F16. This speculation, which agrees with the biostratigraphic results (see "Biostratigraphy," p. 9), suggests that records of normalized field intensity might be obtained from Site 1144, provided the magnetic mineralogy is proven to be uniform. This will be tested in a postcruise study.

SEDIMENTATION AND ACCUMULATION RATES

The chronostratigraphy of Site 1144 is primarily derived from calcareous nannofossil and planktonic foraminiferal zones and events. Because of the extremely high sedimentation rates at this location, only eight biostratigraphic zones and markers were identified (see "Biostratigraphy," p. 9). Unfortunately, the magnetopolarity stratigraphy was also limited because of high sedimentation rates and magnetic overprint; only the Laschamp Event (0.04 Ma) is tentatively identified at 23.5 to 25.5 mcd. Although not highly detailed, the biostratigraphic control points proved adequate for calculating sedimentation rates (Table T6). Because of intensive bioturbation, sediment redeposition is extremely difficult to identify at this site.

Figure F17 (also given as Synergy Software KaleidaGraph plots and Microsoft Excel data files [see the "Supplementary Materials" contents list]) shows the linear sedimentation rate and mass accumulation rate curves based on calculations described in "Sedimentation and Accumulation Rates," p. 13, in the "Explanatory Notes" chapter. The sedimentation rates varied from a maximum of ~1000 m/m.y. over the interval ~100–242 mcd to a minimum of 324 m/m.y. for the interval 242–396 mcd (Table T9). When converted to mass accumulation rates (g/cm²/k.y.) and partitioned into carbonate and noncarbonate components, extremely high accumulation rates are observed over the past 0.26 m.y. (Fig. F17). Accumulation rates in the mid-Pleistocene (1.05–0.78 Ma) are high (~60 g/cm²/k.y.) with noncarbonate components dominating. From 0.78 to 0.26 Ma, the mass accumulation rate was relatively constant (~37 g/cm²/k.y.). Then it increased dramatically to a maximum of >100 g/cm²/k.y. (especially the noncarbonate). The rate remained high but decreased gradually toward the present. These extremely high noncarbonate accumulation rates likely reflect the onset of active drift-type deposition at Site 1144. This onset may be related to changes on the shelf that direct more fine-grained sediment to the site or to a change in the circulation that transports the material.

F17. Age-depth model, LSR, and MAR, p. 51.

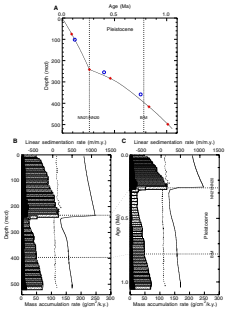

T9. Sedimentation and accumulation rates for selected intervals, p. 83.

ORGANIC GEOCHEMISTRY

Overview

The concentration of methane found by headspace (HS) analysis in sediments at Site 1144 was generally high, varying by more than an order of magnitude between 3,000 and >60,000 ppmv. Traces of ethane (<2 ppmv) were found in just three samples between 375 and 420 mcd, associated with the highest methane concentrations at depth. Carbonate concentrations were generally low, increasing at 180 mcd from 10–

15 wt% in the upper interval to between 10 and 23 wt% in the lower interval, accompanied by greater amplitude fluctuations. Total organic carbon (TOC) obtained by difference (total carbon [TC] – inorganic carbon [IC]) decreases systematically from >1% above 50 mcd to <0.5% toward the base (below 420 mcd). Most sediments exhibit low C/N values, suggesting a predominantly marine organic source. Total chlorin abundance was measured to 316 mcd. Bulk concentrations exhibit strong fluctuations indicative of glacial–interglacial changes.

Hydrocarbon Gases

Headspace gas analysis was performed on every core from Hole 1144A, usually taken midcore. Analysis was conducted as described in "Organic Geochemistry," p. 14, in the "Explanatory Notes" chapter. Concentrations of methane rise rapidly in the first three cores (to 20 mcd) (see Table T10; Fig. F18); this is related to the depletion of dissolved sulfate to essentially zero (<0.5 mM) in interstitial waters within the first core (see "Inorganic Geochemistry," p. 17). Such a relationship has been observed frequently (e.g., Kvenvolden and Kastner, 1990; Stein et al., 1995) and is attributed predominantly to microbial generation of methane below the interval of sulfate reduction. Sediment methane concentrations decline fairly uniformly from 20 to 200 mcd (Fig. F18), apparently reflecting decreasing organic matter (OM) availability (Fig. F19). A marked increase in methane is observed between 220 and 420 mcd, especially below 370 mcd. This is accompanied by traces of ethane in Cores 184-1144A-37X, 39X, and 40X. However, the C_1/C_2 ratio never drops below 50,000 because of the high methane concentrations. Methane rapidly decreases below 420 mcd. Without a strong thermal gradient, it is hard to explain the minimum and secondary peak in CH_4 with depth. Dissolved sulfate measurements indicate that sulfate reduction is complete below 10 mcd. Density shows a marked increase and porosity a corresponding decrease at 420 mcd (see "Physical Properties," p. 19), indicating a change in the sediment. This reduction in pore space reduces the volume available for hydrocarbons and may account for the low methane levels in headspace samples at the base; any free gas generated may have escaped during XCB coring. Organic carbon abundance is also lowest in this deep zone. However, the increase in methane with depth between 220 and 420 mcd remains unexplained; a conclusion implicating increasing organic maturity awaits further postcruise analysis.

Soon after core recovery, the sediment was inspected through the transparent core liner for the presence of gas voids, from which gas was extracted using a steel piercing tool and gas-tight syringe. Voids were sampled in Cores 184-1144A-3H through 35X; below this level, voids were too scarce to routinely sample. Samples were analyzed as described in "Organic Geochemistry," p. 14, in the "Explanatory Notes" chapter. Such void-space (VS) concentrations of methane as analyzed by the natural gas analyzer are approximately an order of magnitude higher than those in HS samples (Table T10; Fig. F18). Concentrations range from 23%–79% by volume with one anomalously low value from Core 184-1144A-23H, which was apparently contaminated by air during collection. The voids also contain 0.5% to 1.5% CO_2 and as much as several percent N_2 (after correction for air N_2 using the O_2 values). The methane data has little trend, although higher values between 190 and 290 mcd might indicate more complete sediment degassing before sampling for

T10. Methane concentrations by headspace and void-space analysis, p. 84.

F18. Methane concentration vs. depth, p. 52.

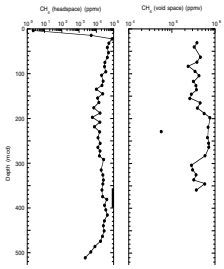

F19. Carbonate, TOC, and organic C/N ratio vs. depth, p. 53.

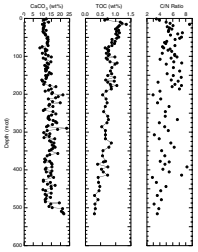

headspace analysis (Fig. F18). This is possibly the result of a change in drilling techniques from APC to XCB drilling, which routinely recovers more compacted sediment and less in situ free gas.

Inorganic Carbon

Three samples per core were analyzed for inorganic carbon, and at least one sample per core for total carbon, total nitrogen (TN), and total sulfur from Hole 1144A (Table T11). Carbonate content varies from 8.6% to 23.5 wt%, with lower average values and amplitudes above 175 mcd (average [AV] of 12.0% and standard deviation [SD] of 1.4), increasing to an AV of 15.1% and SD of 2.9 between 175 and 310 mcd. Values again decrease to ~10%–17% (AV of 13.7%; SD of 2.0) between 310 and 485 mcd until a final further increase below ~425 mcd to >20% (AV of 18.9%; SD of 3.3) (Fig. F19). The marked fluctuations in carbonate concentration between 175 and 310 mcd suggest a cyclic input of carbonate. Further, coulometer reaction times for >99.9% (complete) reaction of carbonate increased over this interval. This may indicate a lithologic change related to increased proportion of dolomite or increased biogenic carbonate.

T11. IC, $CaCO_3$, TC, TOC, TN, and TS contents, p. 85.

Organic Carbon

The TOC concentration by difference (TC – IC) was determined for three samples per core to Core 184-1144A-12H and one sample per core below that. TOC values are higher (0.5%–1.3%; AV of 0.90%; SD of 0.17) above 195 mcd than below (AV of 0.56%; SD of 0.15%). Marked peaks (Samples 184-1144A-2H-5, 107–108 cm; and 12J-3, 107–108 cm) appear to correlate with a tentative assignment of oxygen isotope stage boundaries 2/1 and 6/5e (i.e., Termination Events I and II) and may well relate to pulsed input from allocthonous organic carbon remobilized by transgression of the continental shelf and/or autochthonous phytoplankton production (e.g., Harris et al., 1996) (see "Chlorin Analysis," p. 16). Sample resolution below 180 mcd is insufficient to explore this hypothesis. Concentrations decline steadily below 190 mcd and are especially low below 420 mcd (<0.5%) (Fig. F19). Rock-Eval TOC values are systematically 10% to 30% lower than those calculated by difference (Fig. F20). The decreasing TOC trend with depth downhole is similar to that seen in benthic foraminifers (see "Biostratigraphy," p. 9).

F20. TOC by Rock-Eval pyrolysis vs. TOC by difference, p. 54.

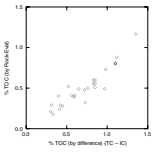

Sulfur

Sulfur values are listed in Table T11 and range from 0.75% to 0.1%. We assume this sulfur occurs as pyrite, which is frequently observed in the cores (see "Lithostratigraphy," p. 6). Ten samples were noted to have visible pyrite in split-core sections during sampling or during carbonate sample preparation. Of these observed sulfide occurrences, approximately half had elevated S contents compared with adjacent samples without visible sulfide. Unlike OM, which is present as ubiquitous, fine-sized material, the sulfide occurs as discrete, irregular concentrations that may or may not be present in the CARB sample analyzed for total S. Six samples gave 0% S values after the detector began to yield unreliable S results (see "Organic Geochemistry," p. 18, in the "Site 1143" chapter) and were subsequently re-analyzed (Table T11). The high values for the samples above Core 184-1144A-15H also correspond to the samples with higher organic carbon as expected from syn-

genetic sulfate reduction and organic carbon-sulfur systematics (Berner, 1984).

Organic Matter Characterization

Our analytical methods allow us to chemically characterize the organic matter in several ways. Ratios of TOC to TN (C/N ratio) range from ~3 to ~9 at Site 1144 (Table T11; Fig. F19). However, these values appear too low and may result from residual NH_4^+ adsorbed on to, or absorbed within, the clay minerals (see "Organic Geochemistry," p. 11, in the "Site 1145" chapter). Figure F21 shows the results for TN vs. TOC by difference. Average C/N values of marine plankton are between 5 and 8, whereas higher land plants have ratios >20. These values, however, may change during diagenesis and thermal maturation (Emerson and Hedges, 1988). Therefore, it is unclear whether a correction for clay-bound nitrogen is applicable. A woody fragment, recovered from Core 184-1144B-24H, can be used as a point of reference for terrestrial organic matter (Tables T11, T12). Overall, the C/N values exhibit no downhole trend, except that the amplitude increases downcore. Two higher C/N values (Sections 184-1144A-38X-1 and 40X-1) do not appear to correlate with any significant changes in TOC or any unusual core observations.

Examination of Rock-Eval S_3 and oxygen index (OI) data (Table T12) indicates that they are not reliable for the first set of analyses. Thus, although the OI data are mainly indicative of type III terrestrial OM, we do not consider them to be definitive. The OI values are always a problem at low TOC and with immature OM. We have rerun several samples and find that the OI is indeed variable, but the results for T_{max} (temperature of maximum release; see "Organic Geochemistry," p. 13, in the "Explanatory Notes" chapter), TOC, and HI (hydrogen index) are repeatable and consistent. An additional problem arises in sediments containing such relatively low TOC content because of adsorption of pyrolyzates (S_2 values leading to low HI values) to clays (Peters, 1986).

Chlorin Analysis

Total chlorin abundance was measured between 0 and 316 mcd at a sampling interval of two samples per section (Table T13; Fig. F22A). Analytical methods are discussed in "Organic Geochemistry," p. 13, in the "Explanatory Notes" chapter. The concentration of pigments determined by solvent extraction and fluorescence spectrophotometry could not be quantified precisely because of the absence of a known standard but is expressed in relative absorbance units per gram dry weight of sediment. Total chlorin abundance varies by more than an order of magnitude (0.34–4.27 units) and exhibits a general decreasing trend downhole. This trend is consistent with that seen in TOC measurements (Fig. F22B) at various sites during Leg 184 and may reflect a dilution signal seen as a corresponding increase in carbonate abundance related to the evolution and deepening of the South China Sea (Fig. F19). However, an alternative explanation requiring diagenetic transformation of chlorins over time awaits further shore-based research.

The distribution of chlorins downhole shows some marked similarities to that of TOC. This confirms the conclusion of previous studies relating chlorin abundance to organic input to sediments (e.g., Harris et al., 1996). However, there are some notable discrepancies within the

F21. TOC (by difference) vs. TN, p. 55.

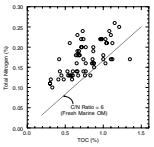

T12. Rock-Eval pyrolysis results, p. 88.

T13. Chlorin concentration per gram dry weight, p. 89.

F22. Chlorin abundance, TOC, and NGR vs. depth, p. 56.

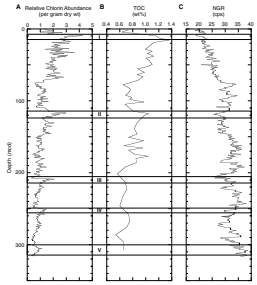

two data sets. Several marked maxima in TOC abundance do not correspond to high chlorin concentrations (e.g., 95–105 mcd and 150–180 mcd). It is suggested that these represent periods of increased nonmarine OM enrichment and coincide with elevated C/N ratio values. Comparison with NGR data indicates that maxima in NGR counts, indicative of higher clay content and (by inference) increased allocthonous input, coincide with such increases in TOC (Fig. F22C). Discrepancies also occur in the exact timing of absolute maxima in chlorins and TOC, which we tentatively conclude coincide with Termination Events (Termination I, 5 mcd; Termination II, 117 mcd; Termination III, 209 mcd; Termination IV, 252 mcd; and Termination V, 309 mcd). The resolution of the TOC data in the upper 180 mcd permits us to conclude that during Terminations I and II, maximum TOC abundance occurs before that in chlorins. This may result from the input of allocthonous OM reworked from the continental shelf during rising sea levels before a climatic and nutrient-related effect on marine phytoplankton productivity. The general pattern observed in NGR data suggests a reverse correlation with chlorin abundance, prompting our conclusion that chlorins are a proxy for autochthonous marine production at Site 1144.

INORGANIC GEOCHEMISTRY

Interstitial water samples were squeezed from 93 whole-round samples at a frequency of two per core in Cores 184-1144A-1H to 20H and 26X to 48X. Additional samples were taken at a frequency of one per core from Cores 184-1144B-22X through 26X to fill a sampling gap in Hole 1144A. Inorganic chemical analyses were conducted on a subset of these interstitial water samples. Salinity was measured in every sample. Alkalinity and pH were measured once per core. The concentrations of Ca^{2+}, Mg^{2+}, K^{+}, Na^{+}, and SO_4^{2-} were measured at a frequency of one per core, except in the sampling gap at Hole 1144A. All other analyses were made one per core for the first nine cores and every third core thereafter. In addition, chloride was measured two per core in Cores 184-1144A-39X through 47X to look for evidence of gas hydrate decomposition. Analytical methods are detailed in "Inorganic Geochemistry," p. 17, in the "Explanatory Notes" chapter. The concentrations of dissolved interstitial constituents are presented in Table T14, and the profiles with depth are shown in Fig F23. Interstitial water profiles at Site 1144 are characteristic of sediments in which sulfate reduction, volcanic ash alteration, and dissolution-recrystallization of biogenic minerals are the primary reactions controlling the concentrations of dissolved constituents.

T14. Interstitial water composition, p. 92.

F23. Interstitial water measurements, p. 57.

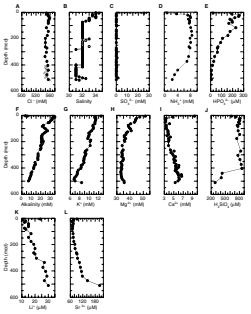

Chloride and Salinity

Chloride (Cl^{-}) concentrations in interstitial waters at Site 1144 are relatively constant, ranging from 549 to 561 mM (Fig. F23A; Table T14). Interstitial water salinities decrease downhole from 35 near the top to 31 near the base of the hole (Fig. F23B; Table T14). The decrease in salinity from 0 to 75 mcd is probably related to the removal of dissolved sulfate from interstitial waters during sulfate reduction. The major goal of the high-density interstitial water sampling at this site was to look for low salinity and chlorinity values, as well as dilution of other interstitial water signals, as evidence of dissociating gas hydrates. At sites where gas hydrates have been observed (e.g., Ocean Drilling Program

Site 994), interstitial waters showed a distinct downhole trend toward lower chlorinity values, as well as very low chlorinity values (<500 mM) in the zone where gas hydrates were observed (Leg 164; Shipboard Scientific Party, 1996). Whereas high-resolution measurements of chlorinity are left to shore-based investigations, the small variation in shipboard chlorinity and salinity measurements suggest that gas hydrates are not present at this site.

Sulfate, Ammonium, Phosphate, Alkalinity, and pH

Sulfate was detected only in interstitial waters from Core 184-1144A-1H (Fig. **F23C;** Table **T14**), and the concentration of dissolved sulfate was essentially zero below this depth. Methane levels increase at this depth, indicating that methanogenesis takes over as the dominant reduction process within the sediments (see **"Organic Geochemistry,"** p. 13). Such a shallow switch from sulfate reduction to methanogenesis suggests that the supply of organic material to this site is high. As a product of both sulfate reduction (see **"Inorganic Geochemistry,"** p. 20, in the "Site 1143" chapter) and methanogenesis (Gieskes, 1983), ammonium concentrations increase rapidly in the top 22 mcd and then remain quite high until 394 mcd, where there is a decrease toward the base of the hole (Fig. **F23D;** Table **T14**). Also in response to sulfate reduction and methanogenesis, dissolved HPO_4^{2-} concentrations peak at 260 mM at 22 mcd and then decrease toward a minimum of 6 mM at the base of the hole (Fig. **F23E;** Table **T14**). Within this overall downhole decrease is an excursion toward lower HPO_4^{2-} values between 39.9 and 117 mcd. Alkalinity increases rapidly between the first and second core in response to sulfate reduction, from 3.9 mM at 3 mcd to a maximum of 34.9 mM at 13 mcd (Fig. **F23F;** Table **T14**). Below this depth, alkalinity generally decreases downhole to a minimum of 7.1 mM at the base of the hole. Superimposed on this downhole trend toward lower alkalinity is a shift toward lower values with a local minimum at 75 mcd, followed by a shift toward higher values with a local maximum at 117 mcd. Throughout Hole 1144A, pH is relatively constant ranging from 7.4–8.2 (Table **T14**).

Potassium, Magnesium, and Calcium

Dissolved potassium (K^+) concentrations decrease downhole from ~12.5 mM near the surface to 6.8 mM at 486 mcd (Fig. **F23G;** Table **T14**). This shift is probably related to uptake of potassium during clay and volcanic ash alteration. Magnesium concentrations (Mg^{2+}) decrease with depth from 51.5 mM at the top to a minimum of ~33 mM at the bottom of the hole (Fig. **F23H;** Table **T14**), with an excursion toward first lower, then higher Mg^{2+} values between 56 and 126 mcd. The profile of dissolved calcium concentration (Ca^{2+}) decreases from 9.2 mM to 4.8 mM between the first and second core (Fig. **F23I;** Table **T14**), and then Ca^{2+} increases slowly downhole to a maximum 9.1 mM at 429 mcd. Below this depth, Ca^{2+} begins to decrease toward the base of the hole. Overall, the alteration of basaltic volcanic ash, which is documented throughout the sediment at this site (see **"Lithostratigraphy,"** p. 6), is likely the dominant process altering the profiles of these two elements.

In the profiles of alkalinity, Mg^{2+}, and HPO_4^{2-}, an excursion between 53 and 188 mcd overprints the overall downhole trends of these con-

stituents. Sharp events like this are unexpected in interstitial water profiles below the zone of organic matter reduction. One possible source of this signal at Site 1144 is the dissolution of pteropod aragonite within the sediments. Within the upper 160 mcd at Site 1144, there are peaks in the ratio of pteropods to foraminifers (see **"Biostratigraphy,"** p. 9) near the surface and at 108 mcd that correspond to the variations in the dissolved Mg^{2+} and alkalinity in interstitial waters. Thus, the interstitial water peaks within these intervals could reflect the dissolution of relatively unstable, Mg-rich aragonite. How this process would lead to lowered phosphate values is less clear.

Silica, Lithium, and Strontium

Dissolved silica (H_4SiO_4) increases in the first three cores and then is high and relatively constant downhole at 795 mM ± 31 until it decreases abruptly to 400 mM between 404 and 440 mcd (Fig. **F23J;** Table **T14**). This shift coincides with a severalfold increase in magnetic susceptibility (see **"Physical Properties,"** p. 19) and a large decrease in the abundance of siliceous microfossils (see **"Biostratigraphy,"** p. 9). Thus, the decrease in dissolved silica is related to the decrease in the siliceous microfossils available to be dissolved. Lithium (Li^+) decreases from 24 mM to 11 mM between the first and second cores and then increases linearly with depth to a maximum of 30 mM (Fig. **F23K;** Table **T14**). Dissolved strontium concentrations (Sr^{2+}) increase from a minimum of 68 mM at 22 mcd to a maximum of 202 mM at the base of the hole (Fig. **F23L;** Table **T14**). The increases in both Li^+ and Sr^{2+} concentrations downcore most likely reflect exclusion of these elements during dissolution of biogenic calcite (Sr^{2+} and Li^+) or dissolution of biogenic silica (Li^+). The gradients with depth in Li^+ and Sr^{2+} at Site 1144 are much lower than those at Site 1143 (see **"Inorganic Geochemistry,"** p. 20, in the "Site 1143" chapter). This is probably a reflection of the much lower percentage of carbonate at this site (see **"Organic Geochemistry,"** p. 13) and the much shorter interval in which the sediments could be chemically altered.

PHYSICAL PROPERTIES

Sampling

At Site 1144, physical properties were measured on whole-round sections, split-core sections, and discrete samples from the latter. Whole-round core logging with the MST included GRA bulk density, MS, and NGR on all cores as well as *P*-wave velocity logging from the top of the holes down to Sections 184-1144A-6H-7, 184-1144B-23X-1, and 184-1144C-21H-9. Sampling intervals were 4 cm for Hole 1144A from the top of the hole down to Section 184-1144A-6H-7 and 8 cm for the rest of Hole 1144A and Holes 1144B and 1144C. The *P*-wave logger (PWL) data were bad as a result of instrument problems and/or cracks or a void in the sediment cores. Two thermal conductivity measurements per core down to Core 184-1144A-12H and one per core for the remaining cores were also performed on whole-round sections. Color spectral reflectance was measured on the archive halves of all split cores at 4-cm sampling intervals. Moisture, density, and *P*-wave velocity (using the *P*-wave velocity sensor 3 [PWS3]) were measured on discrete samples from split-core sections at intervals of one measurement per section (1.5 m)

(see "Physical Properties," p. 18, in the "Explanatory Notes" chapter). The PWS3 could not detect the ultrasonic signals below Section 184-1144A-5H-1 because of core disturbance associated with gas expansion. Therefore, the *P*-wave velocity values are not presented here.

Results

Multisensor Track Measurements

Results from core logging with the MST reveal three characteristic intervals. The first interval (0–100 mcd) is defined by a trend of steadily increasing GRA density and NGR (Figs. F24, F25). This trend is related to the compaction in the top of the sediment column, at least for the GRA and probably also for the NGR because the intensity counted is density dependent. Superposed on this first-order trend are smaller but well-defined fluctuations. Rather surprisingly, MS—which often shows patterns similar to the NGR—does not follow this trend (Fig. F26). Instead, the MS signal is low (~20 × 10^{-5} SI) and flat except for a distinct depression at 8–18 mcd.

The second interval (100–420 mcd) is defined by a trend of a markedly decreased rate of downhole increase in GRA and NGR compared to the first interval. The superposed variations in these signals are of relatively large amplitude (Figs. F24, F25). The MS continues the rather featureless and low-amplitude downhole trend that it exhibits in the upper interval, except for some spikes associated with ash layers (Fig. F26; see "Lithostratigraphy," p. 6).

The third interval is defined by a very distinct increase in MS, GRA, and NGR at 420 mcd (Figs. F24, F25, F26). Overall, this transition is the most conspicuous feature in the core logs. The MS values increase abruptly from ~20 × 10^{-5} SI to 60 × 10^{-5} SI, then increase further to 120 × 10^{-5} SI. This indicates a major change in supply or, less likely, in the chemical or biogenic production of magnetic minerals. The GRA values increase from ~1.7 to >1.8 g/cm³ over this transition and suggest a markedly reduced porosity and/or a significant change to a higher density mineralogy.

Bulk density estimates from GRA and from moisture and density (MAD) measurements show a generally good agreement in the lower part of the hole and significant offset in the upper part (Figs. F24, F27). The great scatter in GRA data, which are biased toward underestimating the true values, decreases downhole, and so does the discrepancy between GRA and MAD bulk density estimates (Figs. F24, F27). Figure F27 demonstrates that the discrepancy is much more severe for lower density values in general and for APC cores in particular. This phenomenon can be attributed to core disturbance by gas expansion (observed directly when cutting the cores into sections) and indirectly from the numerous voids created in the cores by the pressure of the escaping gas.

Grain Density, Bulk Density, and Porosity

Grain density values vary between 2.60 and 2.75 g/cm³ and show a generally increasing downhole trend (Fig. F28), suggesting an increase in carbonate (see Fig. F19; "Organic Geochemistry," p. 13). This trend is disrupted by significant excursions (~0.5 g/cm³) at 70–120 mcd, 120–150 mcd, 280–320 mcd, and 320–360 mcd. Porosity reveals a steep decrease from 80% to 65% in the uppermost interval (0–100 mcd), compatible with the increase in bulk density from 1.35 to 1.65 g/cm³ (Figs.

F24. Bulk density measurements from GRA core logging and MAD methods, p. 58.

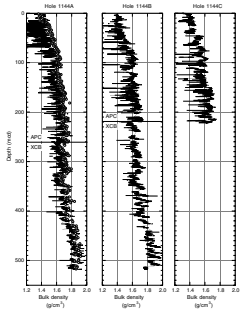

F25. Natural gamma radiation from core logging for Holes 1144A, 1144B, and 1144C, p. 59.

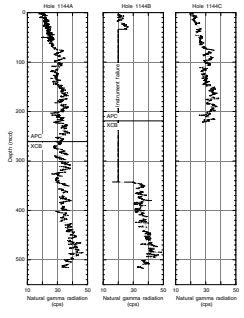

F26. Magnetic susceptibility from core logging for Holes 1144A, 1144B, and 1144C, p. 60.

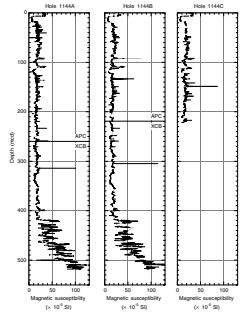

F27. Comparison of bulk density measurements from GRA and MAD methods at Hole 1144A, p. 61.

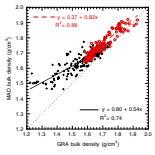

F24, F28) and indicating a strong downhole compaction of the sediments over that interval. In the middle interval (100–420 mcd), porosity decreases further at a lower rate from 65% to 55%. At 420 mcd, porosity abruptly decreases to 50%. This lowermost interval corresponds to the abruptly increased MS values (Fig. F26). Postcruise studies will determine if this abrupt transition is strictly a change in mineralogy and lithology affecting porosity and density or (less likely) if it is a hiatus or fault that brings into contact strata with different compaction histories.

The transition from APC to XCB coring (260.15 mcd in Hole 1144A; 219.54 mcd in Hole 1144B), which had a severe effect on the data from Site 1143, has only a minor effect here. This is probably less because of better XCB core quality than because of severe gas expansion that affected APC and XCB cores alike to a depth of ~350 mcd.

F28. Porosity, grain density, and dry density from MAD measurements at Hole 1144A, p. 62.

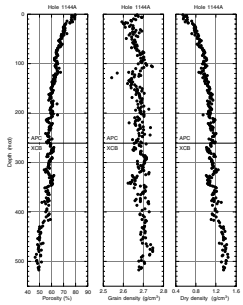

P-wave Velocity

Neither the PWL sensors on whole cores nor the PWS3 measurements of *P*-wave velocity from split-core sections yielded useful results because of abundant voids and cracks from gas expansion.

Color Reflectance

The CSR data are presented as records of two parameters from the L*a*b* color system: L*, representing the lightness in percent; and a*/b*, the ratio of the two chromaticity parameters (Fig. F29). Although L* can generally be used as a first-order approximation of the relative concentration of carbonate, the relationship between L* and shipboard carbonate measurements is not apparent, perhaps because of the low carbonate sampling resolution. A general correspondence with the three intervals defined by the MST core-logging data is recognizable. Most of the uppermost interval (18–100 mcd) is characterized by an increase in L* from 33% to 40%; the uppermost 18 m shows the opposite trend. The middle interval (100–420 mcd) denotes a very gentle general increase from 40% to 44%, with larger fluctuations (~5%) superimposed on the general trend. The lowermost interval below 420 mcd (but only to 500 mcd) reveals a decrease from 44% to 40%. The trends of the a*/b* ratio, a proxy for color change that can be related to a combination of carbonate or organic matter content, clay mineralogy, oxidation, and so forth, are quite different. From 0 to 150 mcd, the parameter has a constant value around 0 with few excursions. Below that interval, high frequency and amplitude variations between 0 and –1.5 are observed and may indicate a color bedding, perhaps the green clay layers. Postcruise spectral analysis will be required to interpret these records.

F29. Color spectral reflectance measurements, p. 63.

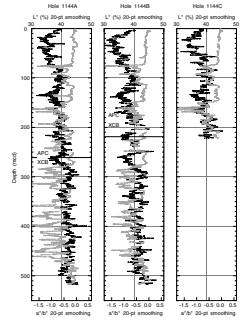

T15. Thermal conductivity measurements, p. 94.

Thermal Conductivity

Thermal conductivity values increase downhole from 0.9 to 1.1 (W/[m·K]) (Table T15, also in ASCII format; Fig. F30). The low sampling resolution reveals one more abrupt increase near 420 mcd, suggesting that the generally positive correlation between thermal conductivity and bulk density is valid here too.

F30. Thermal conductivity measurements for Hole 1144A, p. 64.

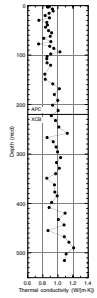

Heat Flow

Four downhole temperature measurements with the APC temperature tool were taken in Hole 1144A at depths of 25.9, 54.4, 101.9, and 149.4 mbsf, respectively. In addition, a bottom-water temperature measurement was taken before coring in Hole 1144B (Fig. F31). The objective was to establish the local heat flow. Original temperature records were analyzed using "Tfit" software to establish the equilibrium temperature at depth. Measurements at 25.9 mbsf seem problematic. The estimated errors in equilibrium temperature vary from 0.2° to 0.5°C, reflecting the amount of frictional heat introduced during the 10-min measurement as a result of heave. Depth errors are on the order of ±0.5 m. The measurements between 0 and 149.4 mbsf yielded a thermal gradient of 24°C/km (Fig. F32), which is less than one-third of the thermal gradient observed in Hole 1143A.

WIRELINE LOGGING

Logging Operations

After reaching the maximum coring depth of 452.6 mbsf, Hole 1144A was filled with viscous mud, reamed, and flushed of debris. We first ran one full pass and a shorter repeat pass with the triple combo tool string, including the hostile environment natural gamma-ray sonde (HNGS), accelerator porosity sonde, hostile environment lithodensity sonde (HLDS), and dual-induction tool (DIT; resistivity). The Lamont-Doherty Earth Observatory temperature/acceleration/pressure tool was not run because it failed during Hole 1143A operation, and attempts to fix it were unsuccessful. Next, we ran two full passes with the FMS, long-spaced sonic (LSS), and natural gamma-ray tool (NGT) string. Finally, we ran two full passes with the GHMT tool string, including the nuclear magnetic remanence sonde, susceptibility measurement sonde, and NGT (Fig. F33; see "Wireline Logging," p. 21, in the "Explanatory Notes" chapter). (The raw data are given on the "Related Leg Data" contents list.) The wireline heave compensator (WHC), which was fixed by Sedco mechanics after Hole 1143A logging, did a fine job. Sea heave was generally <1 m for the duration of the logging. All of the tool strings went to the bottom of the hole without any trouble, and a pipe trip was not required. Logging operations started at 1145 hr on 15 March and finished at 0530 hr on 16 March (Table T16).

Log Quality

All three tool strings reached within several meters of the bottom, indicating that little debris fell from the borehole wall. The two passes for the three tool-string runs showed generally excellent repeatability for all the log parameters.

The hole was mostly in good shape. Borehole caliper measurements revealed that the lower part of the hole typically had a 10-in diameter, yielding good data. However, the area between 320 and 380 mbsf showed zones of washout reaching an 18.1-in diameter (Fig. F34). The washed-out zones resulted in poor contact with the borehole wall and, hence, bogus spikes on both the density and porosity logs. The shallow resistivity values from the spherically focused log (SFL) yielded a constant offset of ~30 ppmv less than the medium and deep resistivity (me-

F31. Downhole temperature measurements, p. 65.

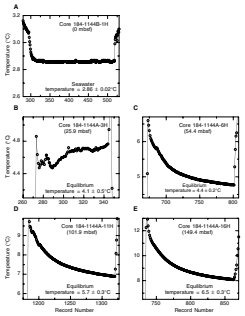

F32. Downhole temperature gradient, p. 66.

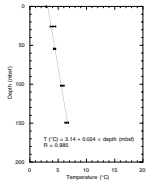

F33. Graphic summary of downhole logging operations for Hole 1144A, p. 67.

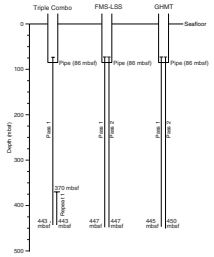

T16. Summary of logging operations, p. 97.

F34. Downhole logs in Hole 1144A, p. 68.

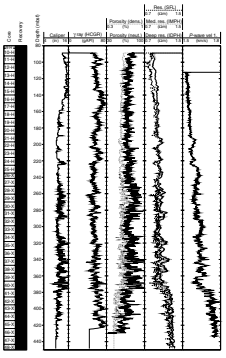

dium induction phasor-processed resistivity [IMPH] and deep induction phasor-processed resistivity [IDPH]) values from the DIT (Fig. F34). The offset is greatest in some of the rugose areas. Despite this, the three resistivity curves show excellent agreement in their variations with depth throughout the entire log interval.

The FMS results once again demonstrated that even when the WHC is working perfectly, it does not provide perfect compensation. The observed stick-slip of the tool string was on the order of 0.25 m. This effect on the data was corrected during the processing of the FMS images with the Geoframe software. Despite an aspect ratio close to unity in the lower part of the hole, the FMS pads in the second pass perfectly tracked the first pass.

The magnetic intensity data recorded during the GHMT runs displayed the typical random spikes that were expected from this tool. Most of these spikes were on the order of 20 nT, but a few were hundreds of nT. In general, the spikes do not repeat between the two passes, so a good splice should be possible. These spikes were edited out in the data presented in Figure F35. Disregarding the spikes, the intensity does not vary by more than 50 nT from top to bottom.

The LSS log is of good quality for the entire hole; the two *P*-wave velocity measurements are almost completely superimposed (Fig. F34). In general, standard gamma ray (HSGR) and computed gamma ray (HCGR) from the HNGS tool in the triple combo run read 10% to 25% higher than spectroscopy gamma ray or computed gamma ray from the NGT tool in the FMS-LSS run, a difference easily accounted for by eccentricity and hole-size correction. Contrary to the NGT, the HNGS corrects for borehole diameter and potassium in the borehole fluid. The HNGS is more sensitive than the NGT; hence, its results are presented in Fig. F34 (column 1).

F35. Comparison of MAD porosity, downhole log bulk density porosity, and NGR, p. 70.

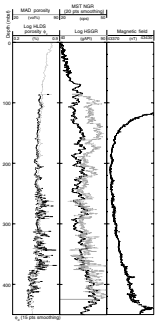

Results

P-wave velocities from the split-core samples were limited to the top 35 m of the core (see "Physical Properties," p. 19; Fig. F34) On the other hand, logging *P*-wave velocities are available below 86 mbsf, precluding comparison between them. Unfortunately, the MST core-logging measurements of the core *P*-wave velocities were also of poor quality because of gas expansion. The most striking features in the logging *P*-wave velocity curve are the major changes in velocity gradient at depths of 230, 290, and 375 mbsf. Above 230 mbsf, the velocity increases slightly with depth; between 230 and 290 mbsf, it decreases with depth. After an sudden increase of 0.06 km/s at 290 mbsf, the velocity again decreases slightly with depth between 290 and 375 mbsf. Another jump of 0.08 km/s occurs at a depth of 375 mbsf. Below this, the velocity increases with depth, showing the common compaction trend also seen in the porosity records. Because no obvious differences in lithology were found between the sediment units defined by these depth intervals (see "Lithostratigraphy," p. 6), we suggest that the discontinuities in the velocity profile may reflect differences in the style of compaction within various sediment units.

Other logging parameters, including bulk density and resistivity as well as magnetic susceptibility, also show significant increases at 375 mbsf (Fig. F34). Magnetic susceptibility shows a jump of ~30%–40% with much higher amplitude variations at 370 mbsf and an increasing trend down to the bottom of the hole. Lithologic description reveals

that the amount of pyrite in the sediments increases below 350 mbsf (see **"Lithostratigraphy,"** p. 6).

The potassium measurements from the NGT of the FMS-LSS run agree reasonably well with those from the HNGS of the triple combo run (Fig. **F36**). Above 160 mbsf, the values from the NGT are consistently lower than those from the HNGS tool by ~0.5%. The thorium values from the NGT, on the other hand, are consistently higher than those from the HNGS tool. The uranium measurements between the NGT and HNGS tools do not agree well; the NGT yields larger amplitude variations (Fig. **F36**).

The absolute values of gamma-ray attenuation bulk density data from cores and downhole logs generally agree (Fig. **F35**). Above 250 mbsf, however, the MST measurements are systematically less than the logging densities by 0.1 g/cm³. We noted that this depth corresponds to where coring changed from APC to XCB. Severe gas expansion in the recovered cores, particularly the APC cores, may be responsible for lower average values from the core-logging data. The trends of the $CaCO_3$ measurements of core samples (see **"Organic Geochemistry,"** p. 13) and photoelectric effect (PEF) from downhole logging are constant from 220 to 330 mbsf (Fig. **F37**). Lithostratigraphic observation reveals that pyrite in the sediments increases at the bottom of the hole (Fig. **F34**; see **"Lithostratigraphy,"** p. 6). Magnetic susceptibility from downhole logging is in excellent agreement with that from the MST whole-core measurements (Fig. **F37**).

The total magnetic field recorded by the GHMT reaches a minimum value at 210 mbsf. Above this depth, the total magnetic field may be influenced by the proximity to the bottom of the drill pipe (Fig. **F35**). Further analysis and interpretation of the total magnetic field awaits shore-based investigation. Natural gamma-ray data from core and downhole logging agree well in their pattern in the entire section (Fig. **F35**) but are offset in value. Above 230 mbsf, where coring changed from APC to XCB, the MST measurements are systematically lower than the logging values. This again may be explained by the gas expansion in the cores. Porosity calculated from downhole bulk density and that calculated from the moisture content of core samples agree well between 100 and 240 mbsf (Fig. **F35**). Between 240 and 380 mbsf, the log density porosity shows much greater amplitude in its variability. We noted that this depth interval corresponds to a rugose section of the hole as shown by the caliper on the triple combo tool string (Fig. **F34**). The FMS records reveal frequent alternation of relatively conductive (dark) and resistive (light) sediment layers in the entire log (Fig. **F38**). The implications of these fine-scale variations are yet to be explored.

F36. Downhole logs of HSGR, HCGR, potassium, thorium, and uranium, **p. 71.**

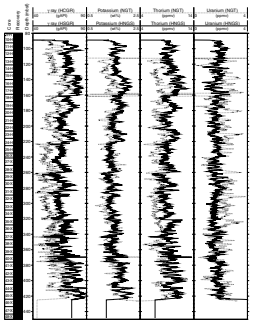

F37. MS from MST measurements of core logs vs. downhole measurements of thorium, **p. 72.**

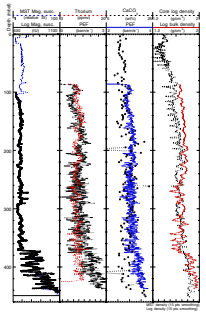

F38. FMS image from downhole logging data, **p. 73.**

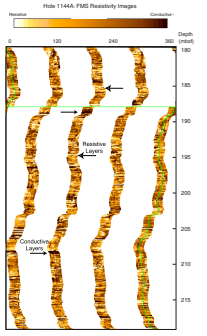

REFERENCES

Berner, R.A., 1984. Sedimentary pyrite formation: an update. *Geochim. Cosmochim. Acta,* 48:605–615.

Blow, W.H., 1969. Late middle Eocene to Recent planktonic foraminiferal biostratigraphy. *In* Brönnimann, P., and Renz, H.H. (Eds.), *Proc. First Int. Conf. Planktonic Microfossils, Geneva, 1967:* Leiden (E.J. Brill), 1:199–422.

Emerson, S., and Hedges, J.I., 1988. Processes controlling the organic carbon content of open ocean sediments. *Paleoceanography,* 3:621–634.

Gieskes, J.M., 1983. The chemistry of interstitial waters of deep-sea sediments: interpretation of deep-sea drilling data. *In* Riley, J.P., and Chester, R. (Eds.), *Chemical Oceanography* (Vol. 8): London (Academic), 221–269.

Guyodo, Y., and Valet, J.-P., 1996. Relative variations in geomagnetic intensity from sedimentary records: the past 200,000 years. *Earth. Planet. Sci. Lett.,* 143:23–36.

Harris, P.G., Zhao, M., Rosell-Melé, A., Tiedemann, R., Sarnthein, M., and Maxwell, J.R., 1996. Chlorine accumulation rate as a proxy for Quaternary marine primary productivity. *Nature,* 383:63–65.

Kvenvolden, K.A., and Kastner, M., 1990. Gas hydrates of the Peruvian outer continental margin. *In* Suess, E., von Huene, R., et al., *Proc. ODP, Sci. Results,* 112: College Station, TX (Ocean Drilling Program), 517–526.

Le, J., and Shackleton, N.J., 1992. Carbonate dissolution fluctuations in the western equatorial Pacific during the late Quaternary. *Paleoceanography,* 7:21–42.

Lehman, B., Laj, C., Kissel, C., Mazaud, A., Paterne, M, and Labeyrie, L., 1996. Relative changes of the geomagnetic field intensity during the last 280 kyr from piston cores in the Azores area. *Phys. Earth Planet. Sci.,* 93:269–284.

Li, B., 1997. Paleoceanography of the Nansha Area, southern South China Sea since the last 700,000 years [Ph.D. dissert.]. Nanjing Inst. Geol. Paleontol., Academica Sinica, Nanjing, China. (in Chinese, with English abstract)

Martini, E., and Locker, S., 1990. Clusters of sponge spicules from Quaternary sediments at Sites 685 and 688 off Peru. *In* Suess, E., von Huene, R., et al., *Proc. ODP, Sci. Results,* 112: College Station, TX (Ocean Drilling Program), 175–180.

Pelejero, C., Grimalt, J.O., Sarnthein, M., Wang, L., and Flores, J.-A., 1999. Molecular biomarker record of sea surface temperature and climatic change in the South China Sea during the last 140,000 years. *Mar. Geol.,* 156:109–121.

Peters, K.E., 1986. Guidelines for evaluating petroleum source rock using programmed pyrolysis. *AAPG Bull.,* 70:318–329.

Pflaumann, U., and Jian, Z., 1999. Modern distribution patterns of planktonic foraminifera in the South China Sea and western Pacific: a new transfer technique to estimate regional sea-surface temperatures. *Mar. Geol.,* 156:41–83.

Prell, W.L., 1984. Variation of monsoonal upwelling: a response to changing solar radiation. *In* Hansen, J.E., and Takahashi, T. (Eds.), *Climatic Processes and Climate Sensitivity.* Geophys. Monogr., Am. Geophys. Union, Maurice Ewing Ser., 29:48–57.

Sarnthein, M., Pflaumann, U., Wang, P.X., and Wong, H.K. (Eds.), 1994. Preliminary Report on Sonne-95 Cruise "Monitor Monsoon" to the South China Sea. *Rep. Geol.-Paläontol. Inst. Univ. Kiel.,* 68.

Schönfeld, J., 1996. The "*Stilostomella* Extinction": structure and dynamics of the last turnover in deep-sea benthic foraminiferal assemblages. *In* Mogurlevsky, A., and Whatly, R. (Eds.), *Microfossils and Oceanic Environments:* Aberystwyth (Univ. Wales, Aberystwyth Press), 27–37.

Shipboard Scientific Party, 1996. Site 994. *In* Paull, C.K., Matsumoto, R., Wallace, P.J., et al., *Proc. ODP, Init. Repts.,* 164: College Station, TX (Ocean Drilling Program), 99–174.

Sirocko, F., Sarnthein, M., Erlenkeuser, H., Lange, H., Arnold, M., and Duplessy, J.C., 1993. Century-scale events in monsoonal climate over the past 24,000 years. *Nature,* 364:322–324.

Stein, R., Brass, G., Graham, D., Pimmel, A., and the Shipboard Scientific Party, 1995. Hydrocarbon measurements at Arctic Gateways sites (ODP Leg 151). *In* Myhre, A.M., Thiede, J., Firth, J.V., et al., *Proc. ODP, Init. Repts.,* 151: College Station, TX (Ocean Drilling Program), 385–395.

Su, X., 1996. Development of Late Tertiary and Quaternary coccolith assemblages in the Northeast Atlantic. *GEOMAR Rep.,* 48.

Sun, X., 1996. Environmental changes of the northern South China Sea since the last 30 k.y. based on pollen data of deep sea Core 17940-2. *IGC-30,* 2:254. (Abstract)

Sun, X., and Li, X., 1999. A pollen record of the last 37 ka in deep sea core 17940 from the northern slope of the South China Sea. *Mar. Geol.,* 156:227–242.

Thompson, P.R., Bé, A.W.H., Duplessy, J.-C., and Shackleton, N.J., 1979. Disappearance of pink-pigmented *Globigerinoides ruber* at 120,000 yr BP in the Indian and Pacific oceans. *Nature,* 280:554–558.

Wang, L., Jian, Z., and Chen, J., 1997. Late Quaternary pteropods in the South China Sea: carbonate preservation and paleoenvironmental variation. *Mar. Micropaleontol.,* 32:115–126.

Wang, L., Sarnthein, M., Erlenkeuser, H., Grimalt, J., Grootes, P., Heilig, S., Ivanova, E., Kienast, M., Pelejero, C., and Pflaumann, U., 1999. East Asian monsoon climate during the late Pleistocene: high-resolution sediment records from the South China Sea. *Mar. Geol.,* 156:245–284.

Wang, P., Wang, L., Bain, Y., and Jian, Z., 1995. Late Quaternary paleoceanography of the South China Sea: surface circulation and carbonate cycles. *Mar. Geol.,* 127:145–165.

Figure F1. Magnetic susceptibility data and the splice for the three holes at Site 1144 (spliced MS data in this figure are also available in ASCII format). The order of the four arrays (the splice and Holes 1144A through 1144C) increases outward from the origin. The hole arrays are offset from each other—and from the splice—by a constant (10.0×10^{-5} SI units) so that only the splice is plotted relative to the absolute MS value. Lines identify the splice tie points. Note the y-axis scale change at 400 mcd. (Continued on next two pages.)

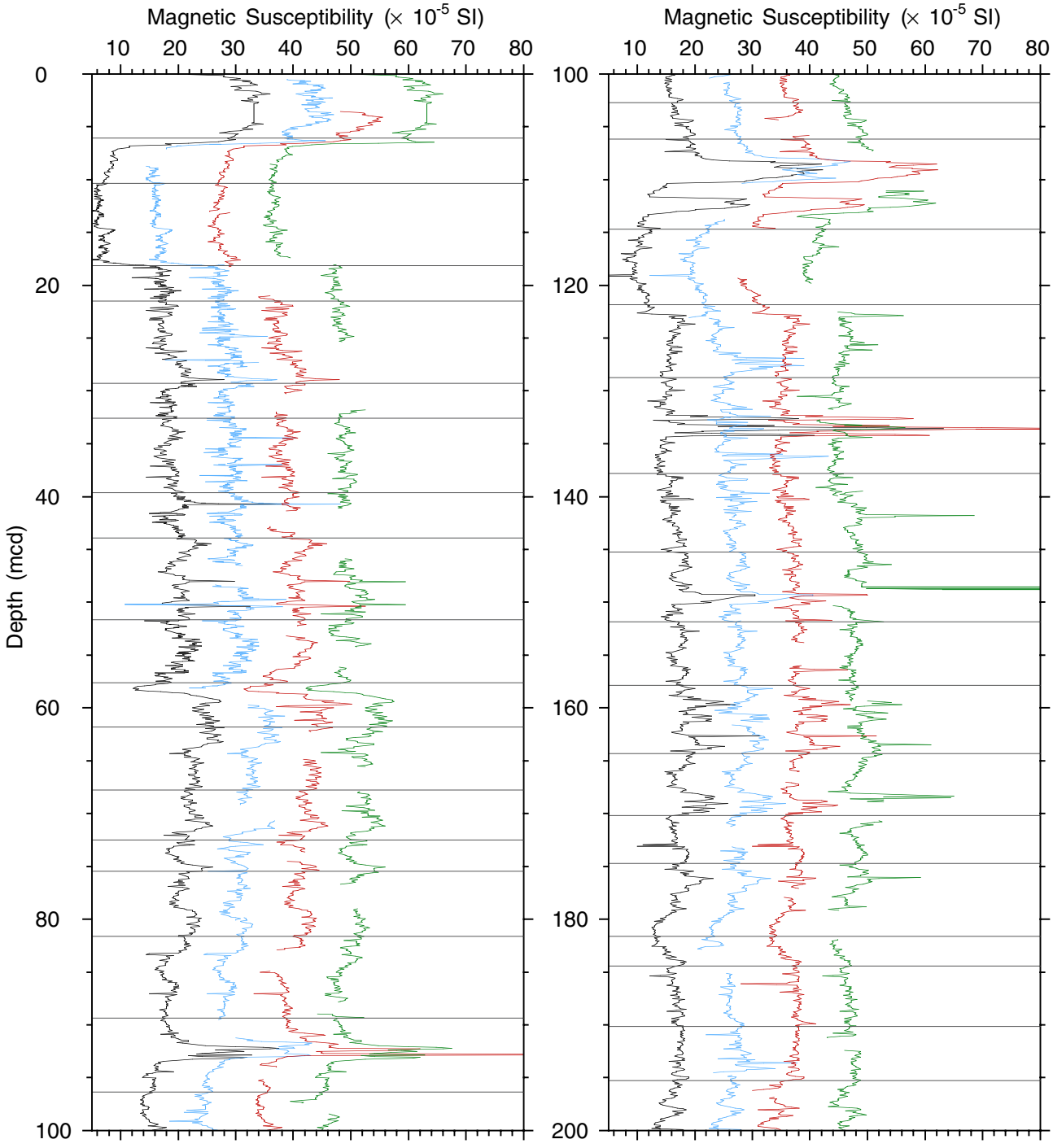

Figure F1 (continued).

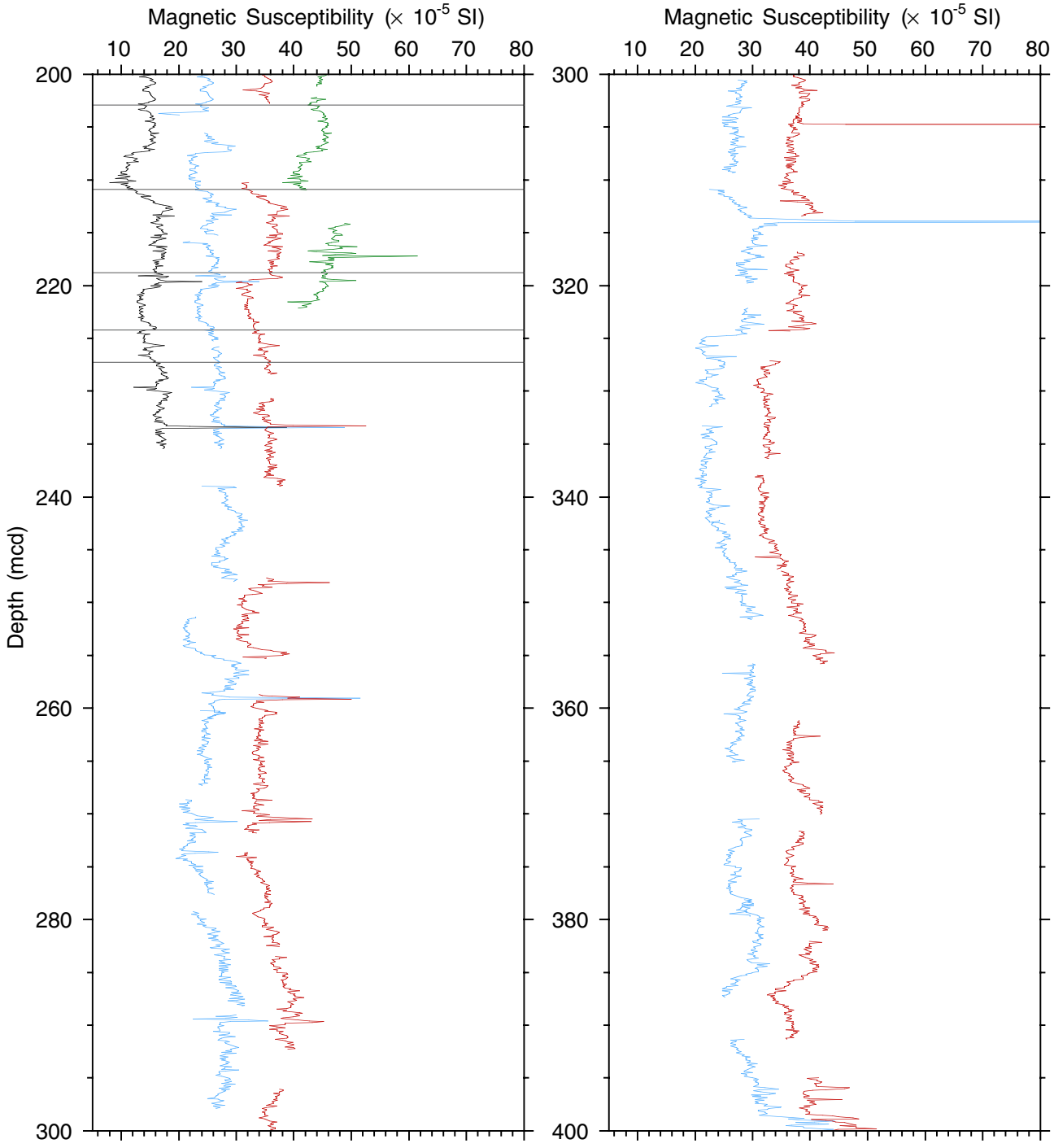

Figure F1 (continued).

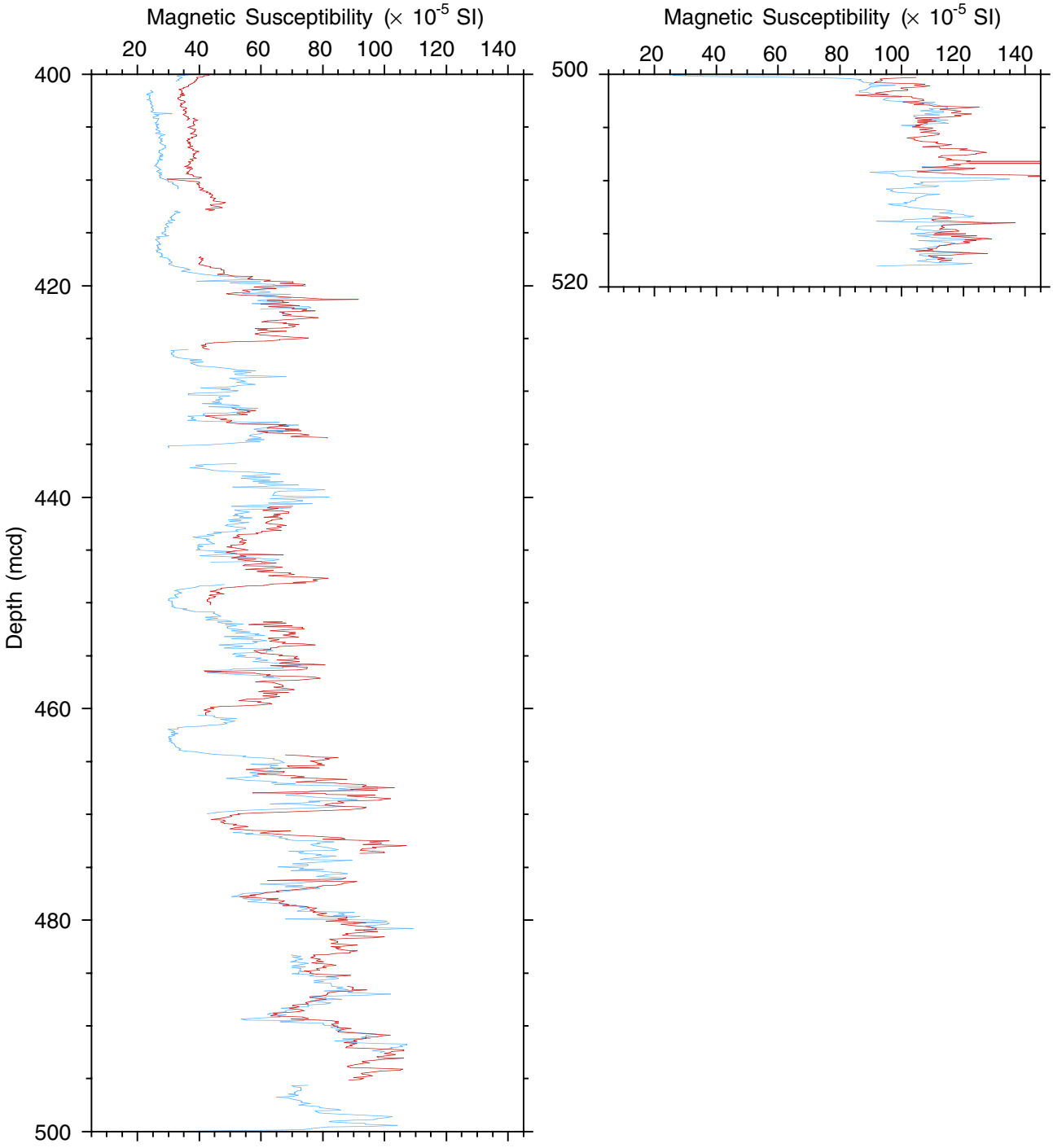

Figure F2. Smoothed (11-point running average)/correlated NGR data and the splice for the three holes at Site 1144 (spliced NGR data in this figure are also available in **ASCII format**). The order of the four arrays (the splice and Holes 1144A through 1144C) increases outward from the origin. The hole arrays are offset from each other—and from the splice—by a constant (9 cps) so that only the splice is plotted relative to the absolute NGR value. Data from the top and bottom 7 cm of the first and last section of each core have been culled. Lines identify the splice tie points. Artificial NGR values of 20 cps were assigned to intervals in Hole 1144B that are part of the splice where NGR data were not collected because of sensor failure. (Continued on next two pages.)

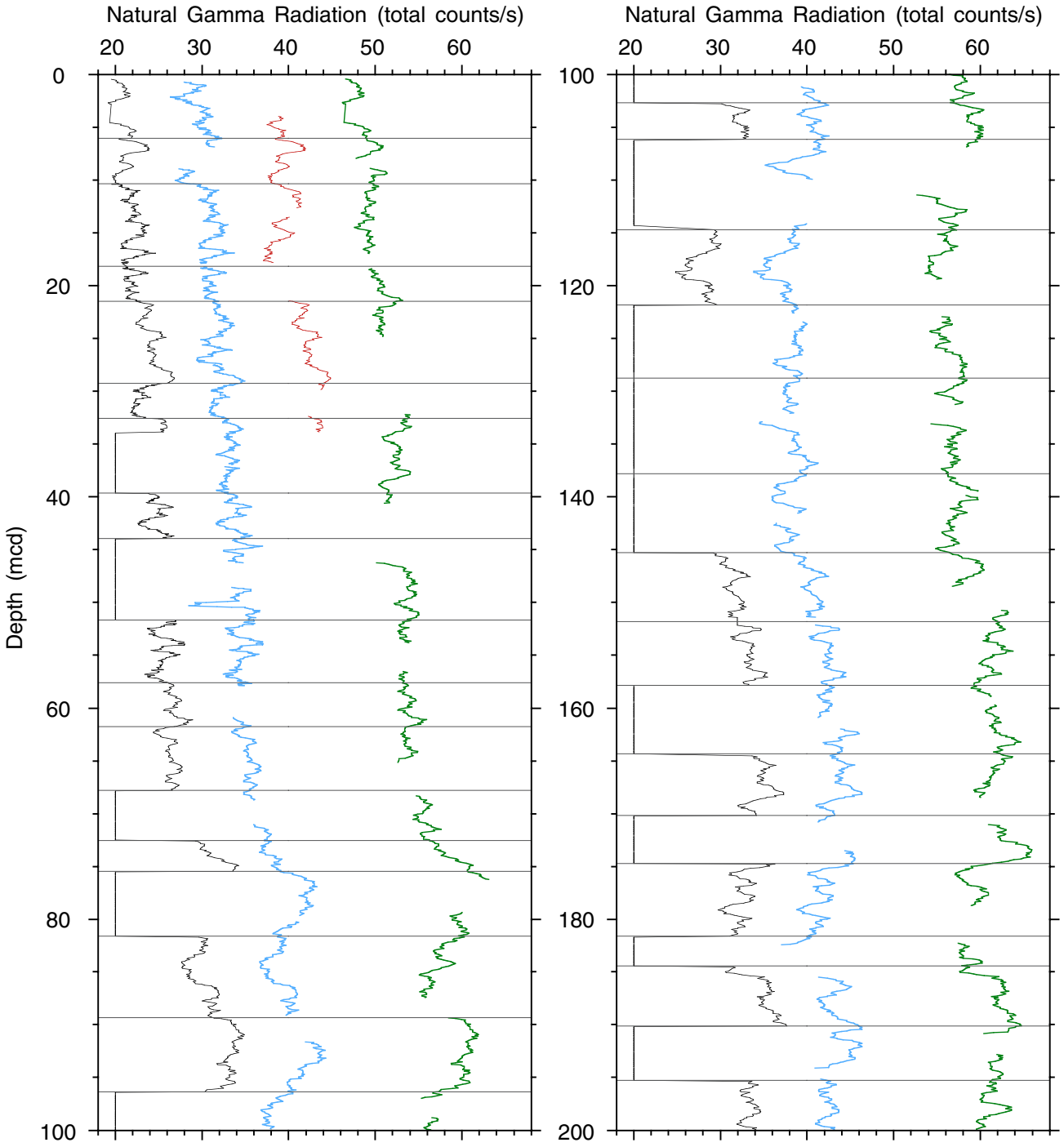

Figure F2 (continued).

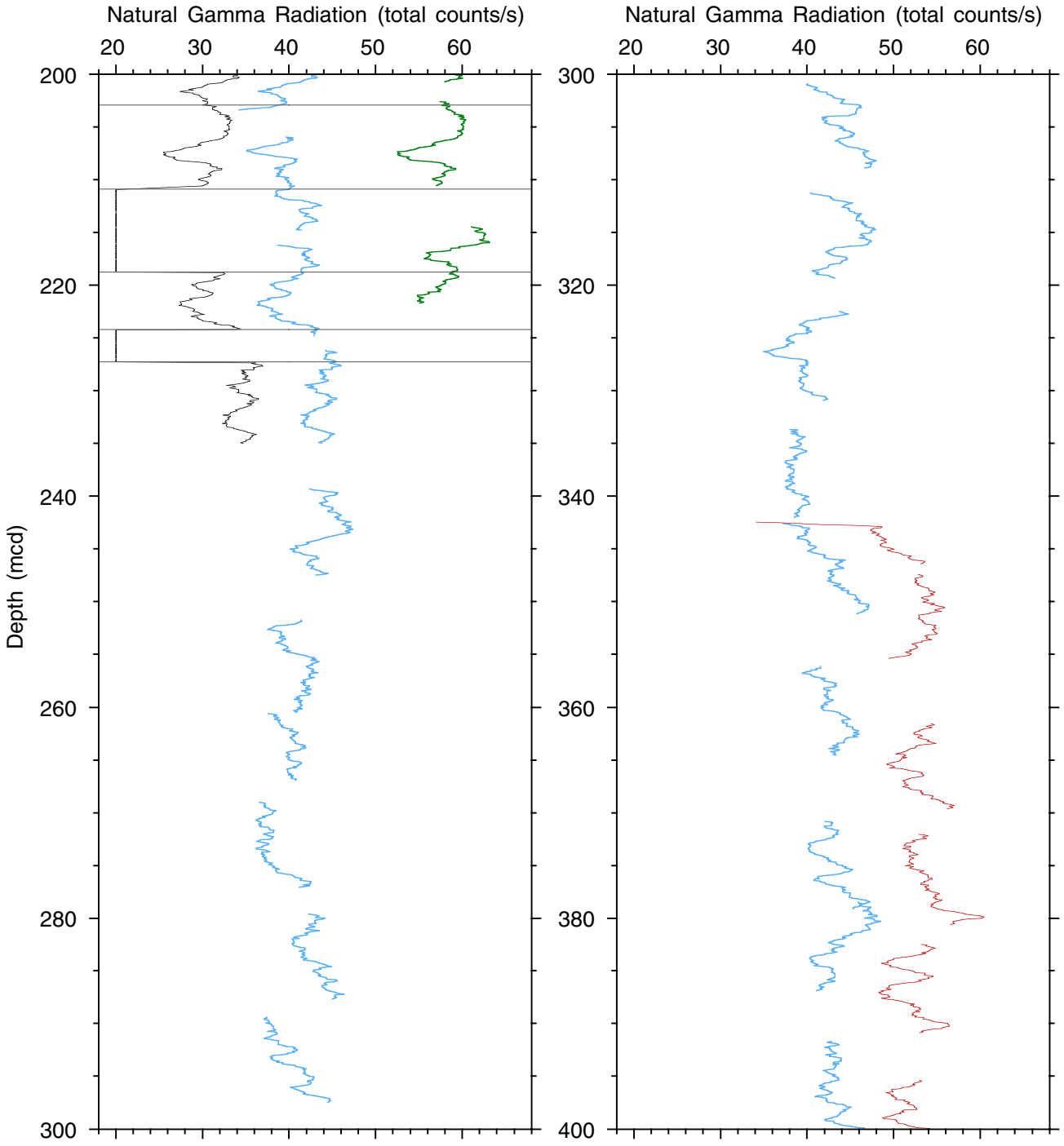

Figure F2 (continued).

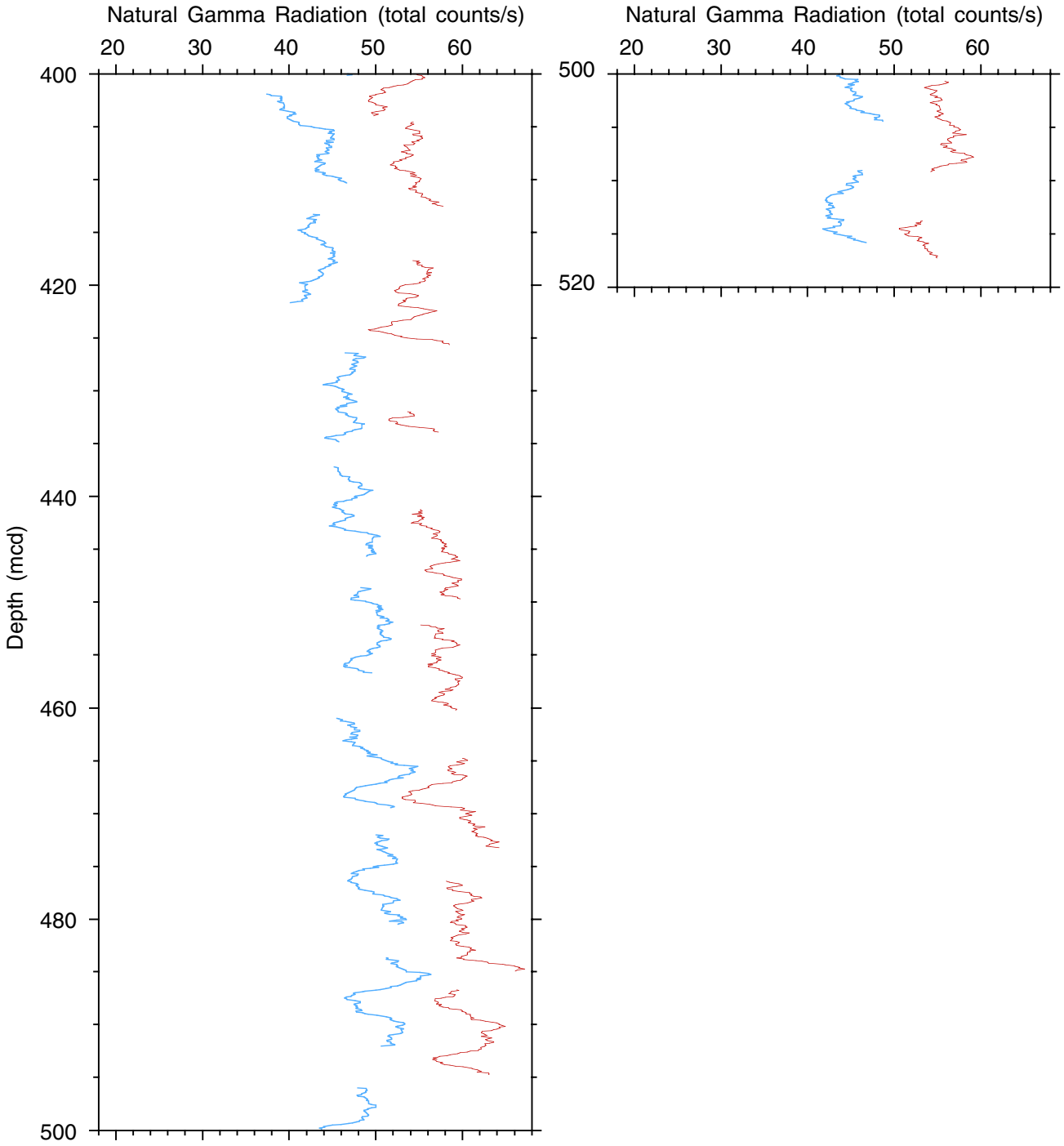

Figure F3. Gamma-ray attenuation data (GRA bulk density) and the splice for the three holes at Site 1144 (spliced GRA data in this figure are also available in **ASCII format**). The order of the four arrays (the splice and Holes 1144A through 1144C) increases outward from the origin. The hole arrays are offset from each other—and from the splice—by a constant (0.15 g/cm³) so that only the splice is plotted relative to the absolute GRA value. Values ≤1.03 and ≥2.4 (g/cm³) have been culled. Lines identify the splice tie points. (Continued on next two pages.)

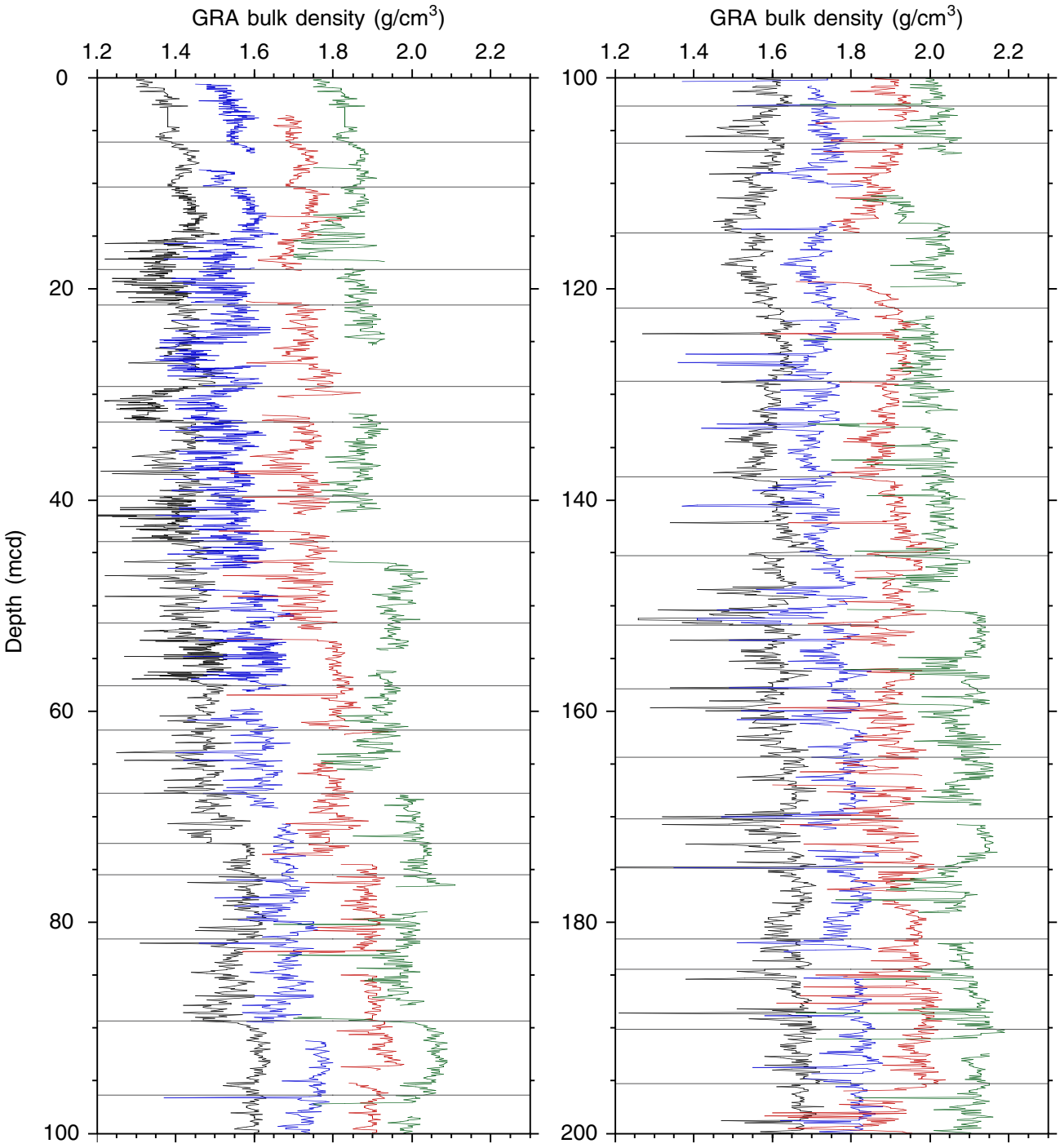

Figure F3 (continued).

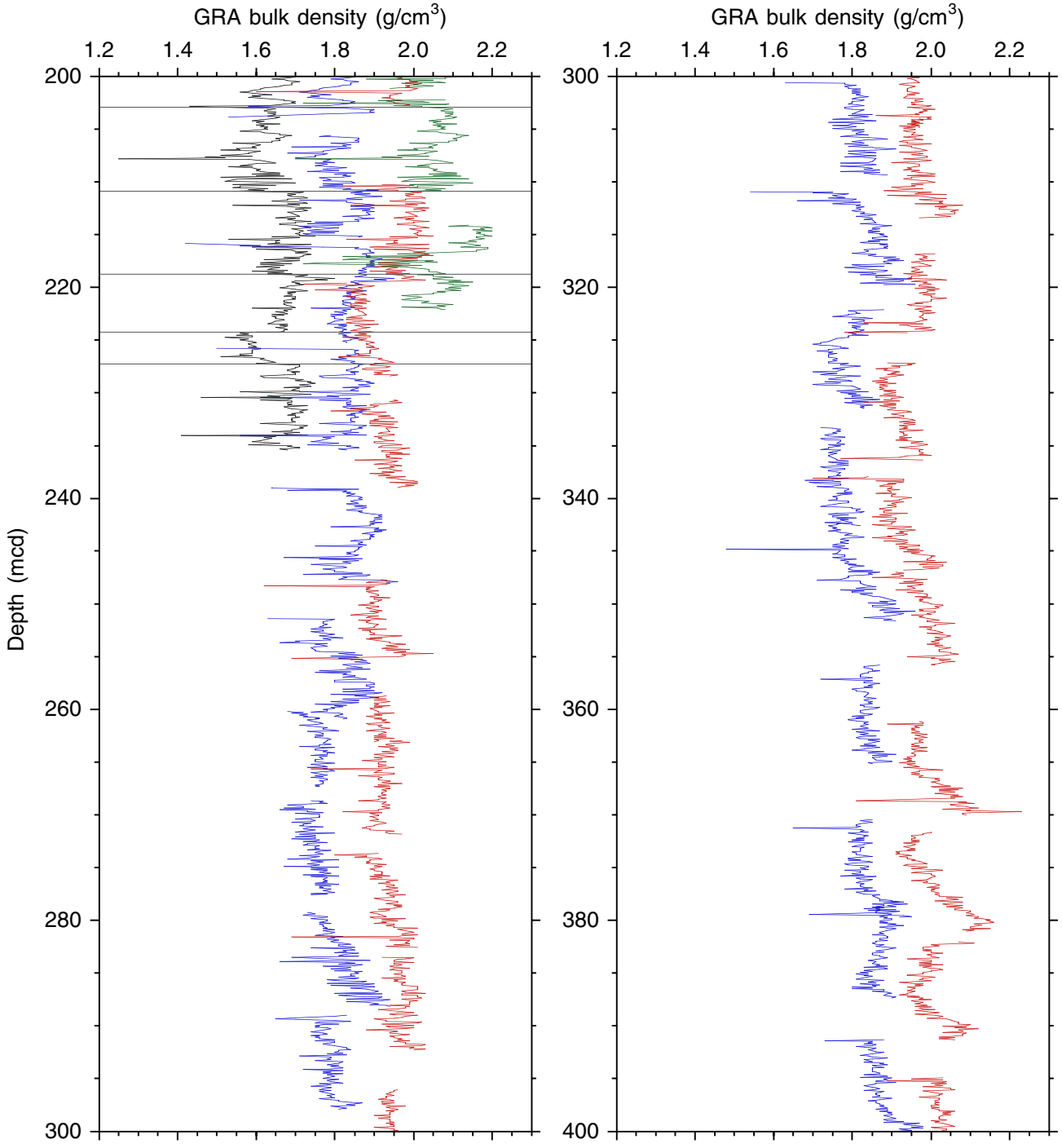

Figure F3 (continued).

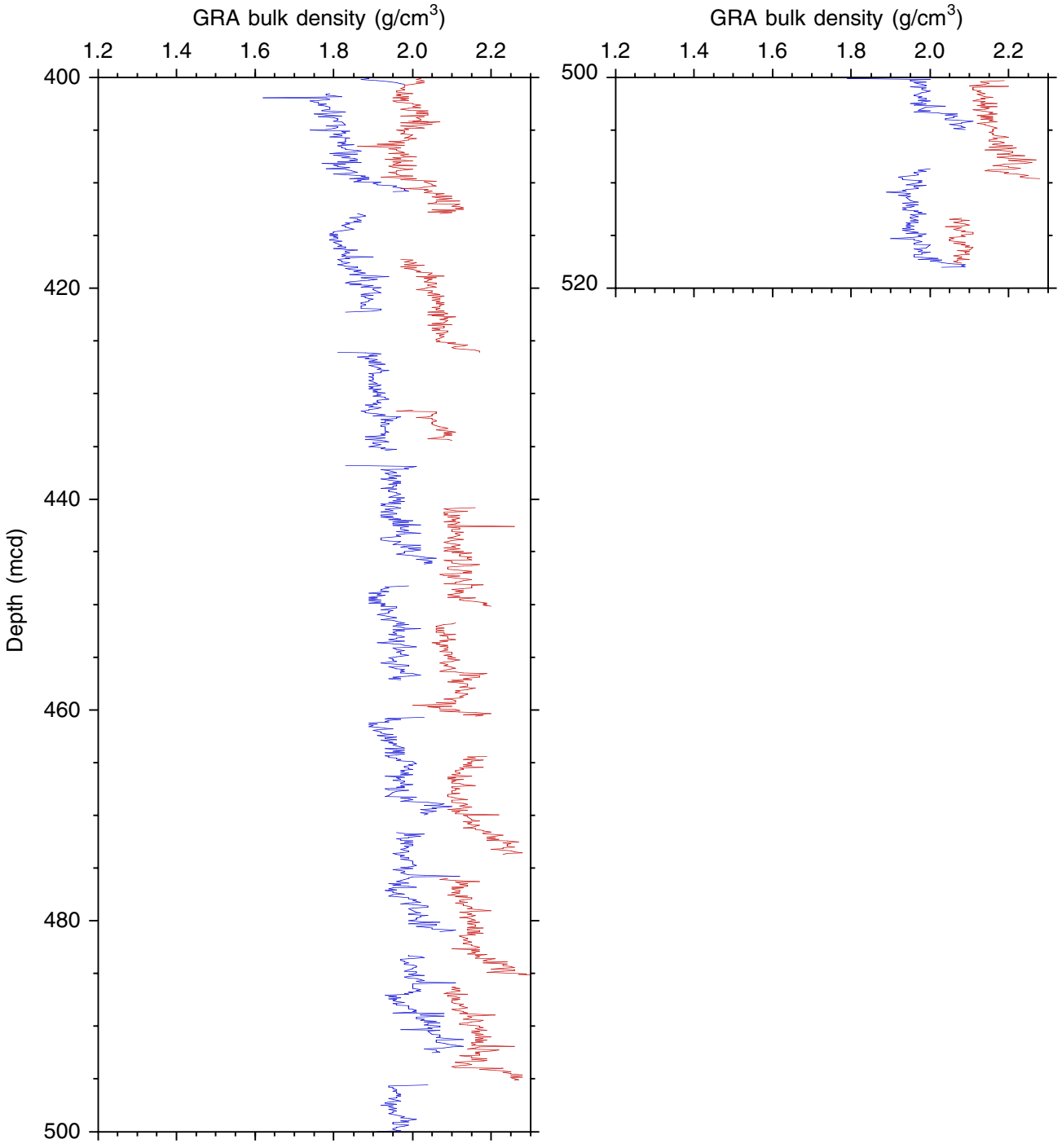

Figure F4. Smoothed (11-point running average)/correlated L* ("lightness") values from the CSR data and the splice for the three holes at Site 1144 (spliced CSR data in this figure are also available in **ASCII format**). The order of the four arrays (the splice and Holes 1144A through 1144C) increases outward from the origin. The hole arrays are offset from each other—and from the splice—by a constant (8%) so that only the splice is plotted relative to the absolute L* value. Values ≤1% have been culled. Lines identify the splice tie points. (Continued on next two pages.)

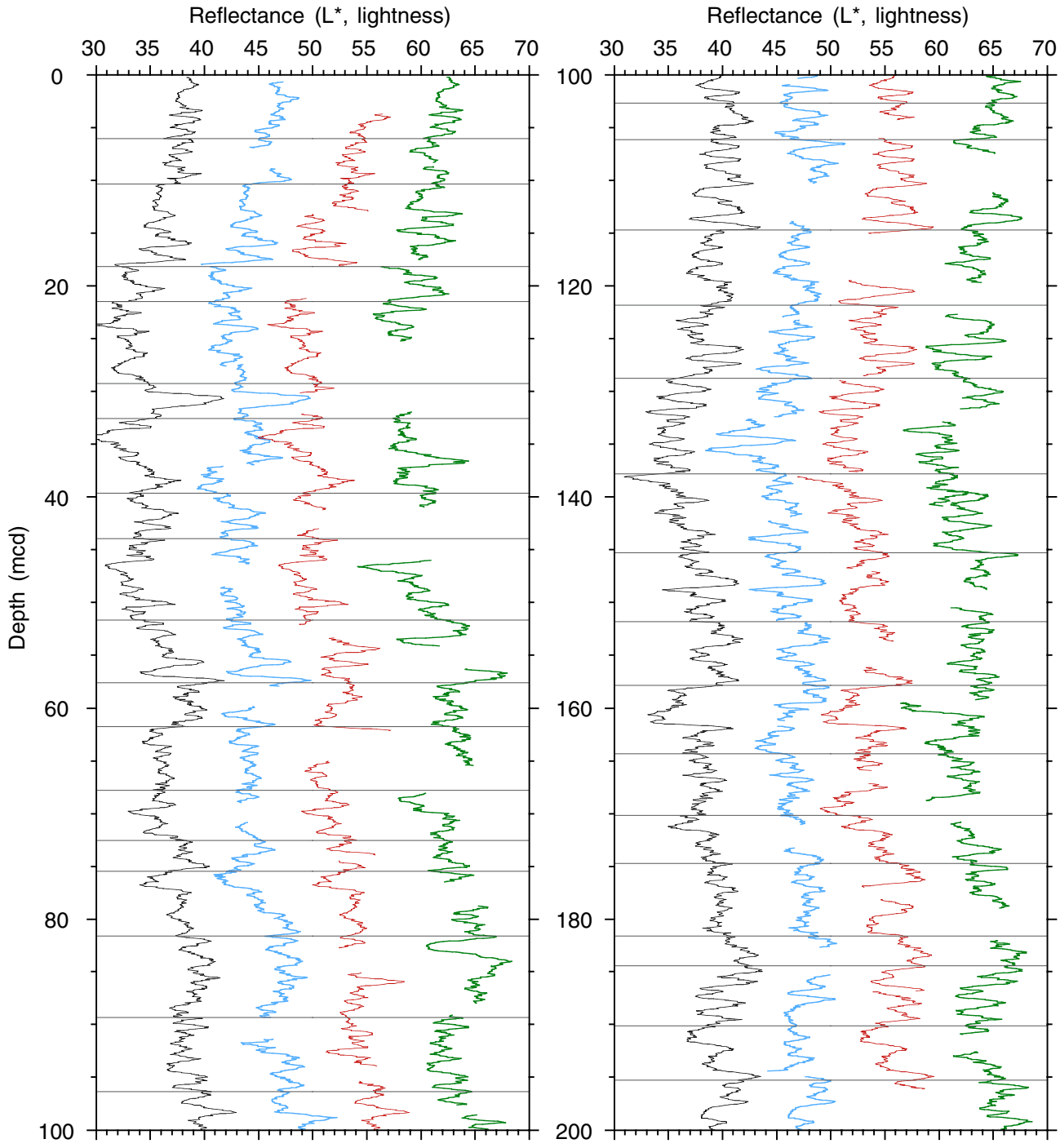

Figure F4 (continued).

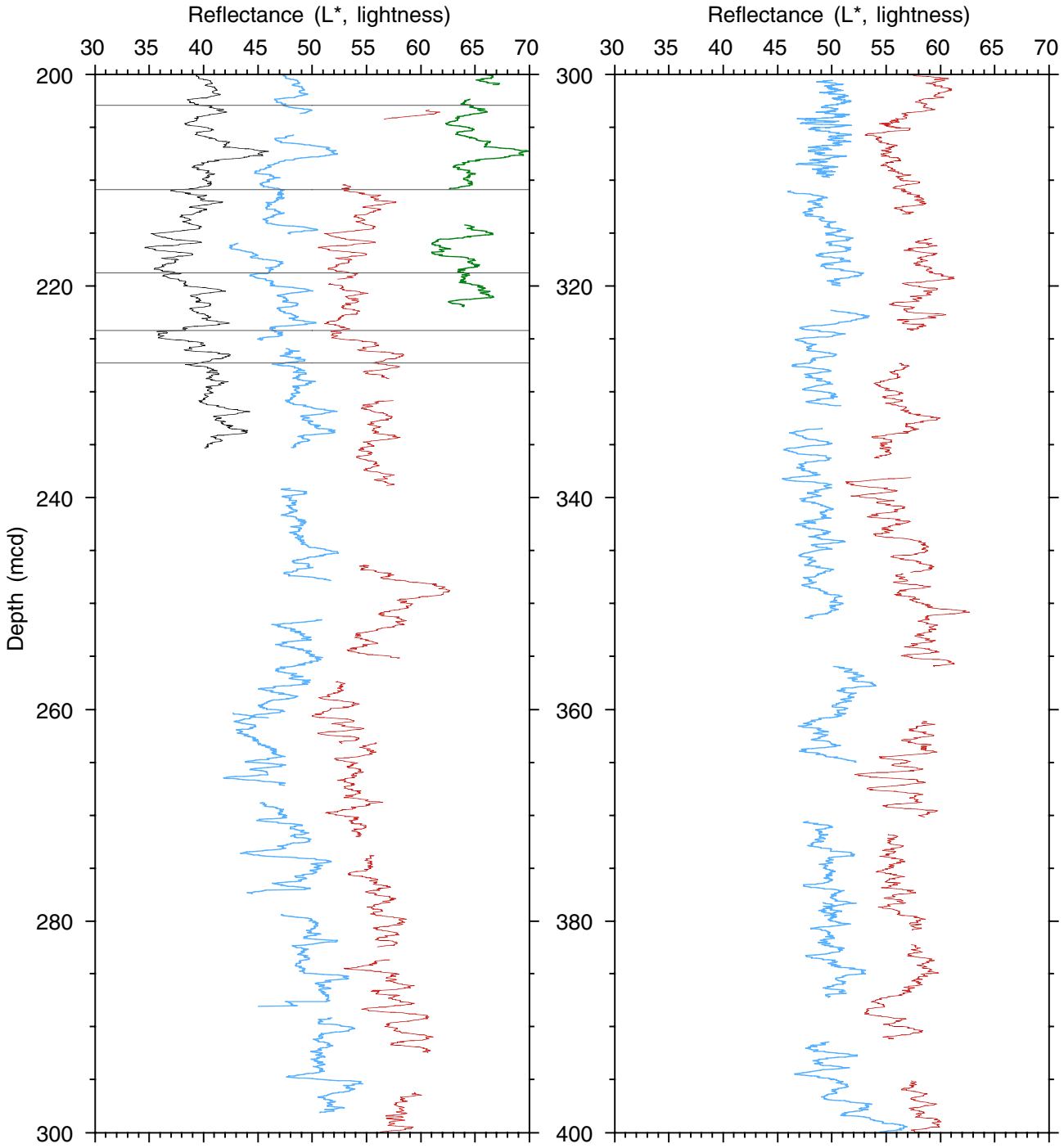

Figure F4 (continued).

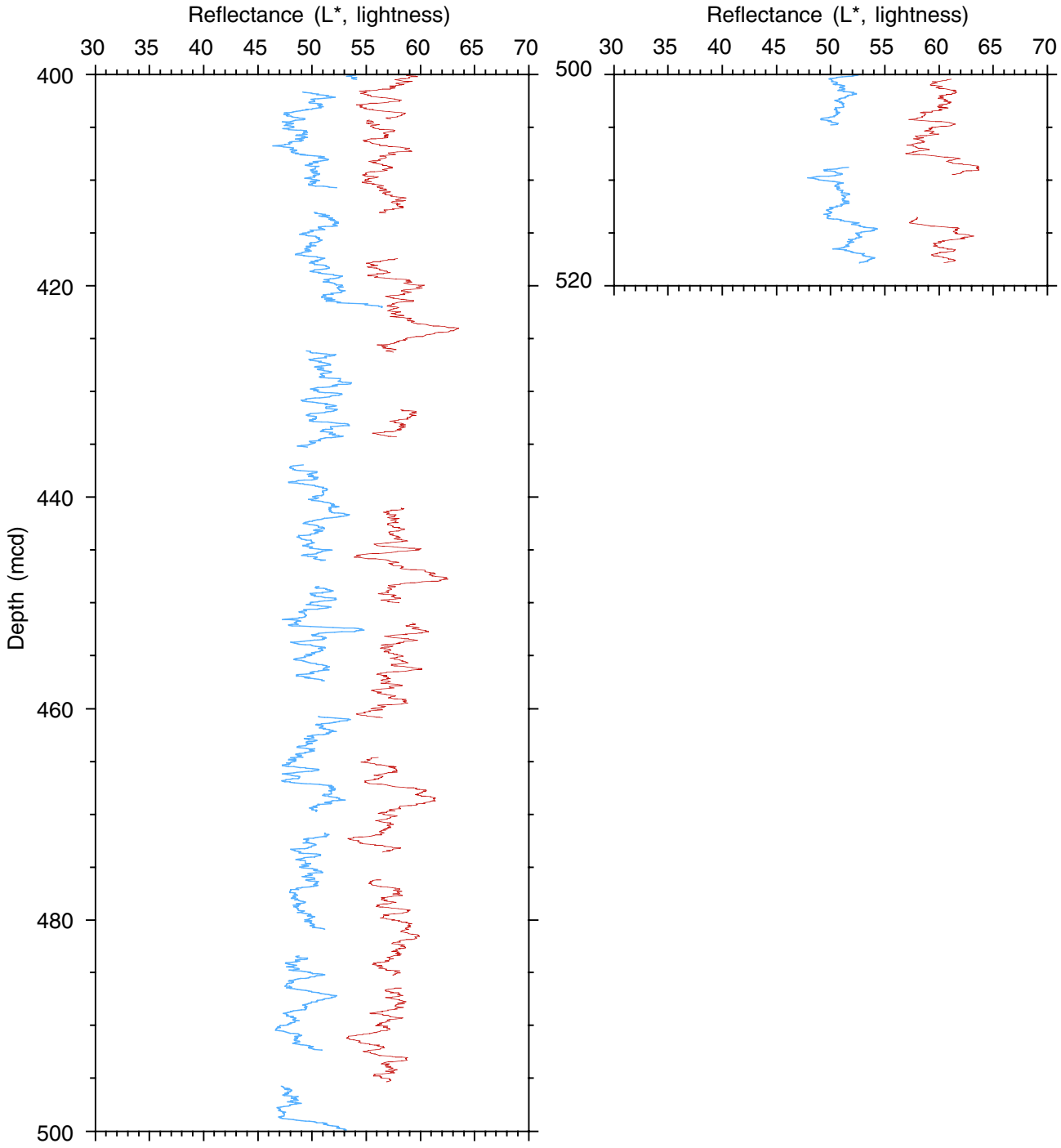

Figure F5. Recovery and lithology of Site 1144.

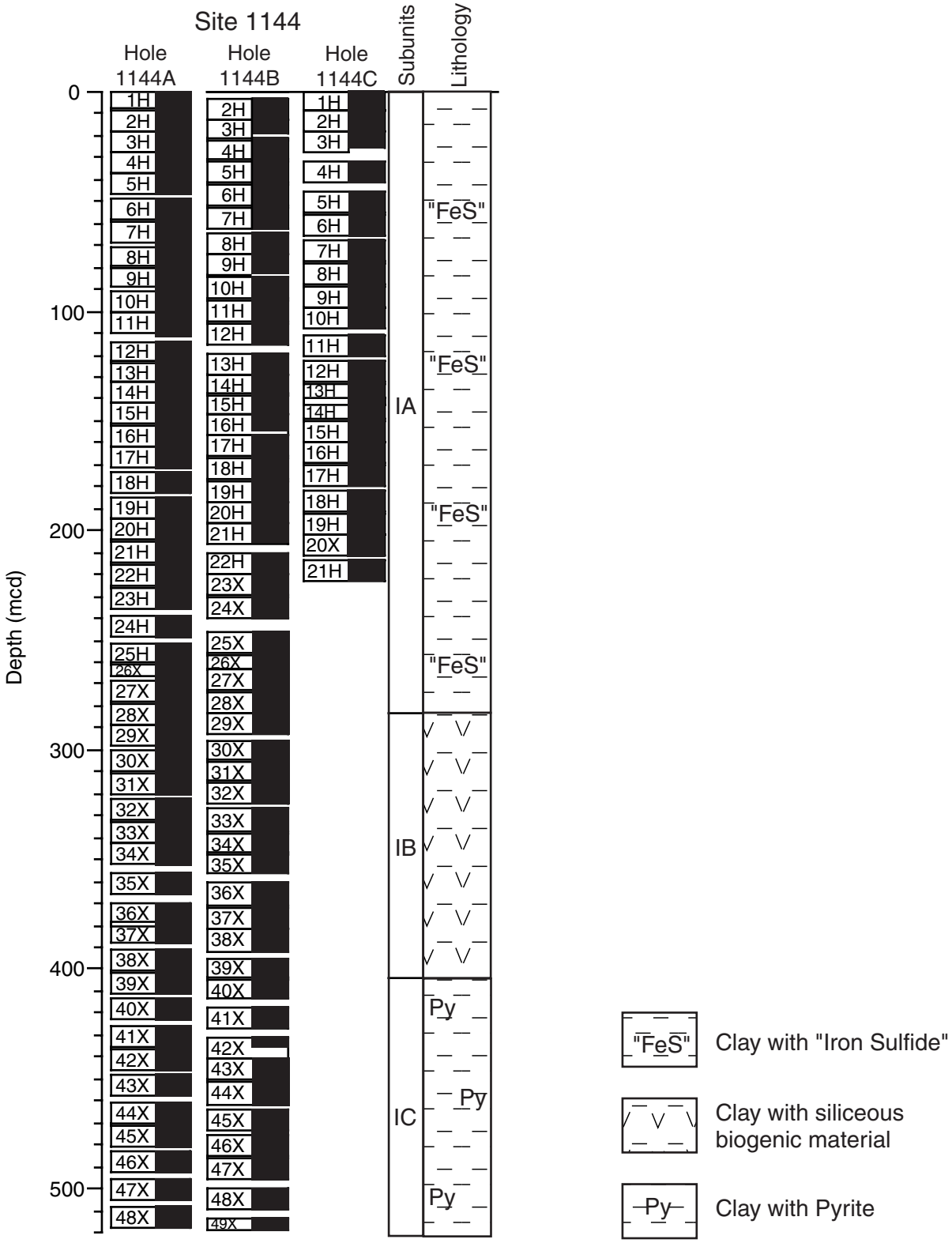

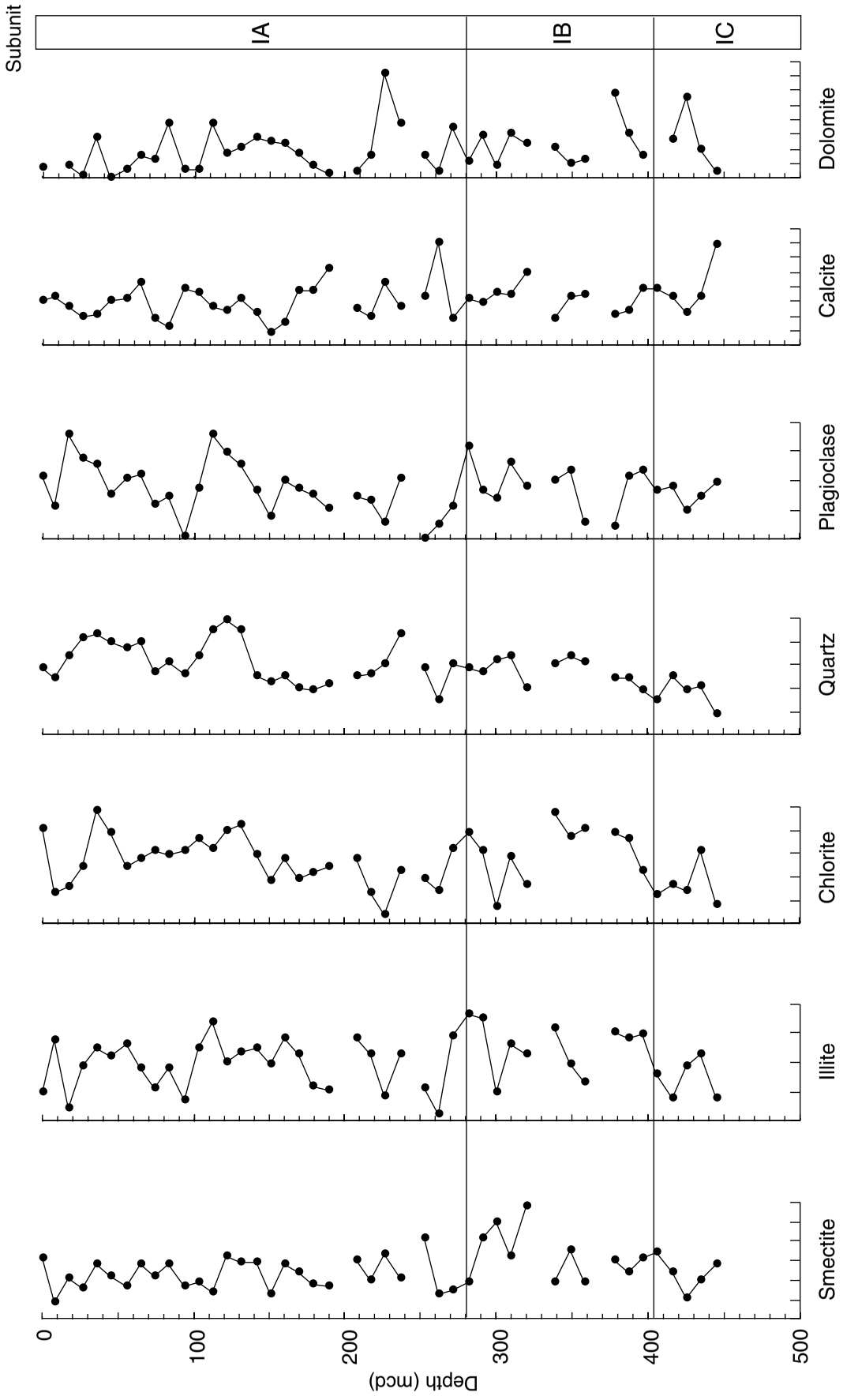

Figure F6. Bulk mineralogy (peak area) for the major mineral phases determined by XRD analysis in Hole 1144A. The peak areas only reflect variations in the relative abundance of each mineral downcore; comparisons of concentration between mineral phases are not possible.

Figure F7. A. Abundance of dispersed "iron sulfide" and macrocrystalline pyrite. Arbitrary units based on core description with the values being averaged over five sections (see **"Core Descriptions"** contents list). **B.** Downhole variation in the content of nannofossils. **C.** Total siliceous organisms (diatoms, sponge spicules, and radiolarians) estimated from smear slides. Note peak in siliceous organisms in Subunit IB and the generally high levels of nannofossils in Subunits IB and IC.

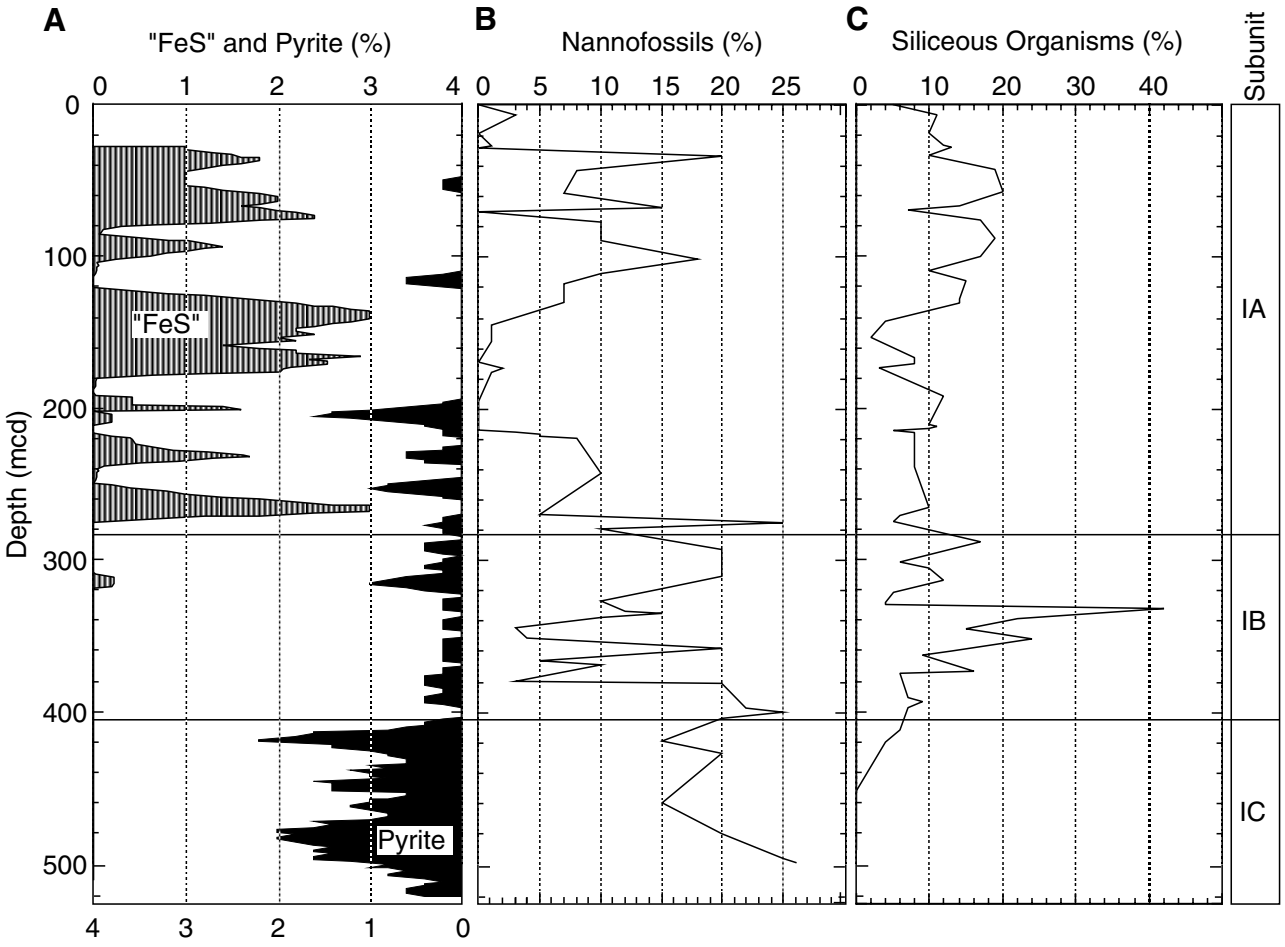

Figure F8. Identified volcanic ash layers from all holes at Site 1144 showing their thickness and depth distribution. Note the coincidence of the ash layers at two levels in Holes 1144A, 1144B, and 1144C at ~179.12 and ~396.63 mcd.

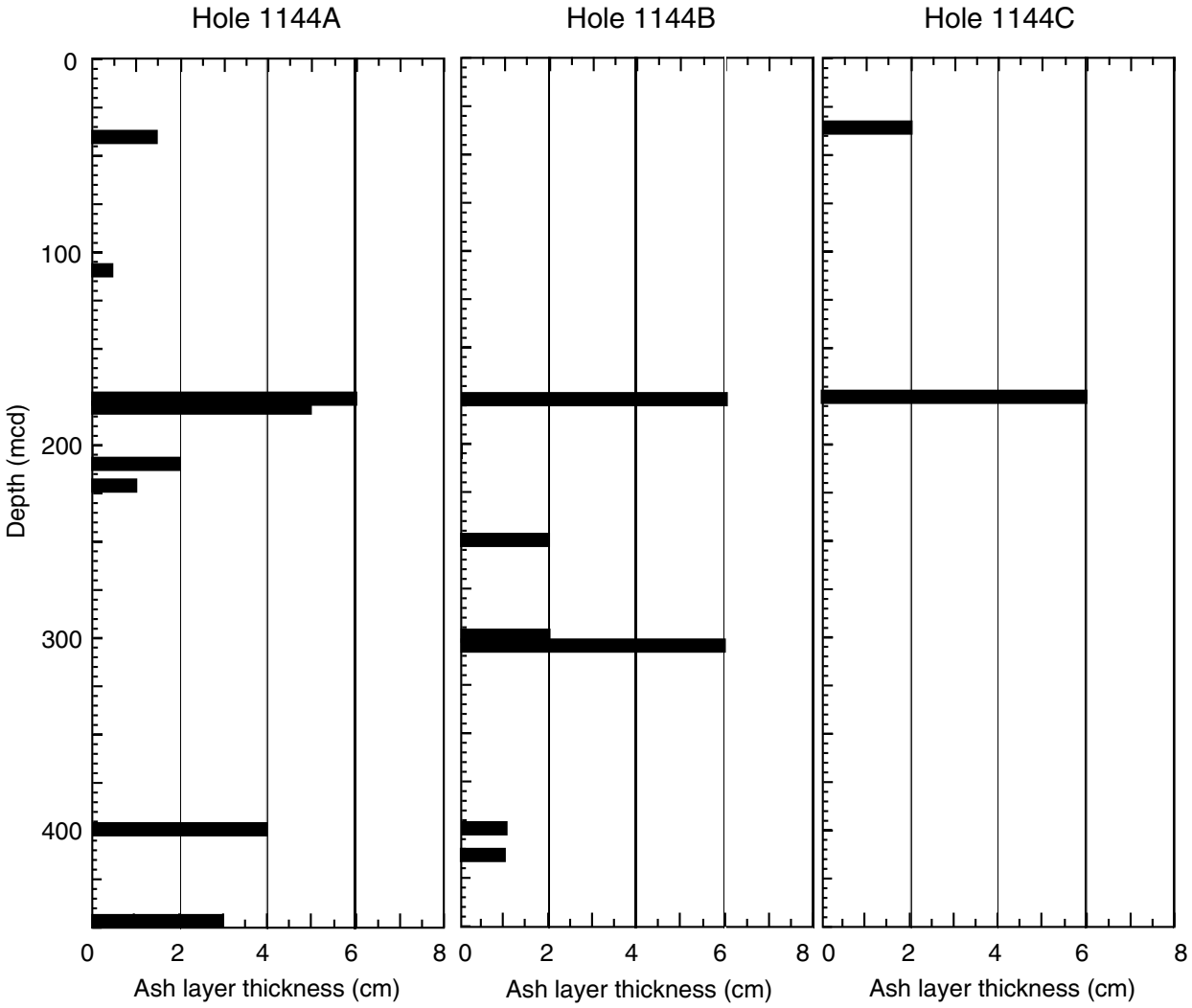

Figure F9. Site 1144 age-depth plot. All biostratigraphic events are listed in Table T6, p. 80. The average sedimentation rate is calculated based on four control points (control points are marked by * in Table T6, p. 80). LO = last occurrence, FO = first occurrence. Dotted lines mark depth intervals over which linear sedimentation rates are calculated.

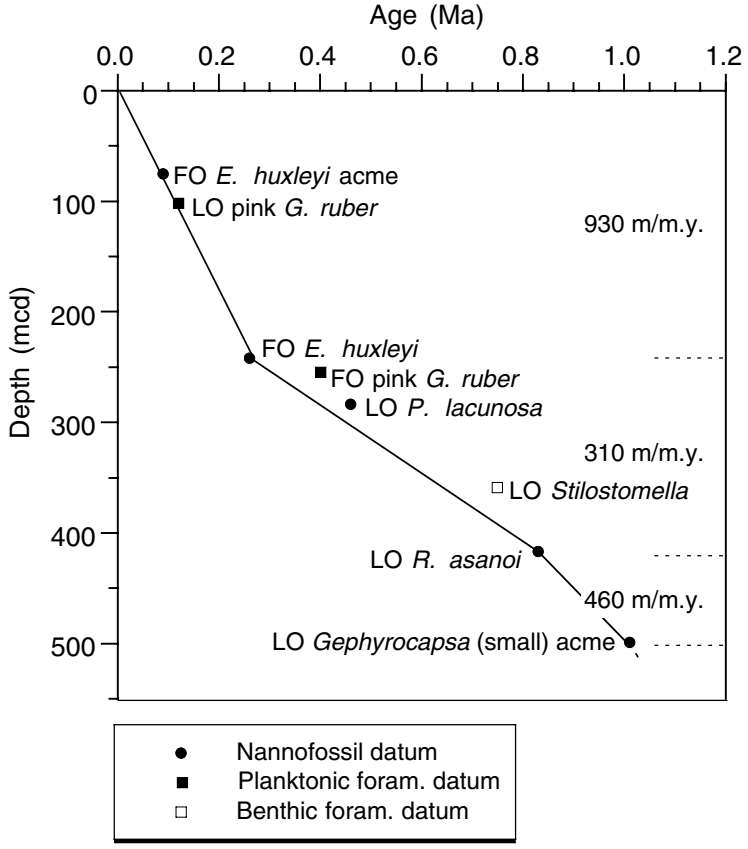

Figure F10. Variations in the relative abundance of (**A**) *Pseudoemiliania lacunosa* and (**B**) *Reticulofenestra asanoi* at Site 1144. LO = last occurrence, marked by the dotted lines.

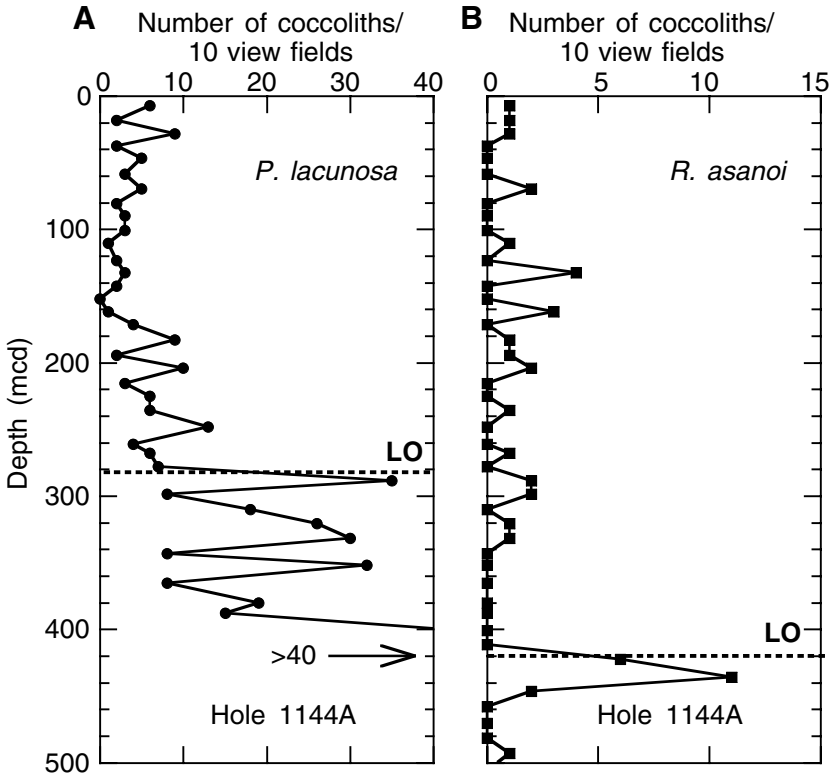

Figure F11. Downhole changes at Site 1144 in (**A**) the group abundance of siliceous microfossils (including radiolarians, diatoms, and their debris), (**B**) the proportion of benthic foraminifers (BF) related to high organic carbon flux (high productivity BF), (**C**) relative abundance of *P. obliquiloculata,* (**D**) fragmentation, (**E**) the ratio between pteropod (PT) and planktonic (PF) foraminifers, and (**F**) the ratio between *G. menardii* and *G. inflata*. Three biostratigraphic events (LO of pink *G. ruber,* FO of *E. huxleyi,* and LO of *R. asanoi*) are shown. The numbers 1, 5, 7, and 9 at the top of the diagram indicate possible marine oxygen isotopic stages. LO = last occurrence, FO = first occurrence. Dotted lines mark the biostratigraphic events of nannofossils; solid bar shows the event of foraminifers.

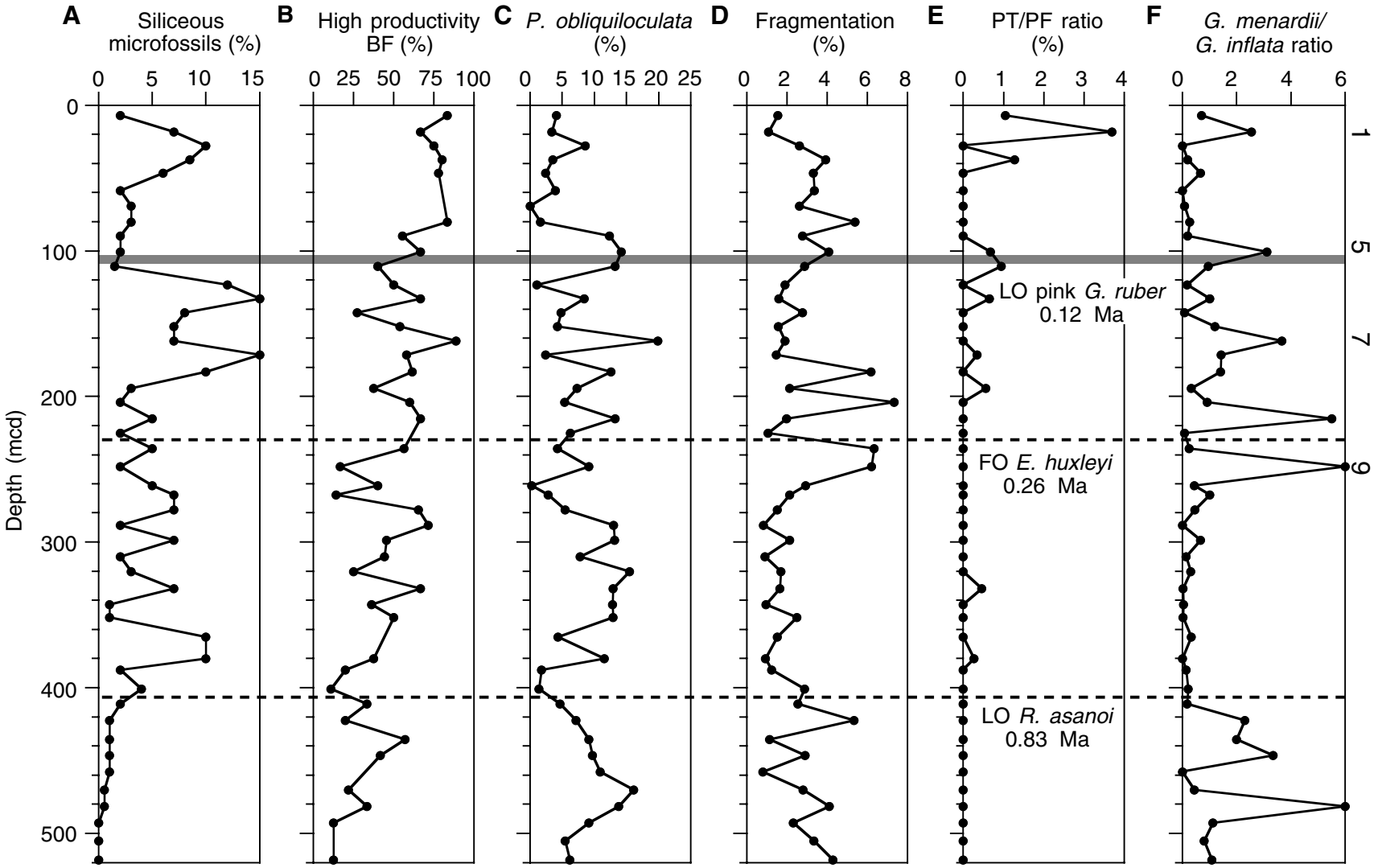

Figure F12. Intensity of magnetization and low-field magnetic susceptibility for Hole 1144A. A number of short-lived features and the increase below 430 mcd are correlated in the two records.

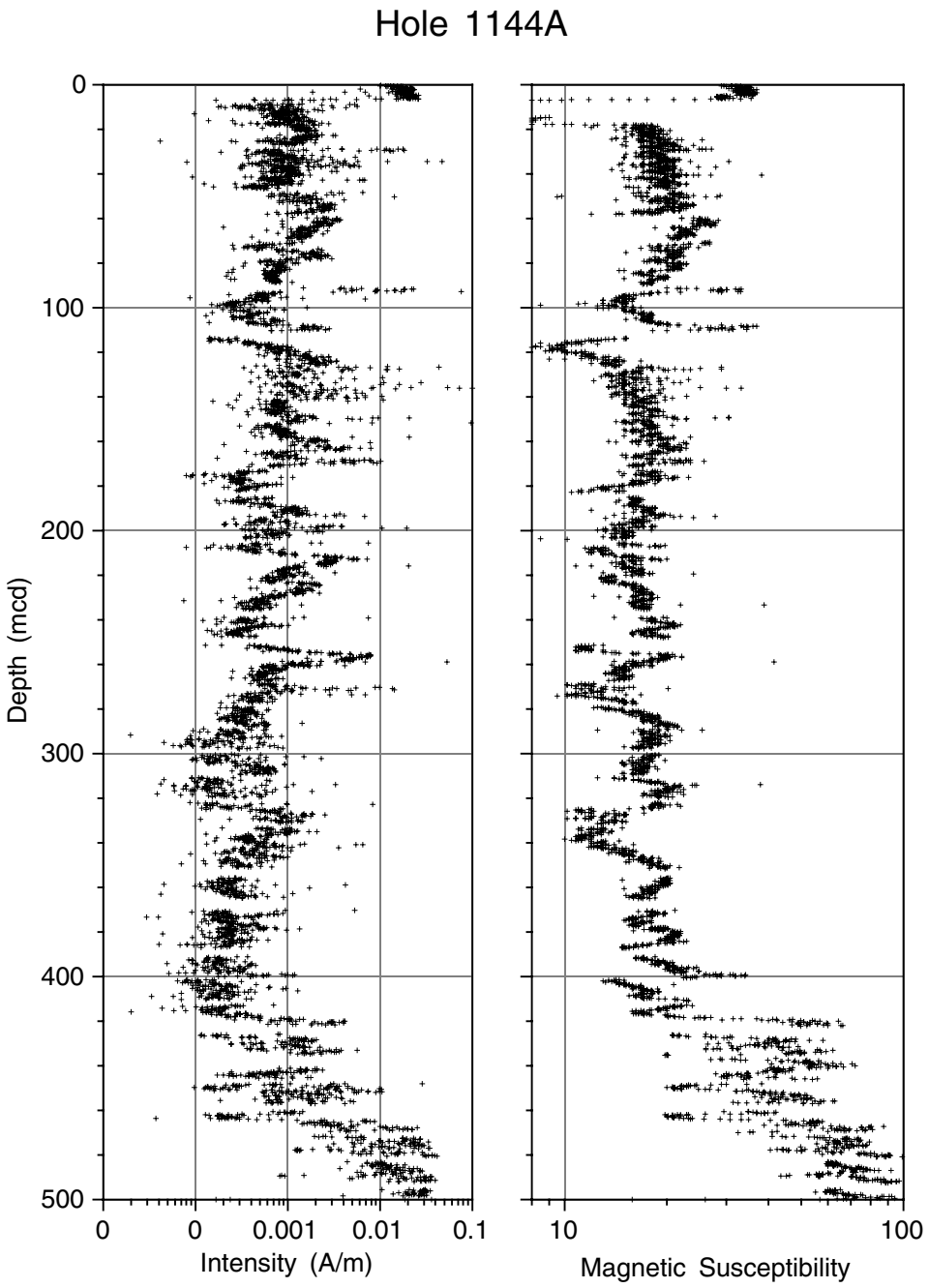

Figure F13. Declination and inclination for Hole 1144A, 0–500 mcd, obtained from long-core measurements (Cores 184-1144A-1H and 2H are not oriented). Normal polarity is observed from 0 to 261 mcd (APC cores). Below 261 mcd (XCB cores), declinations and inclinations are very scattered. A strong overprint (revealed by inclinations steeper than the expected value) makes it difficult to retrieve the primary polarity.

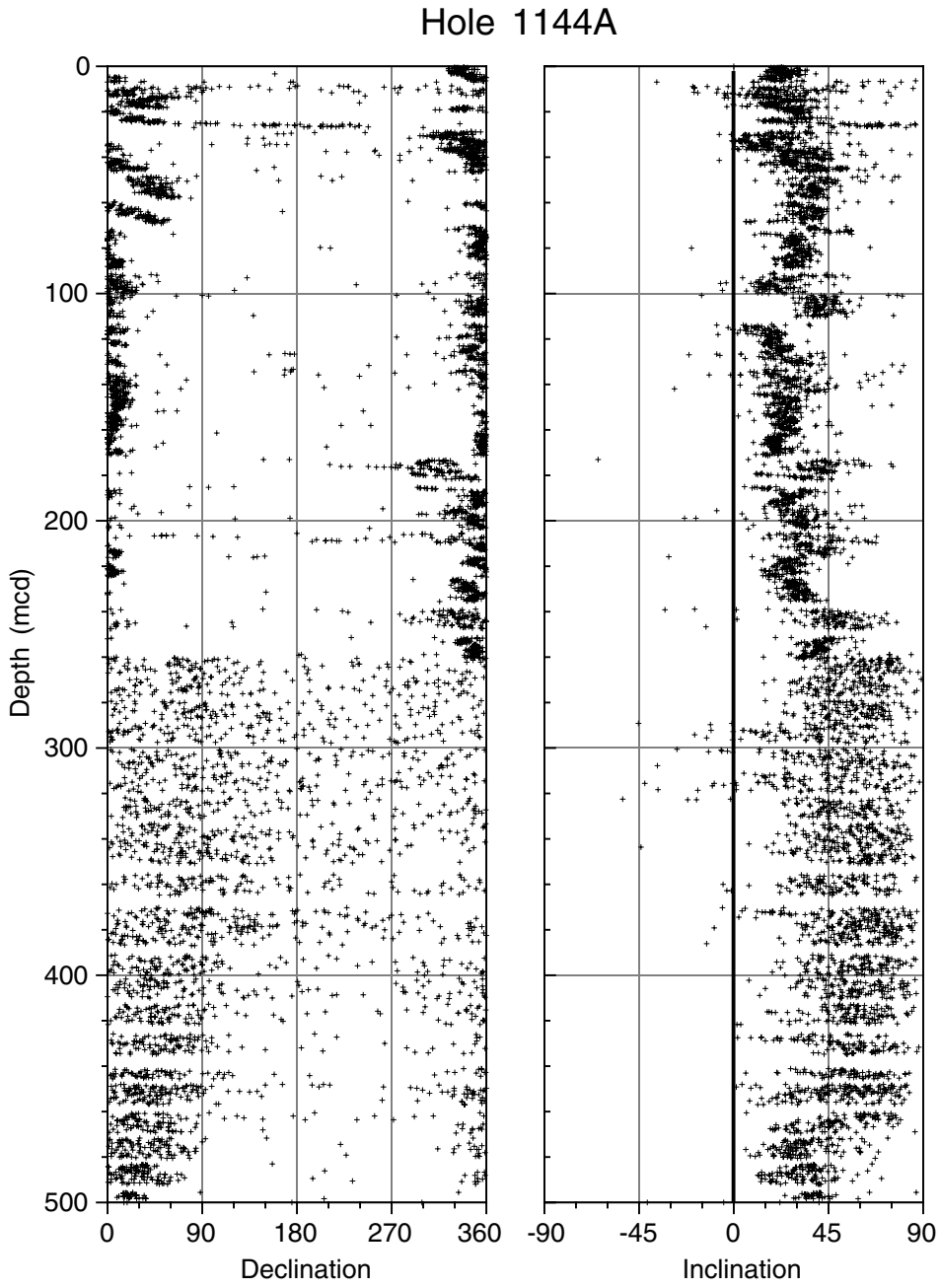

Figure F14. Enlarged view of the declination and inclination for Hole 1144A, 0–50 mcd. A swing to reverse declinations is observed between ~24 and ~25.6 mcd in Core 184-1144A-3H. This could represent a partial record of the Laschamp Event.

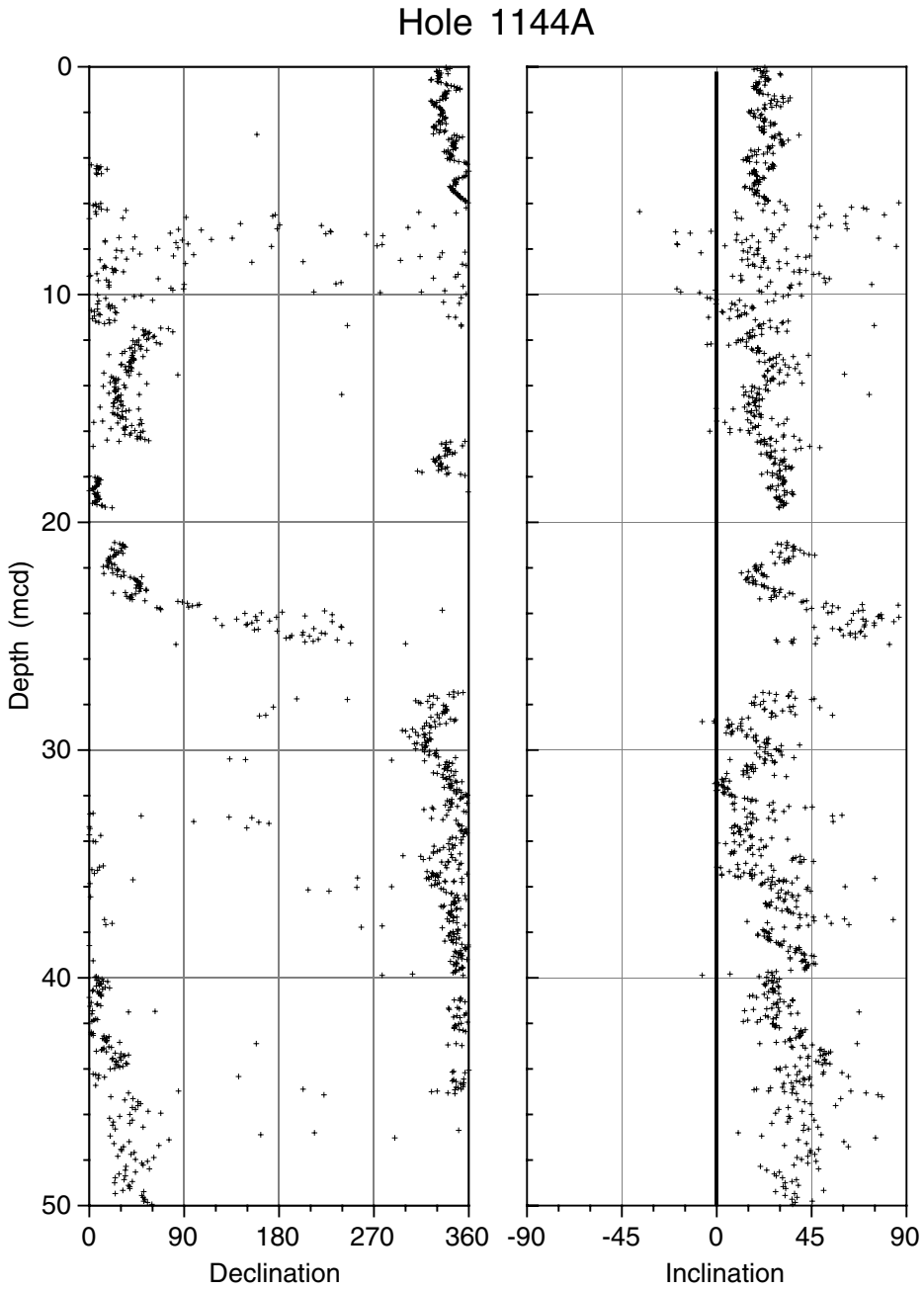

Figure F15. Alternating field demagnetization to 70 mT of (**A**) Sample 184-1144A-45X-4, 86 cm, and (**B**) Sample 184-1144A-47X-2, 86 cm. Demagnetization reveals the reverse polarity of (A), whereas only normal polarity is documented for (B).

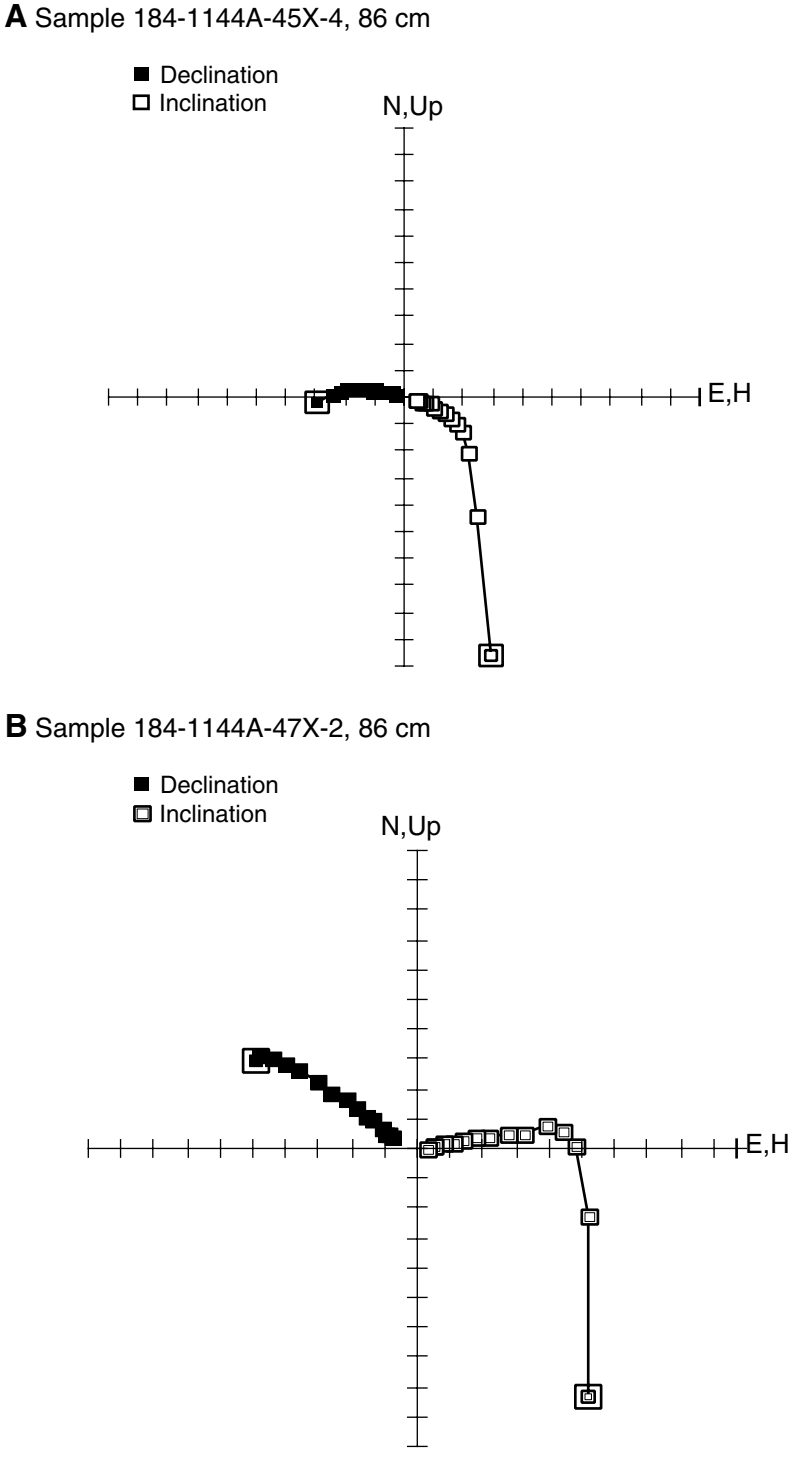

Figure F16. Preliminary normalized intensity (magnetization after 20 mT AF demagnetization divided by magnetic susceptibility) for Holes 1144A, 1144B, and 1144C. Three lows identified at ~40, ~95, and ~165 mbsf are assigned ages based on records of known lows by Lehman et al. (1996) and Guyodo and Valet (1996). These tentative assignments are supported by biostratigraphic results (see **"Biostratigraphy,"** p. 9).

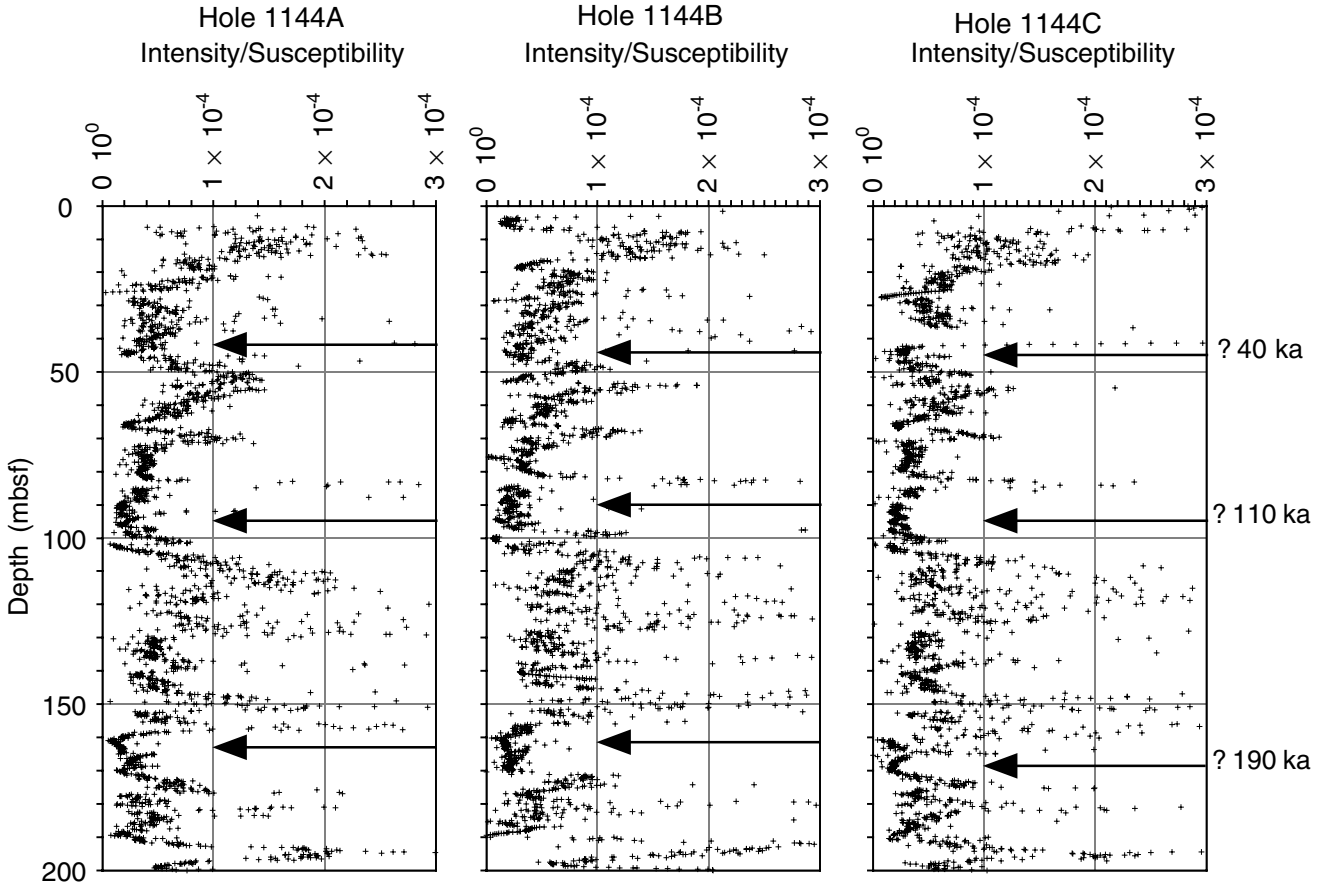

Figure F17. (A) Age-depth model, (B) linear sedimentation rate (LSR) and mass accumulation rate (MAR) vs. depth, and (C) LSR and MAR vs. age for Site 1144. Construction of model rates, LSR, and MAR is explained in "Sedimentation and Accumulation Rates," p. 13, in the "Explanatory Notes" chapter. In (A), diamonds = calcareous nannofossils, circles = foraminifers; in (B) and (C), solid lines = total sediment LSR, dashed lines = carbonate LSR, stippled columns = total sediment MAR, solid column = carbonate MAR. B/M = Brunhes/Matuyama (expected location).

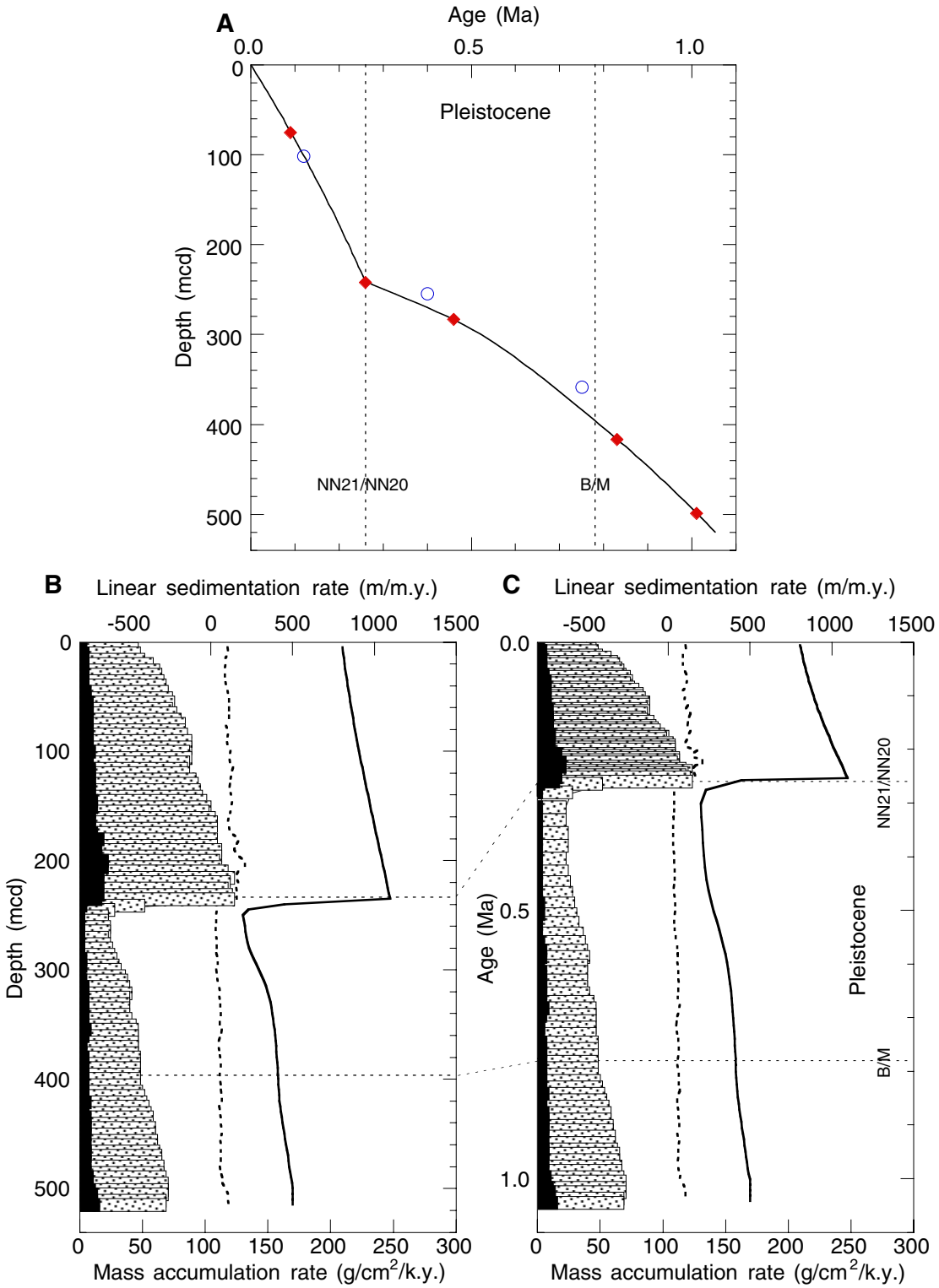

Figure F18. Methane concentration (ppmv, log scale) vs. depth at Site 1144, as obtained by the headspace technique normalized for sample mass (dark line = interval of ethane detection) and from gas voids (void space) in Hole 1144A.

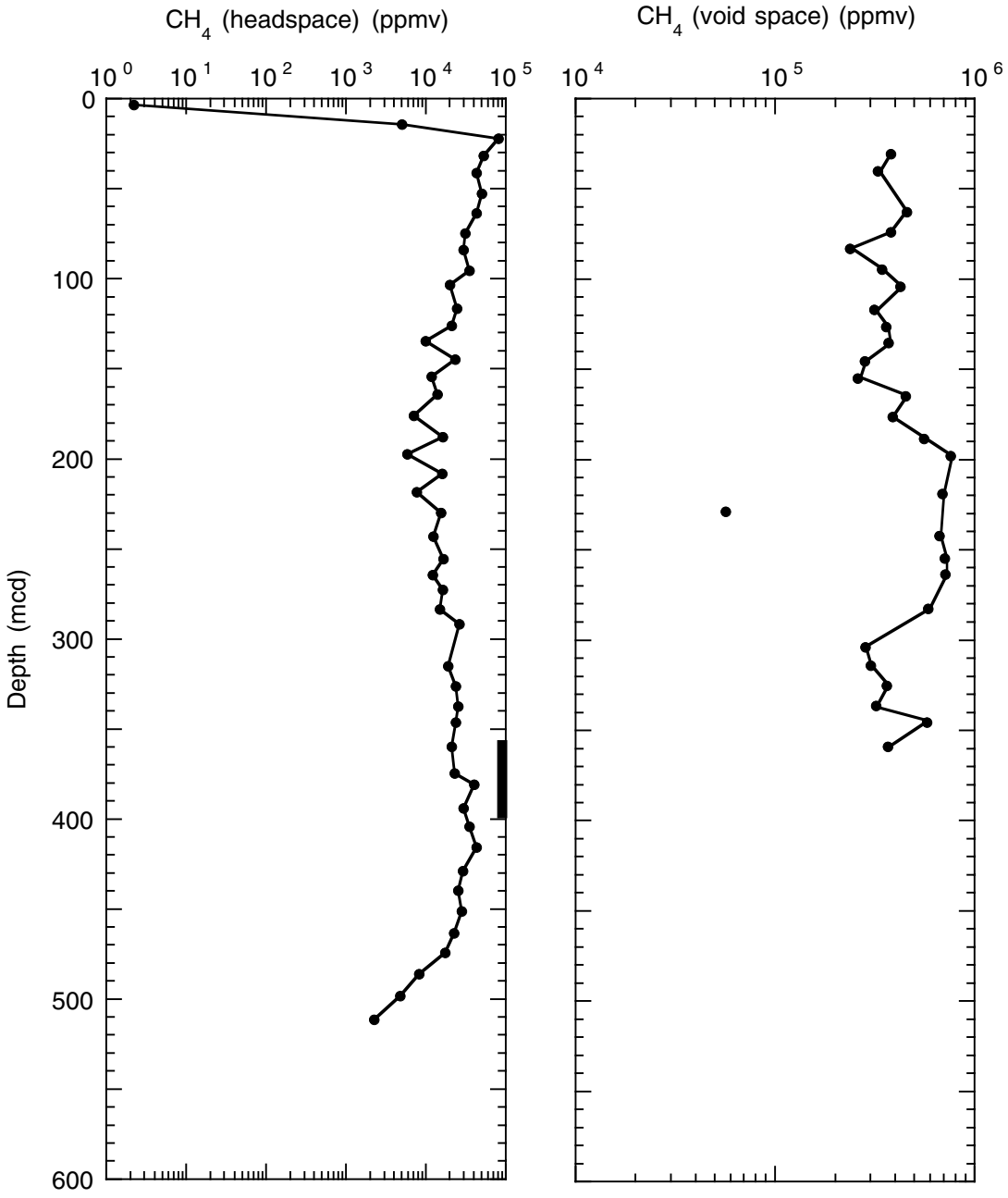

Figure F19. Carbonate, total organic carbon, and organic C/N ratio at Site 1144 vs. depth (Hole 1144A).

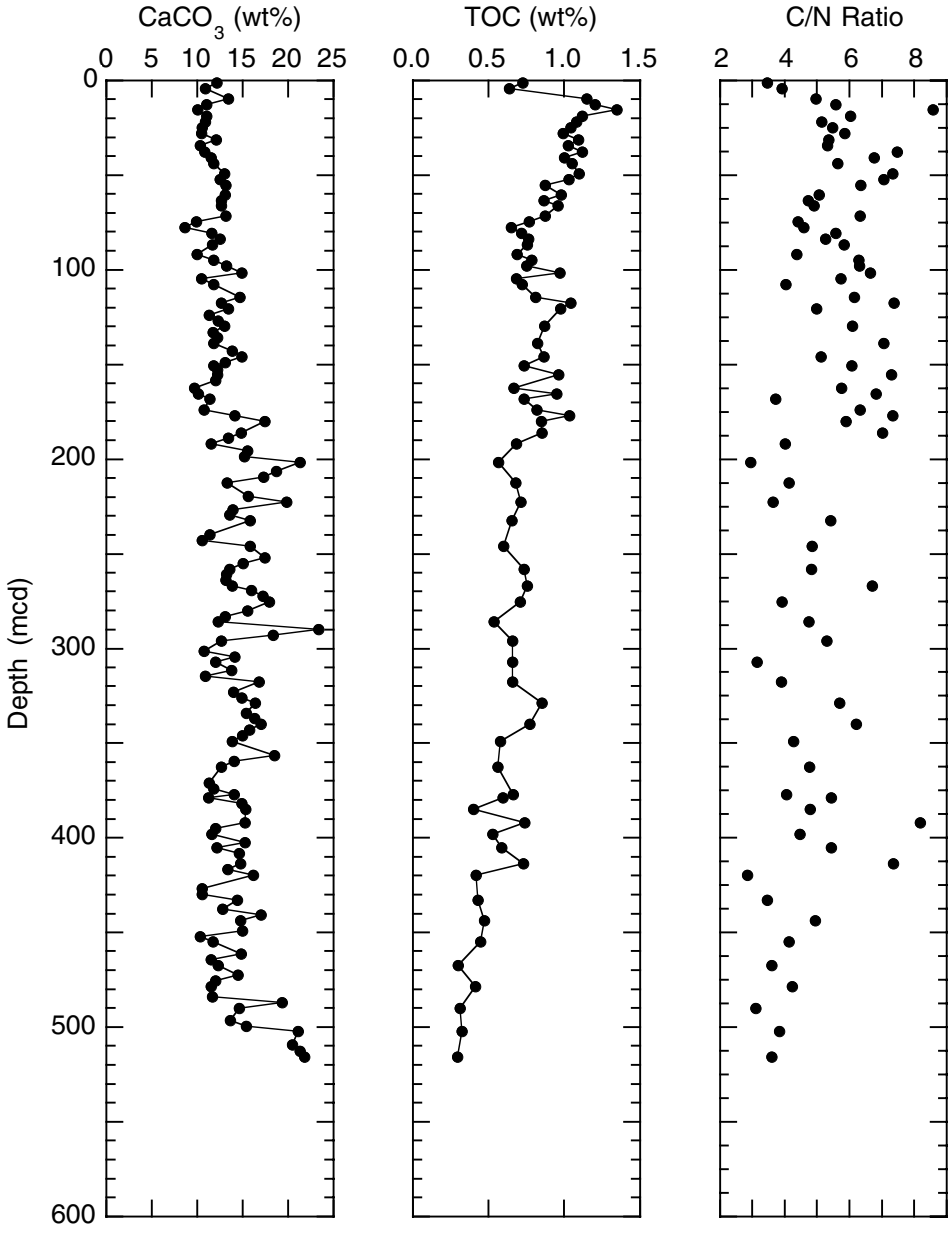

Figure F20. TOC by Rock-Eval pyrolysis vs. TOC by difference.

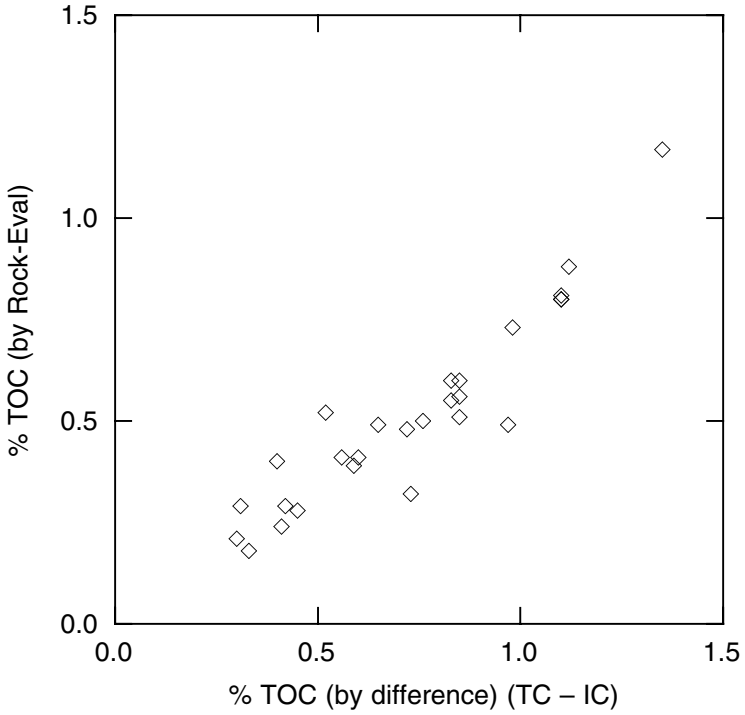

Figure F21. Total organic carbon (by difference) vs. total nitrogen at Site 1144 (see "Organic Matter Characterization," p. 16). OM = organic matter.

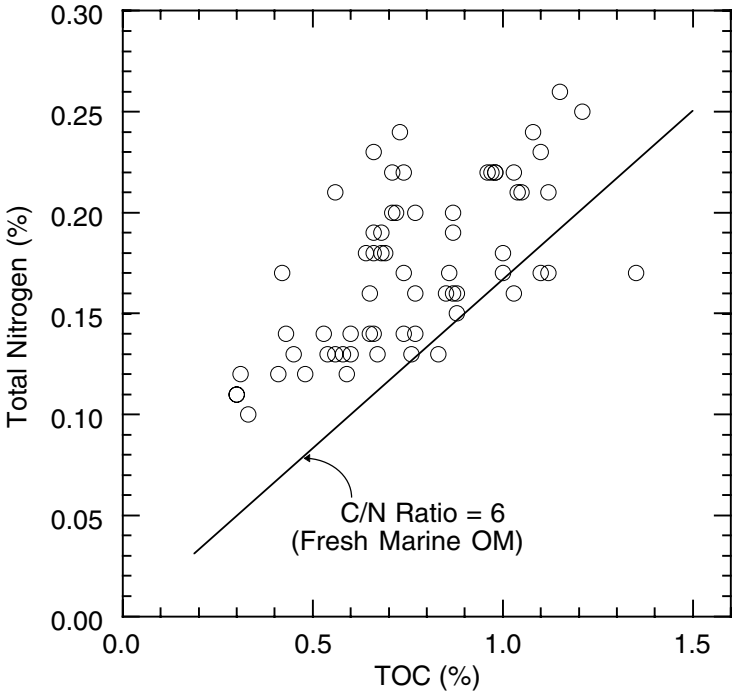

Figure F22. (A) Chlorin abundance, (B) total organic carbon, and (C) NGR at Site 1144 vs. depth (Hole 1144A). Tentative assignments of Termination Events I–V are indicated.

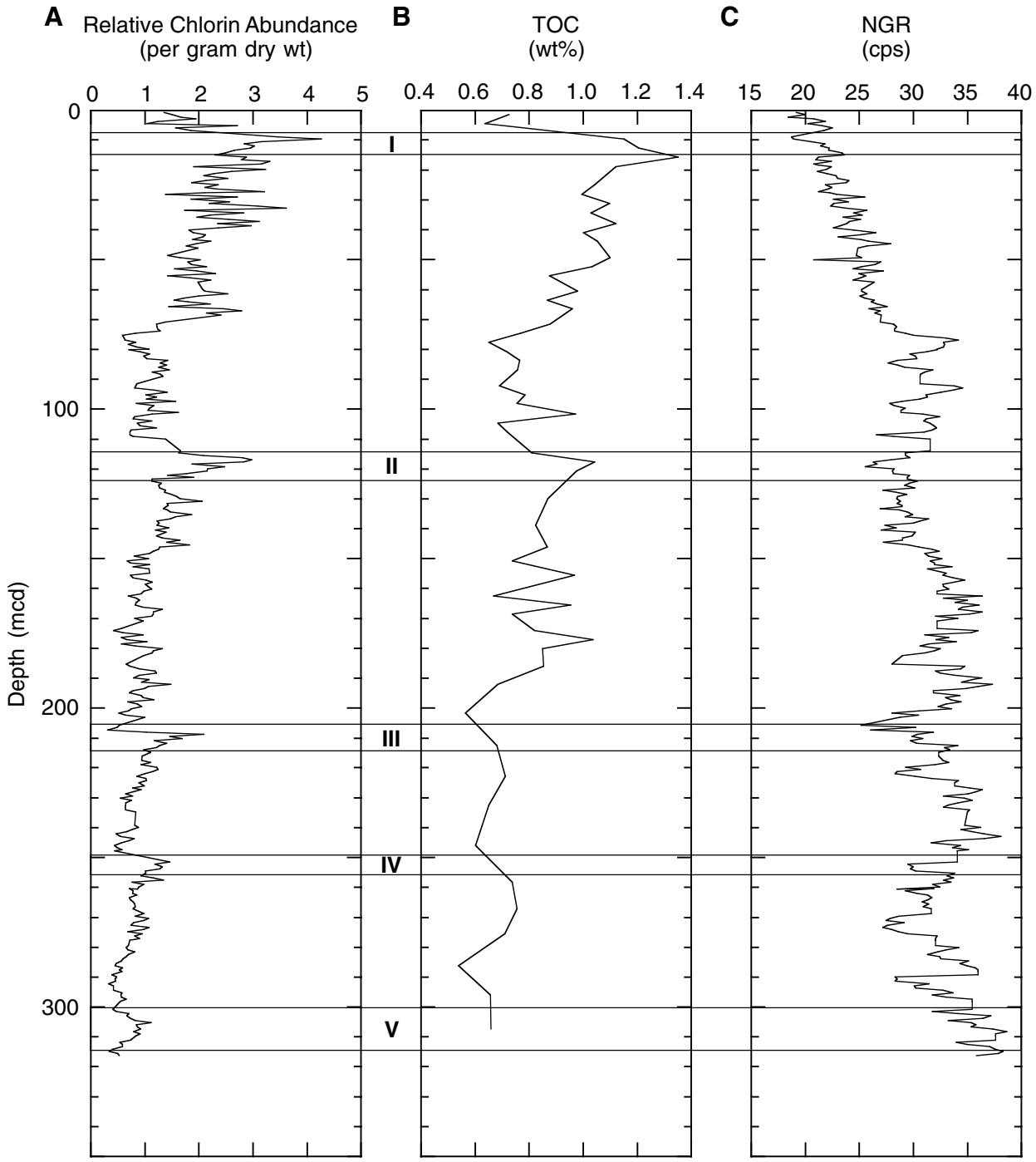

Figure F23. Vertical profiles of interstitial water measurements at Site 1144. **A.** Chloride at normal interstitial water sampling resolution (solid circles) and at higher resolution (crosses). **B.** Salinity at Holes 1144A (solid circles) and 1144B (open circles). **C.** Sulfate. **D.** Ammonium. **E.** Phosphate. **F.** Alkalinity at Holes 1144A (solid circles) and 1144B (open circles). **G.** Potassium. **H.** Magnesium. **I.** Calcium. **J.** Silica. **K.** Lithium. **L.** Strontium concentrations.

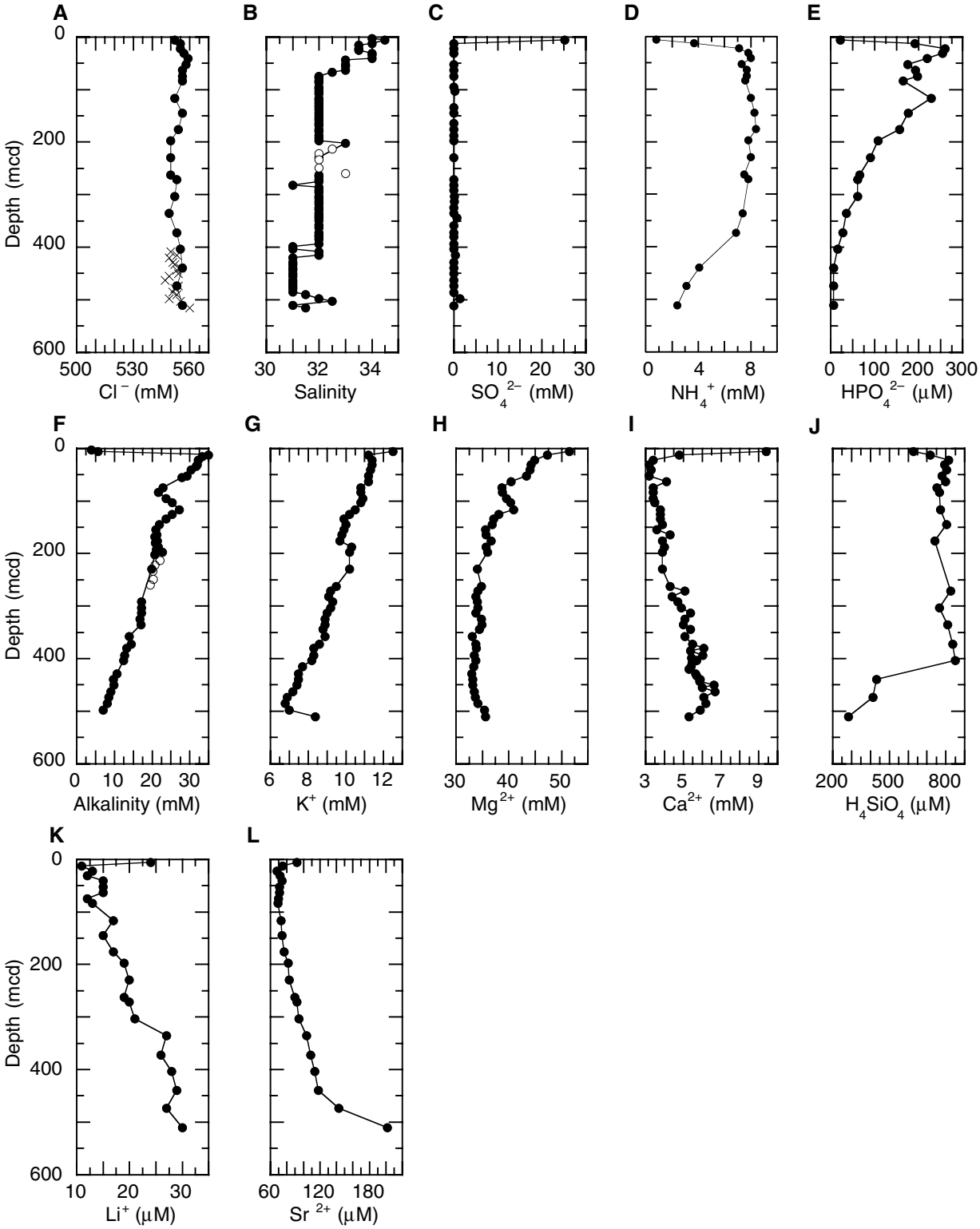

Figure F24. Bulk density measurements from GRA core logging (line) and MAD methods (open circles). The bulk density measurements are plotted for each hole at Site 1144; the MAD measurements were made only on samples from Hole 1144A. APC = advanced hydraulic piston corer, XCB = extended core barrel.

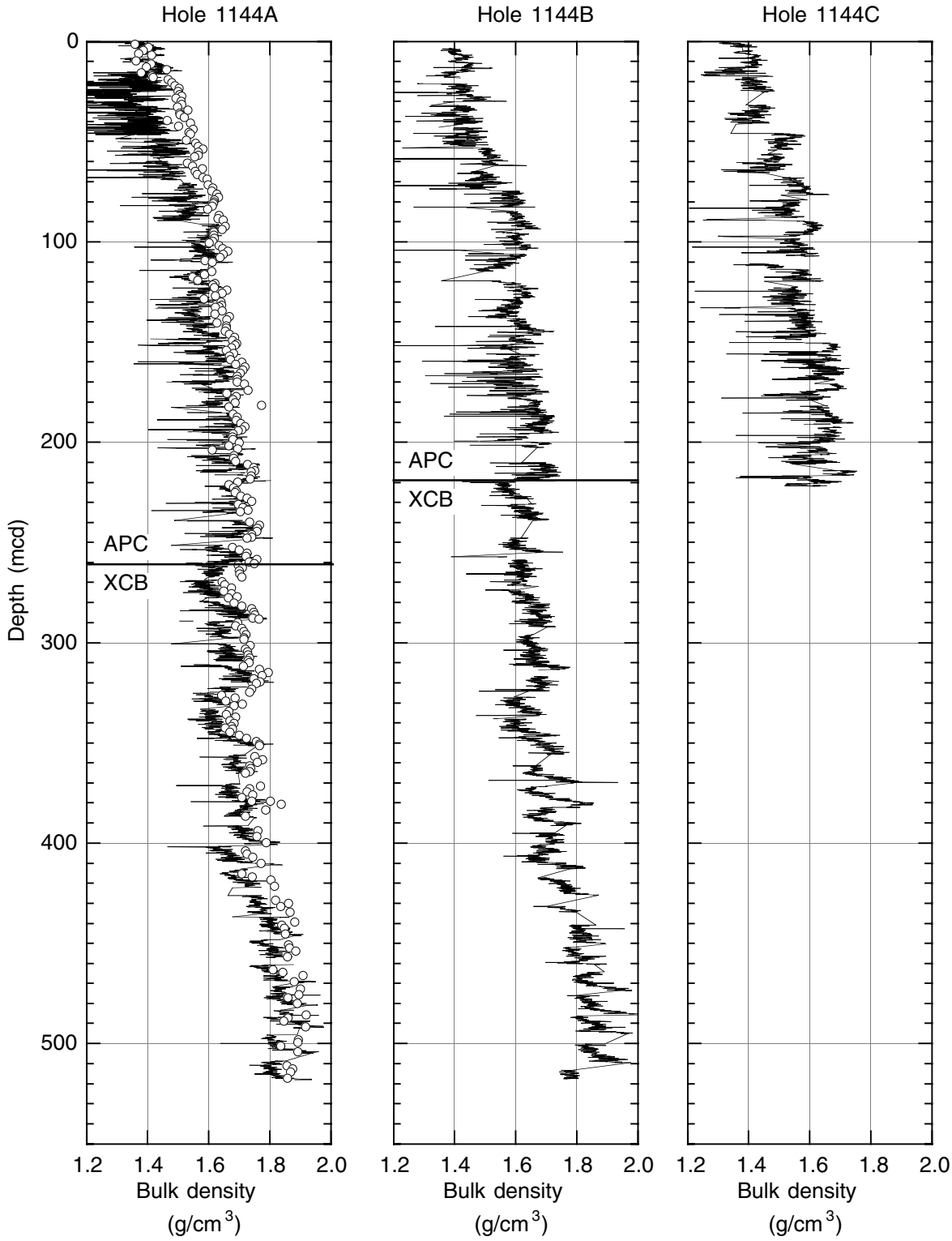

Figure F25. Natural gamma radiation from core logging for Holes 1144A, 1144B, and 1144C smoothed with a 20-point moving average. APC = advanced hydraulic piston corer, XCB = extended core barrel.

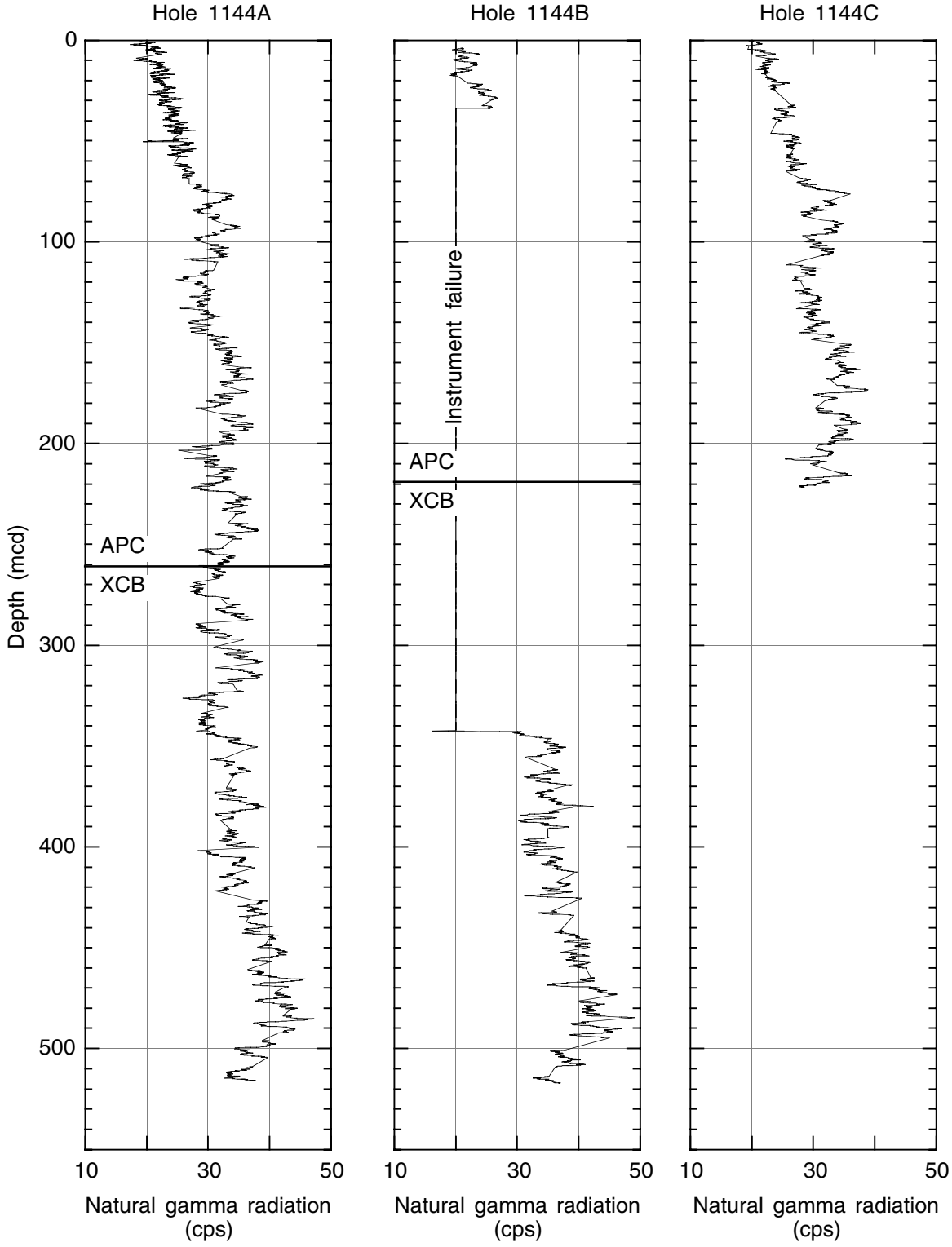

Figure F26. Magnetic susceptibility from core logging for Holes 1144A, 1144B, and 1144C. APC = advanced hydraulic piston corer, XCB = extended core barrel.

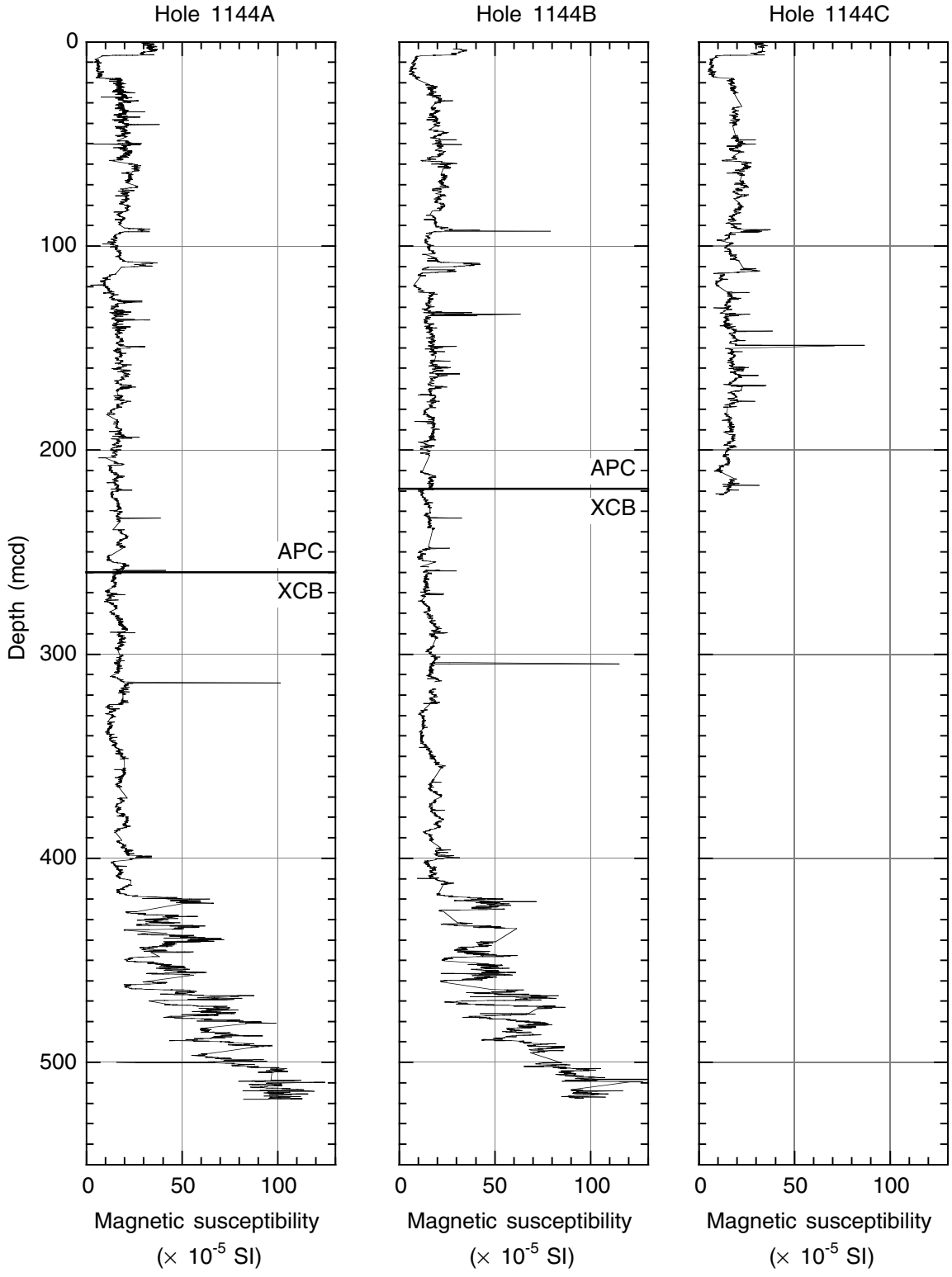

Figure F27. Comparison of bulk density measurements from gamma-ray attenuation (GRA) and moisture and density (MAD) methods at Hole 1144A. Crosses = APC cores, circles = XCB cores.

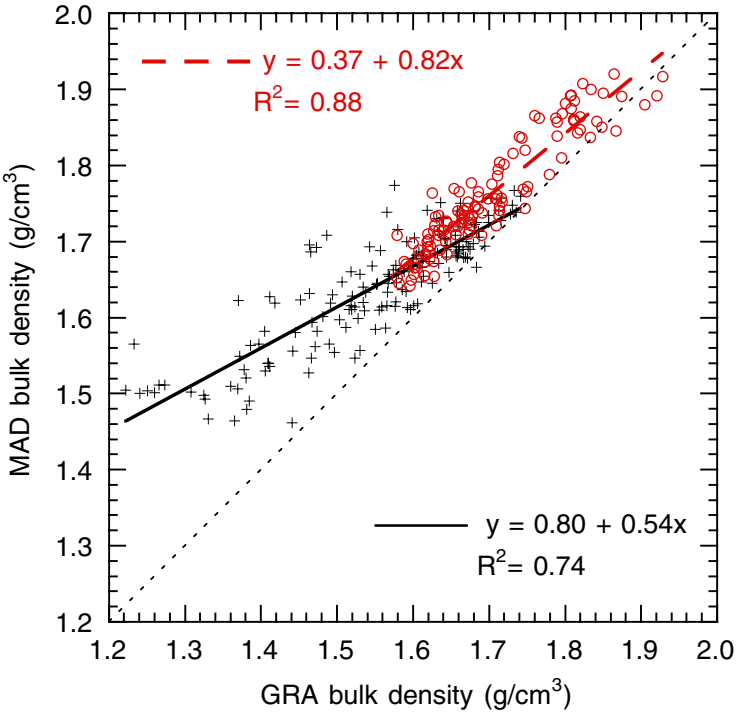

Figure F28. Porosity, grain density, and dry density from MAD measurements at Hole 1144A. APC = advanced hydraulic piston corer, XCB = extended core barrel.

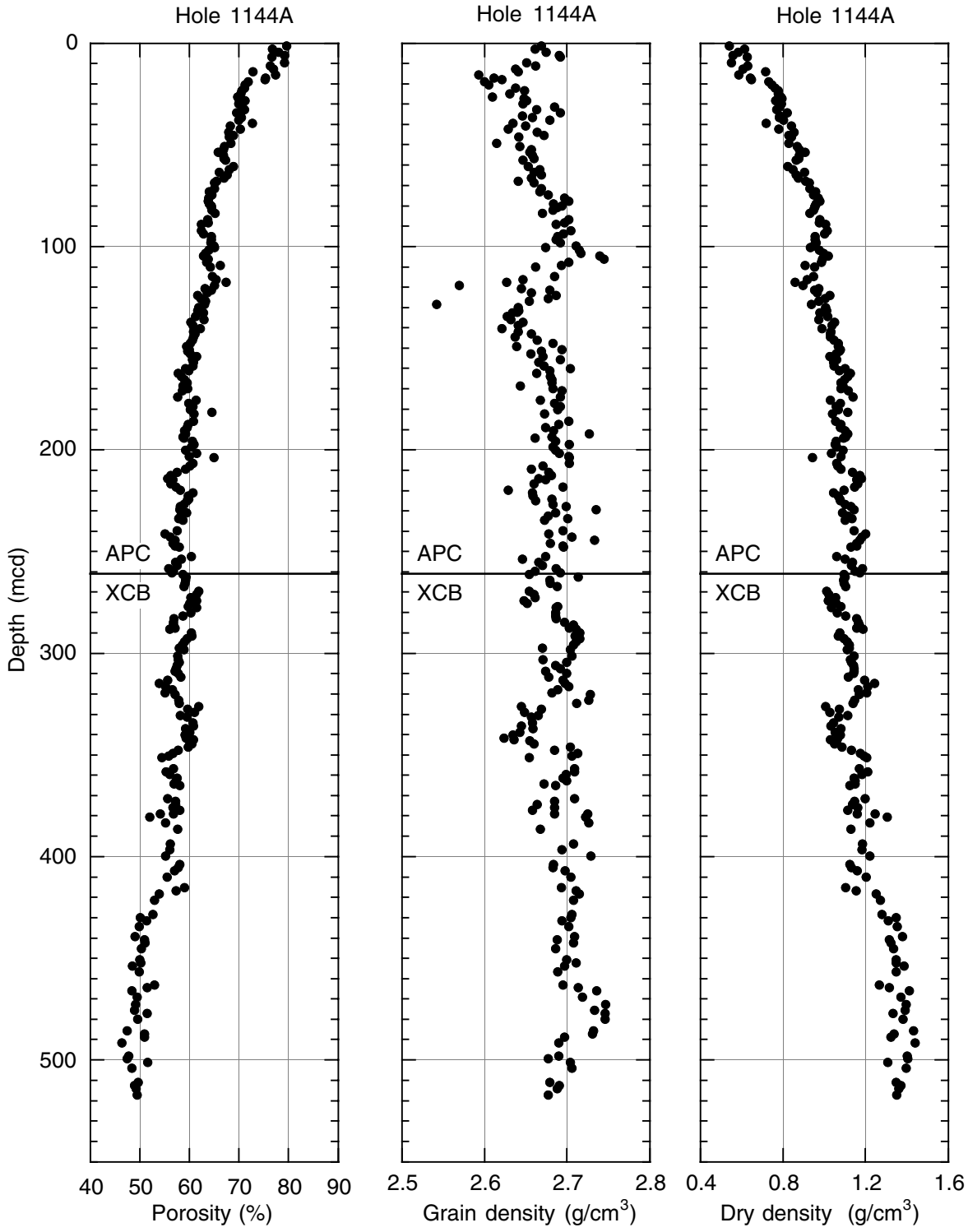

Figure F29. Color spectral reflectance measurements from split-core surfaces, smoothed with a 20-point moving average, plotted for each hole at Site 1144. L*, a*, and b* are standard parameters calculated by the Minolta CM-2002 photospectrometer from the spectral data. L* = black line, a*/b* = gray line, APC = advanced hydraulic piston corer, XCB = extended core barrel.

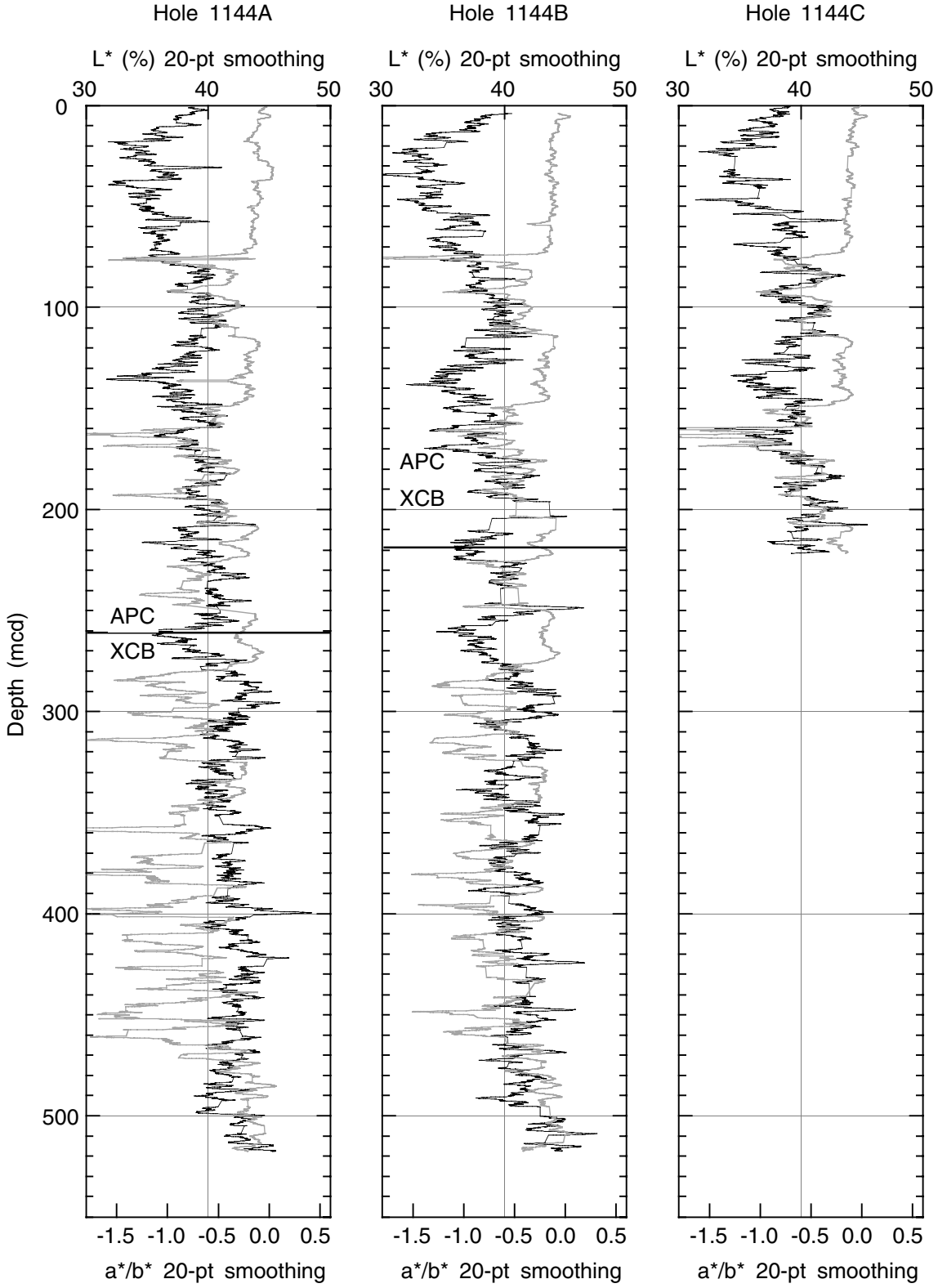

Figure F30. Thermal conductivity measurements for Hole 1144A. APC = advanced hydraulic piston corer, XCB = extended core barrel.

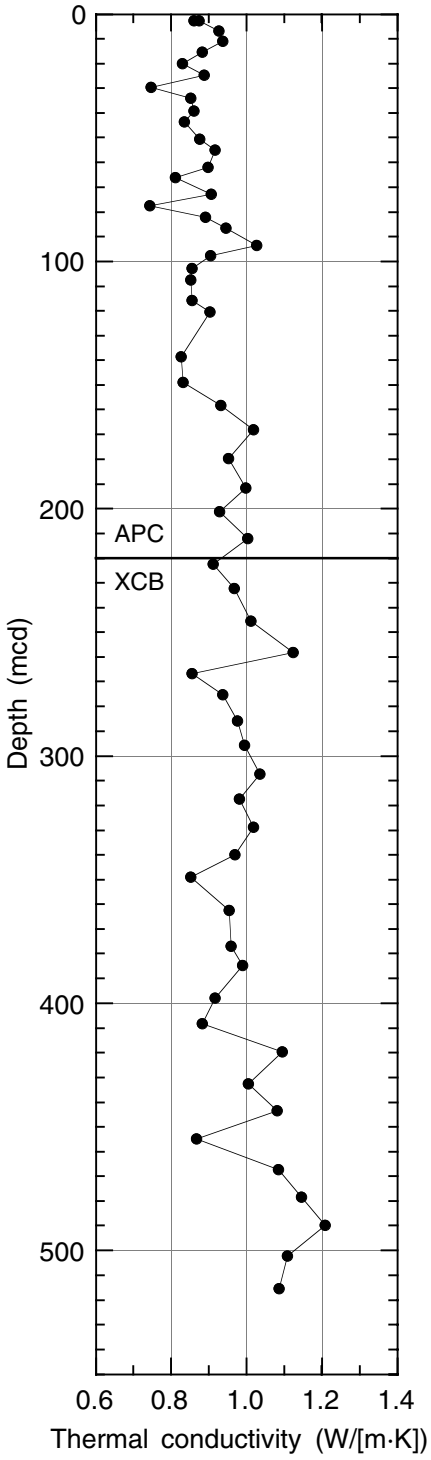

Figure F31. Downhole temperature measurements at Site 1144. **A.** Bottom-water temperature at Hole 1144B taken before Core 184-1144B-1H was shot. This value is taken as approximate bottom-water temperature at Site 1144. **B–E.** Downhole sediment temperature records and calculated equilibrium temperatures at Hole 1144A. Open circles = original temperature measurements, solid circles = selected section of data used in calculating the equilibrium temperature.

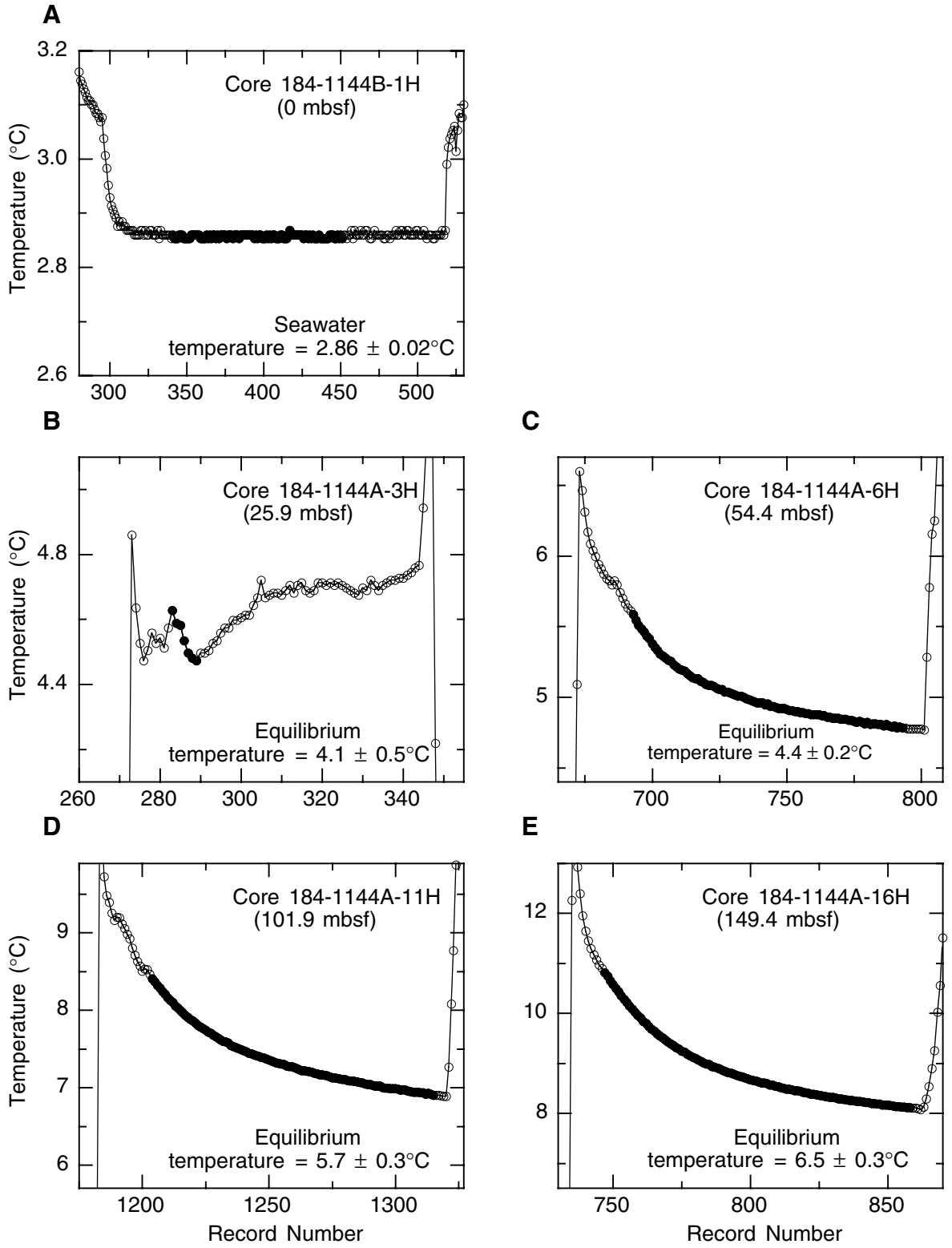

Figure F32. Downhole temperature gradient at Site 1144. T = temperature (°C) at depth (mbsf), R = correlation coefficient.

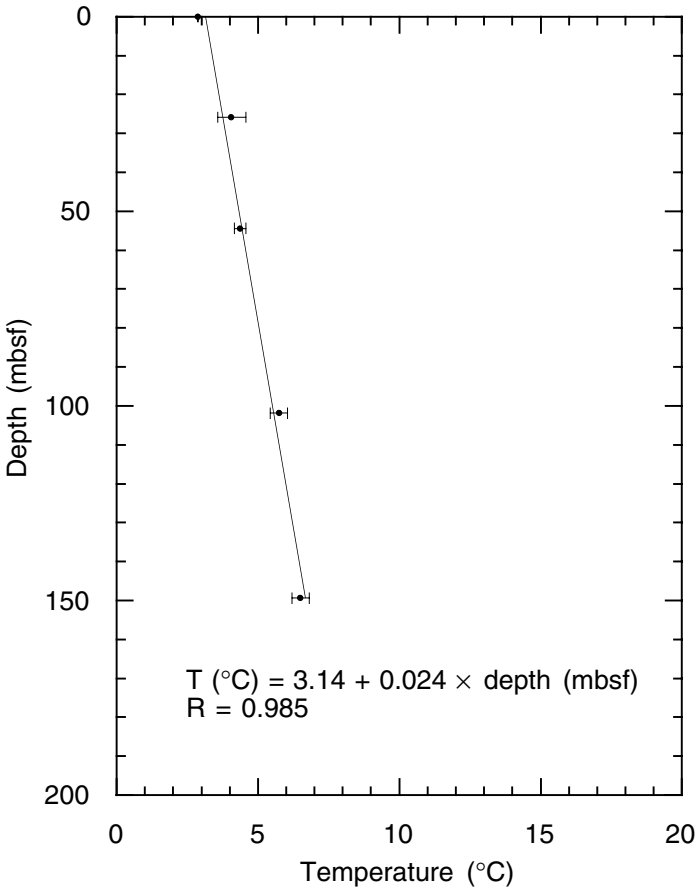

Figure F33. Graphic summary of downhole logging operations for Hole 1144A. The seafloor was identified based on a step in natural gamma activity at the sediment/water boundary. FMS = Formation MicroScanner, LSS = long-spaced sonic, GHMT = geological high-resolution magnetic tool.

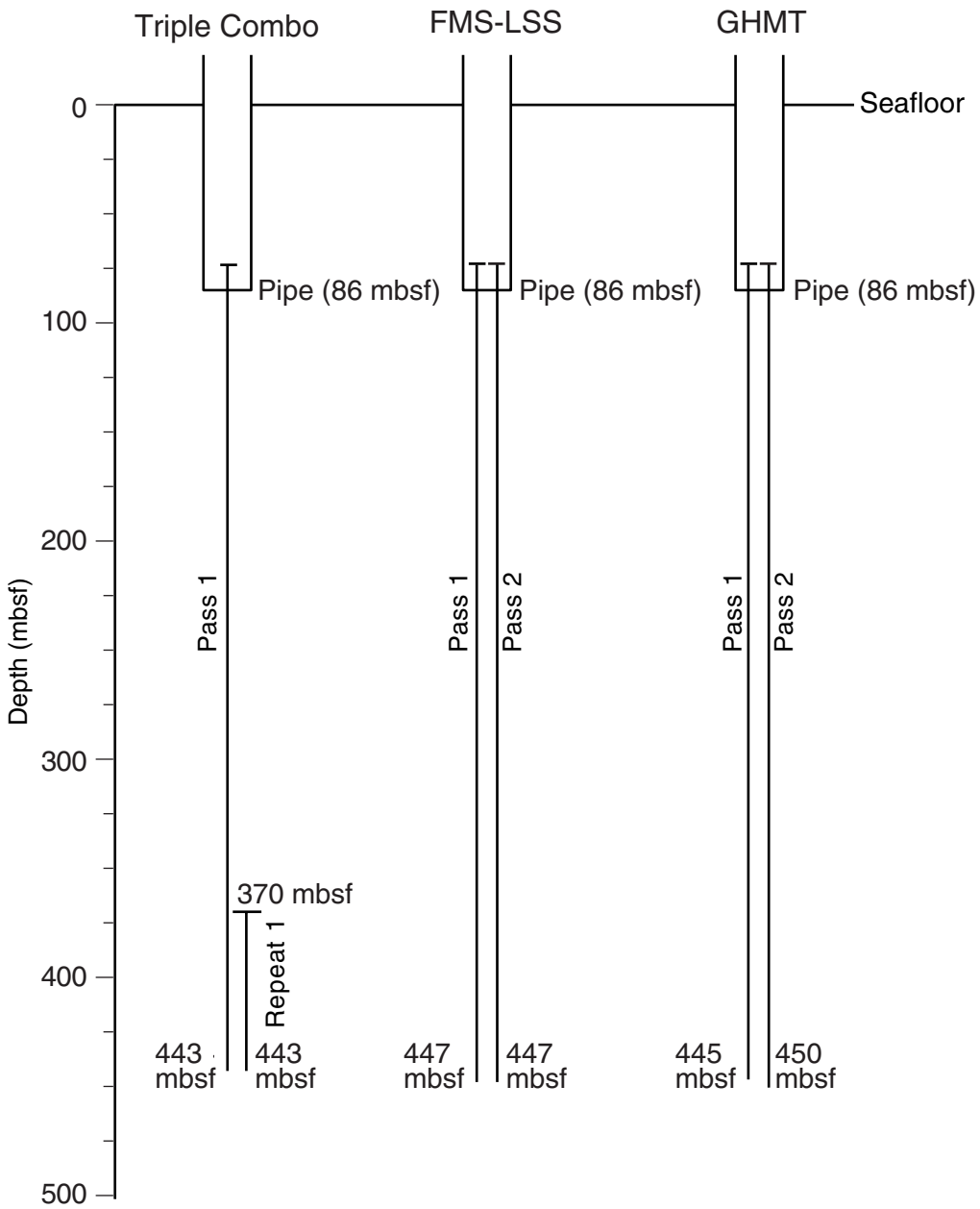

Figure F34. Downhole logs of hole diameter (as measured by caliper opening), computed gamma ray (HCGR), neutron porosity (neut.), density-derived porosity (dens.), electrical resistivity (SFL = spherically focused log, IMPH = medium induction phasor-processed resistivity, IDPH = deep induction phasor-processed resistivity), and *P*-wave velocity from Hole 1144A. (**Figure shown on next page.**)

Figure F34. (Caption on previous page.)

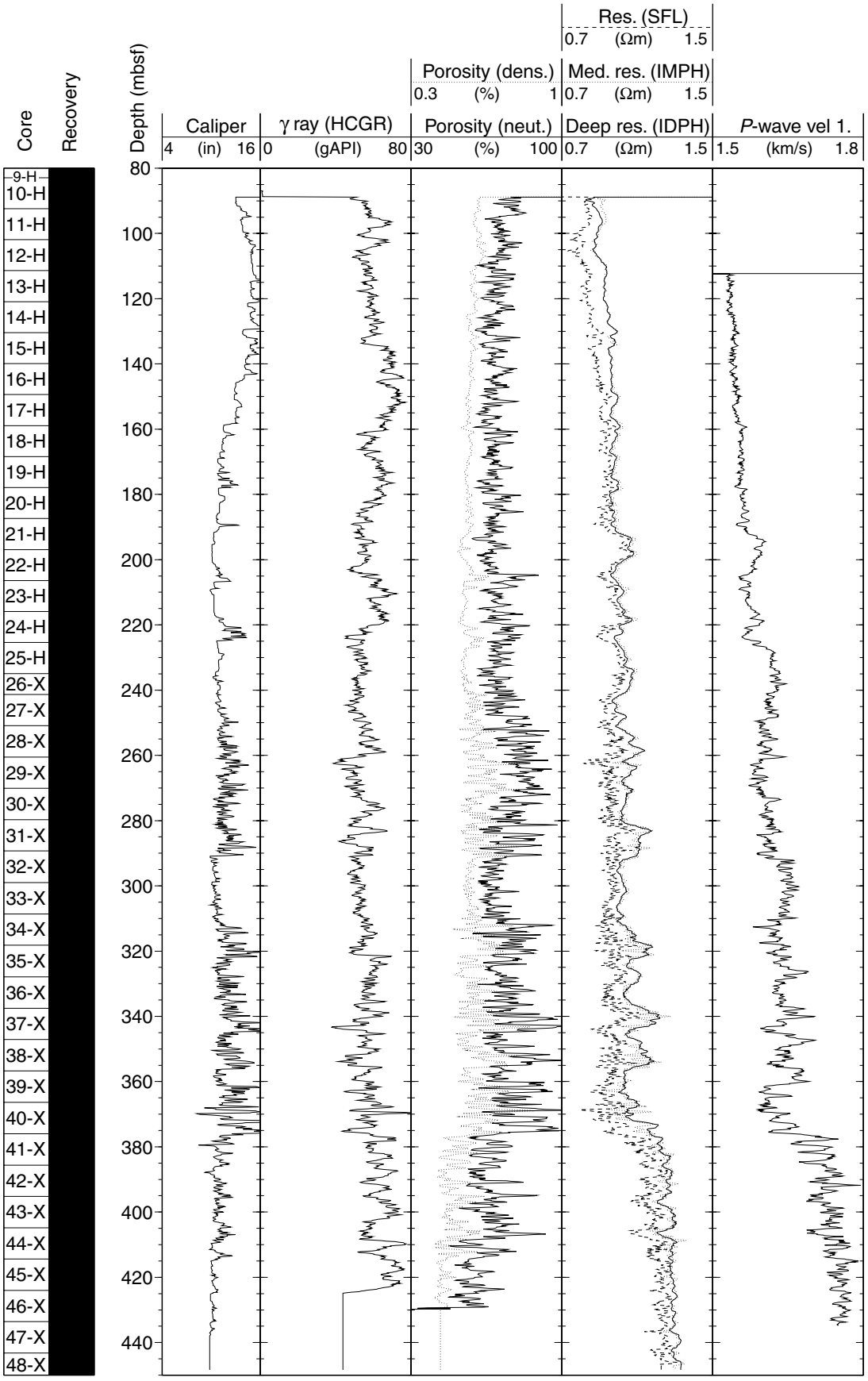

Figure F35. Comparison of core moisture and density (MAD) porosity and downhole log bulk density porosity, and of natural gamma radiation (NGR) from downhole and core logging. Also shown is total magnetic field from downhole logging. Large-amplitude spikes in the magnetic field were edited out. MST = multisensor track, HSGR = standard gamma ray, HLDS = hostile environment lithodensity sonde.

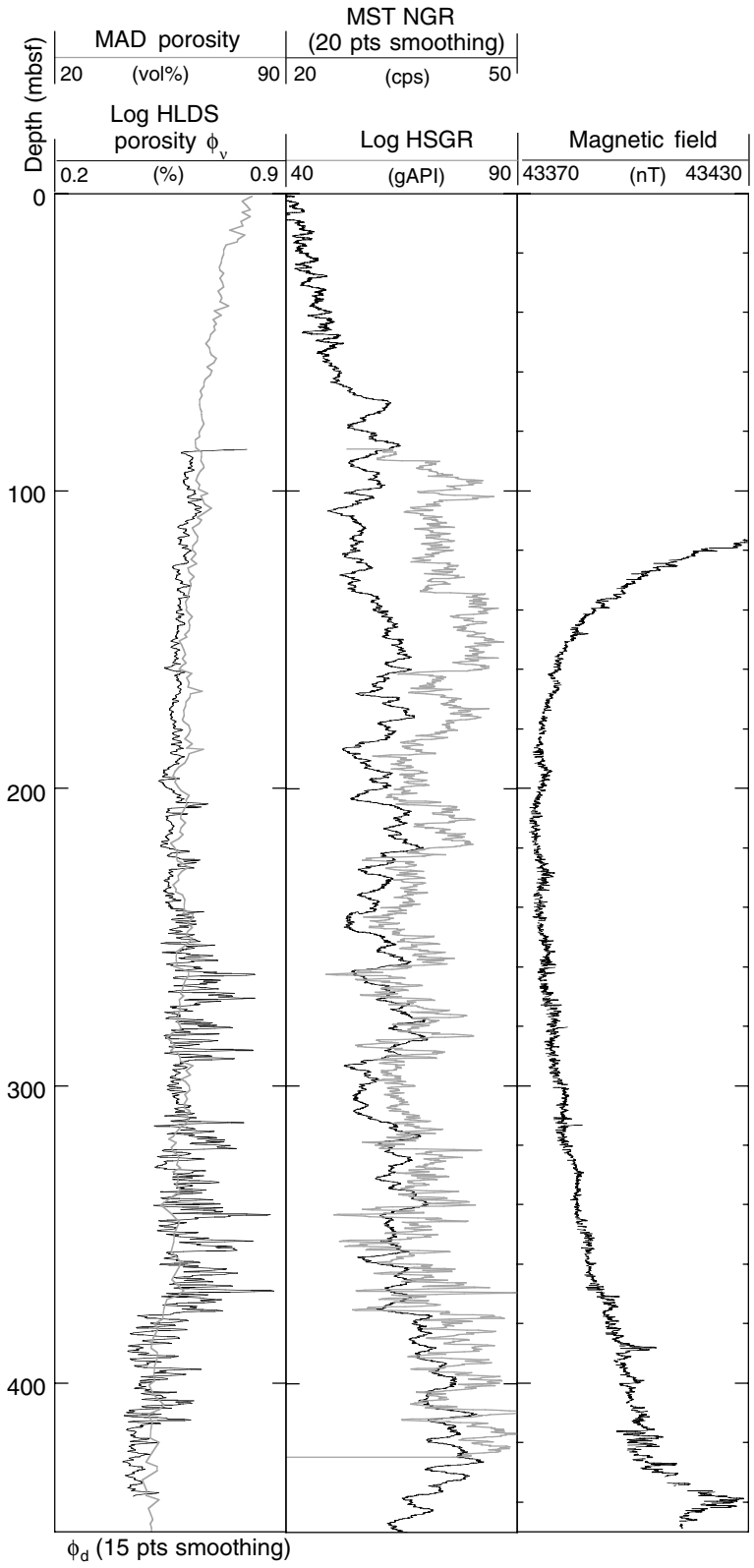

Figure F36. Downhole logs of gamma ray (HSGR = standard gamma ray), computed gamma ray (HCGR = HSGR minus uranium contribution), and potassium, thorium, and uranium from the natural gamma-ray tool (NGT) and hostile environment natural gamma-ray sonde (HNGS). The gamma-ray and computed gamma-ray values are from the HNGS tool.

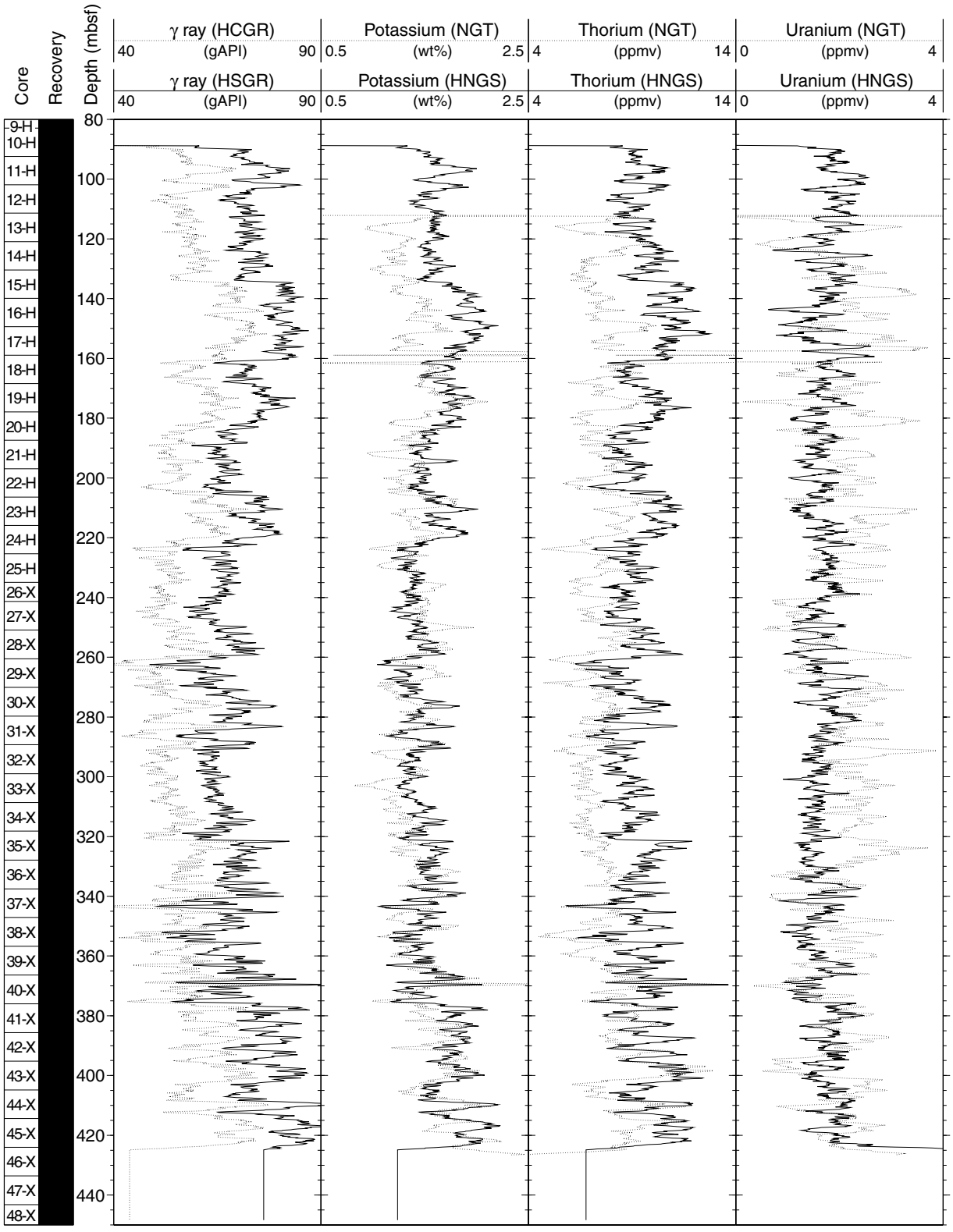

Figure F37. Comparison of magnetic susceptibility from multisensor track (MST) measurements of whole-core sections and downhole measurements (pass 1 of the GHMT tool string) and of thorium measured by the NGT tool string and photoelectric effect (PEF) from the hostile environment lithodensity sonde (HLDS). Also shown are $CaCO_3$ from core samples and PEF as well as bulk density from downhole and core logging. IU = instrument units.

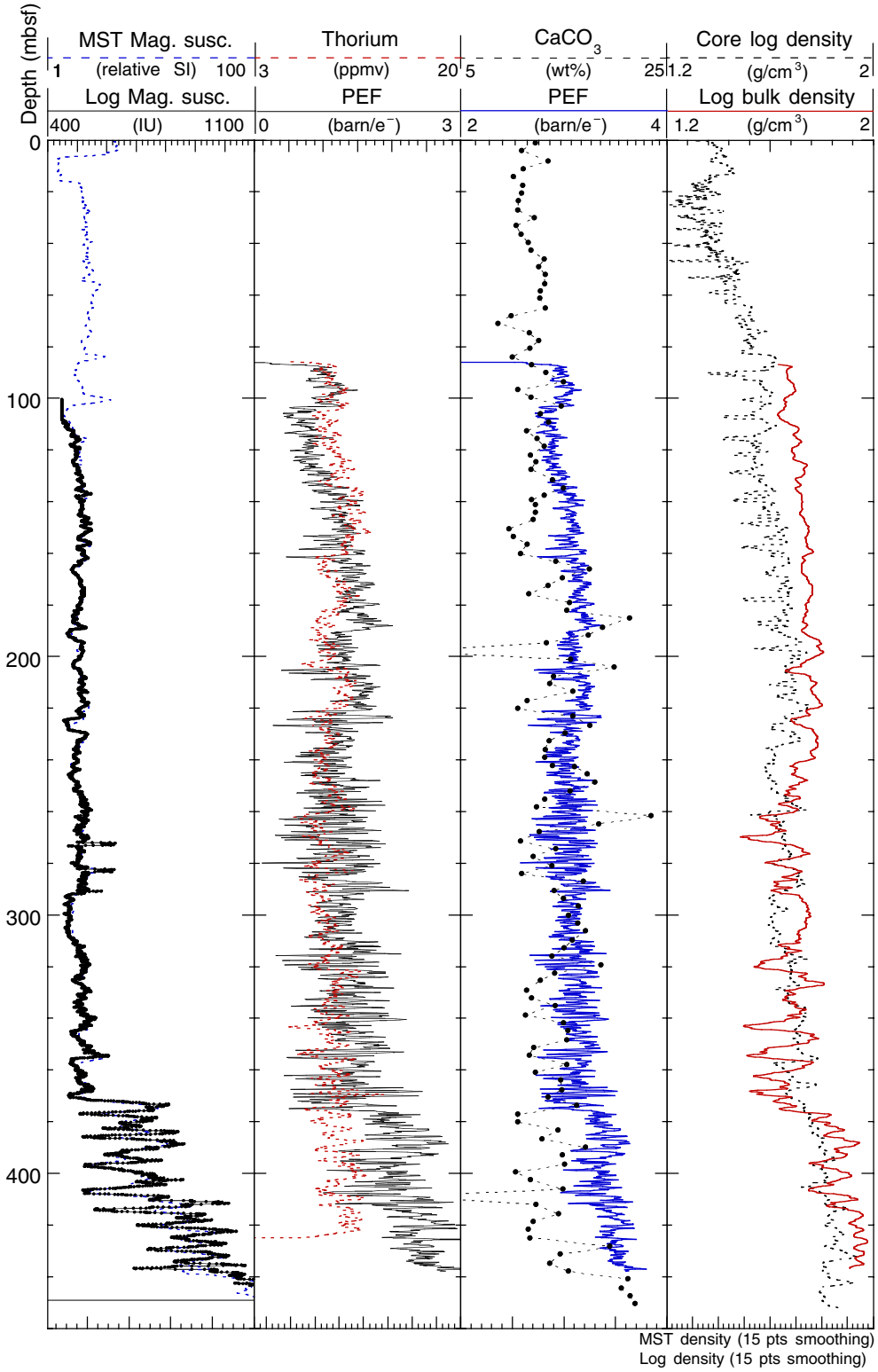

Figure F38. Formation MicroScanner (FMS) image from downhole logging data displaying alternation of relatively conductive (darker) and resistive (lighter) intervals.

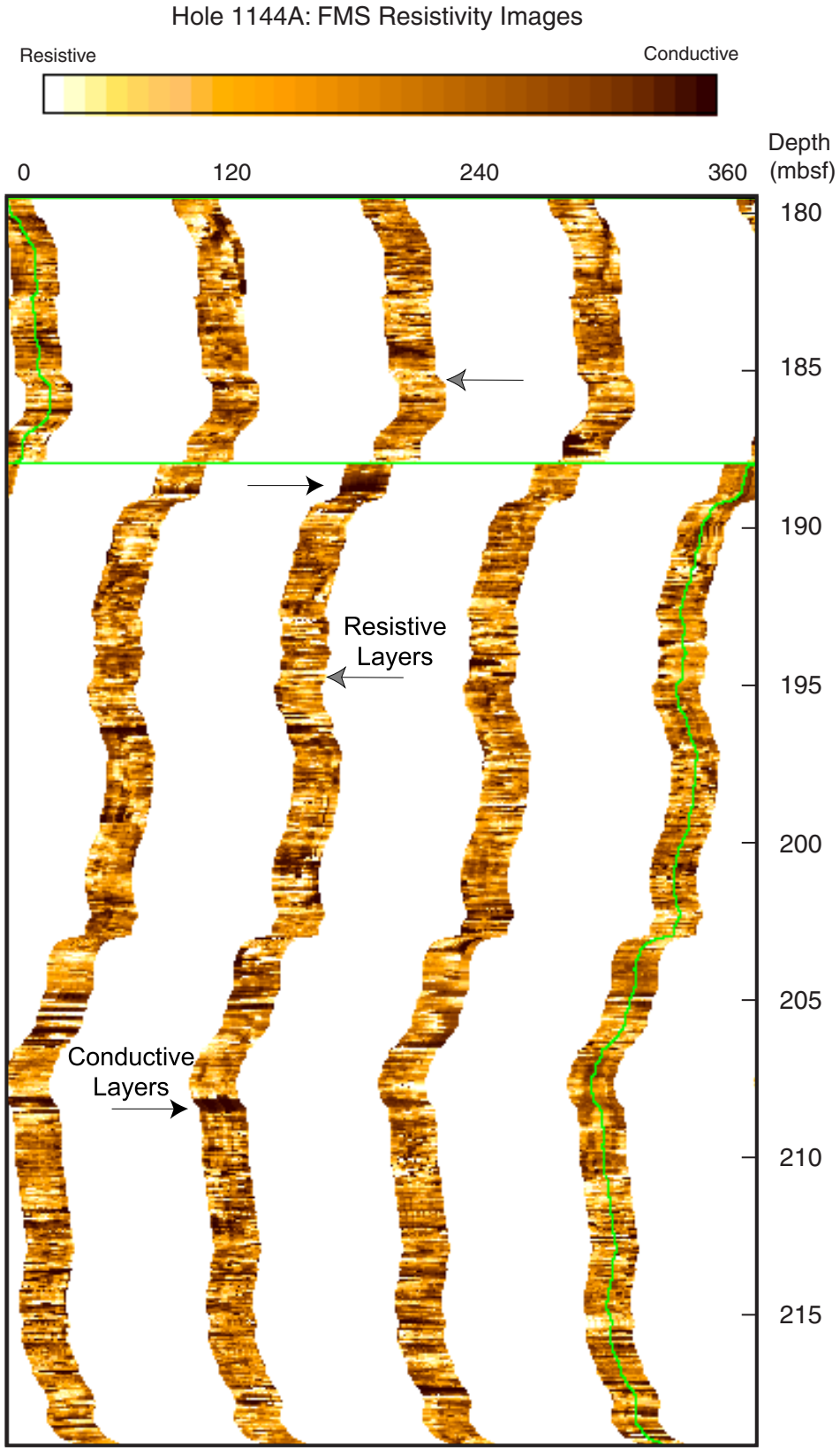

Table T1. Site 1144 coring summary. (See table note. Continued on next page.)

Core	Date (March 1999)	Time (UTC + 8 hr)	Depth Top (mbsf)	Depth Bottom (mbsf)	Depth Top (mcd)	Length (m) Cored	Length (m) Recovered	Recovery (%)
184-1144A-								
1H	13	2305	0.0	6.9	0.46	6.9	6.83	99.0
2H	13	2355	6.9	16.4	8.69	9.5	9.75	102.6
3H	14	0045	16.4	25.9	17.97	9.5	10.21	107.5
4H	14	0125	25.9	35.4	27.25	9.5	10.24	107.8
5H	14	0200	35.4	44.9	36.89	9.5	9.99	105.2
6H	14	0255	44.9	54.4	48.33	9.5	10.27	108.1
7H	14	0330	54.4	63.9	59.66	9.5	9.93	104.5
8H	14	0410	63.9	73.4	70.63	9.5	9.87	103.9
9H	14	0445	73.4	82.9	79.79	9.5	10.12	106.5
10H	14	0540	82.9	92.4	91.17	9.5	9.67	101.8
11H	14	0625	92.4	101.9	100.73	9.5	9.93	104.5
12H	14	0715	101.9	111.4	113.70	9.5	9.79	103.0
13H	14	0755	111.4	120.9	123.03	9.5	9.83	103.5
14H	14	0830	120.9	130.4	132.42	9.5	10.10	106.3
15H	14	0905	130.4	139.9	142.06	9.5	10.29	108.3
16H	14	1005	139.9	149.4	151.70	9.5	10.26	108.0
17H	14	1045	149.4	158.9	161.52	9.5	10.07	106.0
18H	14	1120	158.9	168.4	173.07	9.5	10.06	105.9
19H	14	1200	168.4	177.9	185.07	9.5	9.65	101.6
20H	14	1240	177.9	187.4	194.71	9.5	9.31	98.0
21H	14	1315	187.4	196.9	205.52	9.5	10.05	105.8
22H	14	1355	196.9	206.4	215.77	9.5	9.64	101.5
23H	14	1435	206.4	215.9	225.72	9.5	10.01	105.4
24H	14	1515	215.9	225.4	238.90	9.5	9.39	98.8
25H	14	1615	225.4	234.9	251.31	9.5	10.02	105.5
26X	14	1730	234.9	241.3	260.15	6.4	7.64	119.4
27X	14	1810	241.3	250.9	268.59	9.6	9.51	99.1
28X	14	1845	250.9	260.5	279.17	9.6	9.55	99.5
29X	14	1920	260.5	270.1	288.95	9.6	9.82	102.3
30X	14	1955	270.1	279.7	300.49	9.6	9.74	101.5
31X	14	2050	279.7	289.3	310.83	9.6	9.66	100.6
32X	14	2130	289.3	299.0	322.08	9.7	9.92	102.3
33X	14	2210	299.0	308.6	333.22	9.6	9.93	103.4
34X	14	2245	308.6	318.2	342.14	9.6	9.90	103.1
35X	14	2320	318.2	327.9	355.74	9.7	9.83	101.3
36X	15	0005	327.9	337.5	370.39	9.6	9.70	101.0
37X	15	0045	337.5	347.1	378.05	9.6	9.79	102.0
38X	15	0125	347.1	356.7	391.25	9.6	9.84	102.5
39X	15	0205	356.7	366.4	401.45	9.7	9.89	102.0
40X	15	0245	366.4	376.0	412.85	9.6	9.86	102.7
41X	15	0335	376.0	385.6	425.97	9.6	9.94	103.5
42X	15	0430	385.6	395.2	436.76	9.6	9.88	102.9
43X	15	0530	395.2	404.8	448.20	9.6	9.89	103.0
44X	15	0615	404.8	414.4	460.54	9.6	9.78	101.9
45X	15	0710	414.4	424.0	471.58	9.6	9.95	103.6
46X	15	0755	424.0	433.6	483.21	9.6	9.87	102.8
47X	15	0845	433.6	443.2	495.53	9.6	9.82	102.3
48X	15	1000	443.2	452.8	508.60	9.6	9.89	103.0
					Totals:	452.6	468.88	103.6
184-1144B-								
1H	16	0825	0.0	0.1	0.00	0.1	0.10	100.0
2H	16	0855	0.1	9.6	3.48	9.5	9.77	102.8
3H	16	0935	9.6	19.1	13.04	9.5	5.68	59.8
4H	16	1010	19.1	28.6	20.96	9.5	9.58	100.8
5H	16	1045	28.6	38.1	31.90	9.5	9.86	103.8
6H	16	1120	38.1	47.6	42.80	9.5	9.93	104.5
7H	16	1155	47.6	57.1	53.10	9.5	9.60	101.1
8H	16	1230	57.1	66.6	64.79	9.5	9.83	103.5
9H	16	1310	66.6	76.1	74.22	9.5	8.88	93.5
10H	16	1345	76.1	85.6	84.85	9.5	9.63	101.4
11H	16	1430	85.6	95.1	95.13	9.5	9.56	100.6
12H	16	1505	95.1	104.6	105.77	9.5	9.66	101.7
13H	16	1545	104.6	114.1	119.25	9.5	9.60	101.1
14H	16	1635	114.1	123.6	128.74	9.5	9.45	99.5
15H	16	1715	123.6	133.1	137.82	9.5	9.32	98.1

Table T1 (continued).

Core	Date (March 1999)	Time (UTC + 8 hr)	Depth Top (mbsf)	Depth Bottom (mbsf)	Depth Top (mcd)	Length (m) Cored	Length (m) Recovered	Recovery (%)
16H	16	1755	133.1	142.6	146.80	9.5	7.69	81.0
17H	16	1940	142.6	152.1	155.92	9.5	10.60	111.6
18H	16	2040	152.1	161.6	166.94	9.5	10.62	111.8
19H	16	2120	161.6	171.1	177.89	9.5	9.20	96.8
20H	16	2200	171.1	180.6	186.65	9.5	9.76	102.7
21H	16	2240	180.6	190.1	196.77	9.5	8.33	87.7
22H	16	2325	190.1	199.6	210.18	9.5	9.43	99.3
23X	17	0025	199.6	209.2	219.54	9.6	9.76	101.7
24X	17	0100	209.2	218.8	230.60	9.6	9.00	93.8
25X	17	0140	218.8	228.5	246.09	9.7	9.67	99.7
26X	17	0215	228.5	234.1	257.15	5.6	6.62	118.2
27X	17	0255	234.1	243.8	262.91	9.7	9.75	100.5
28X	17	0330	243.8	253.5	273.57	9.7	9.64	99.4
29X	17	0410	253.5	263.2	283.43	9.7	9.72	100.2
30X	17	0450	263.2	272.8	295.99	9.6	9.64	100.4
31X	17	0525	272.8	282.5	303.95	9.7	9.75	100.5
32X	17	0610	282.5	292.2	315.25	9.7	9.71	100.1
33X	17	0650	292.2	301.9	327.06	9.7	9.85	101.6
34X	17	0730	301.9	311.5	337.88	9.6	9.89	103.0
35X	17	0805	311.5	321.1	346.96	9.6	9.83	102.4
36X	17	0850	321.1	330.7	360.85	9.6	9.90	103.1
37X	17	0925	330.7	340.3	371.57	9.6	9.90	103.1
38X	17	1005	340.3	350.0	382.01	9.7	9.77	100.7
39X	17	1045	350.0	359.7	394.89	9.7	9.94	102.5
40X	17	1135	359.7	369.3	404.07	9.6	9.59	99.9
41X	17	1255	369.3	378.9	417.19	9.6	9.70	101.0
42X	17	1340	378.9	388.5	431.49	9.6	3.61	37.6
43X	17	1425	388.5	398.1	440.78	9.6	9.83	102.4
44X	17	1510	398.1	407.8	451.68	9.7	9.80	101.0
45X	17	1600	407.8	417.5	464.32	9.7	9.91	102.2
46X	17	1645	417.5	426.9	475.95	9.4	9.94	105.7
47X	17	1735	426.9	436.5	486.21	9.6	9.85	102.6
48X	17	1840	436.5	446.1	500.24	9.6	9.88	102.9
49X	17	1930	446.1	452.0	513.29	5.9	5.30	89.8
					Totals:	452.0	445.93	98.7
184-1144C-								
1H	17	2245	0.0	8.7	0.00	8.7	8.66	99.5
2H	17	2315	8.7	18.2	8.46	9.5	9.48	99.8
3H	18	0000	18.2	27.7	17.96	9.5	7.70	81.1
4H	18	0035	27.7	37.2	31.74	9.5	9.81	103.3
Drilled interval			37.2	42.2				
5H	18	0110	42.2	51.7	45.80	9.5	8.96	94.3
6H	18	0150	51.7	61.2	56.10	9.5	9.97	105.0
7H	18	0220	61.2	70.7	67.87	9.5	9.09	95.7
8H	18	0300	70.7	80.2	78.55	9.5	10.10	106.3
9H	18	0335	80.2	89.7	88.89	9.5	9.28	97.7
10H	18	0405	89.7	99.2	98.35	9.5	9.67	101.8
11H	18	0440	99.2	108.7	110.97	9.5	9.18	96.6
12H	18	0515	108.7	118.2	122.49	9.5	9.84	103.6
13H	18	0555	118.2	127.7	132.66	9.5	8.98	94.5
14H	18	0625	127.7	137.2	139.20	9.5	10.11	106.4
15H	18	0705	137.2	146.7	150.28	9.5	9.24	97.3
16H	18	0740	146.7	156.2	159.28	9.5	10.03	105.6
17H	18	0815	156.2	165.7	170.61	9.5	9.17	96.5
18H	18	0850	165.7	175.2	181.66	9.5	9.75	102.6
19H	18	0925	175.2	184.7	192.04	9.5	9.77	102.8
20H	18	1010	184.7	194.2	201.77	9.5	9.94	104.6
21H	18	1045	194.2	203.7	0.00	9.5	9.50	100.0
					Cored totals:	198.7	198.17	99.7
					Drilled:	5.0		
					Total:	203.7		

Note: UTC = Universal Time Coordinated. This table is also available in **ASCII format.**

Table T2. Site 1144 coring summary by section.

Core	Date (March 1999)	Time (UTC + 8 hr)	Core depth (mbsf) Top	Core depth (mbsf) Bottom	Length (m) Cored	Length (m) Recovered	Recovery (%)	Section	Length (m) Liner	Length (m) Curated	Section depth (mbsf) Top	Section depth (mbsf) Bottom	Top depth (mcd)	Catwalk samples	Comments
184-1144A-															
1H	13	2305	0.0	6.9	6.9	6.83	99.0								
								1	1.50	1.50	0.00	1.50	0.46		
								2	1.50	1.50	1.50	3.00	1.96	IW, IWGM	
								3	1.50	1.50	3.00	4.50	3.46	HS	
								4	1.50	1.50	4.50	6.00	4.96	IW, IWGM	
								5	0.70	0.70	6.00	6.70	6.46		
								CC(w/5)	0.13	0.13	6.70	6.83	7.16	PAL	
								Totals:	6.83	6.83					
2H	13	2355	6.9	16.4	9.5	9.75	102.6								
								1	1.50	1.50	6.90	8.40	8.69		
								2	1.50	1.50	8.40	9.90	10.19		
								3	1.50	1.50	9.90	11.40	11.69	IW, IWGM	
								4	1.50	1.50	11.40	12.90	13.19		
								5	1.50	1.50	12.90	14.40	14.69	IW, HS, IWGM	
								6	1.50	1.50	14.40	15.90	16.19		
								7	0.56	0.56	15.90	16.46	17.69		
								CC(w/7)	0.19	0.19	16.46	16.65	18.25	PAL	
								Totals:	9.75	9.75					
3H	14	0045	16.4	25.9	9.5	10.21	107.5								Adara; oriented
								1	1.50	1.50	16.40	17.90	17.97		
								2	1.50	1.50	17.90	19.40	19.47		
								3	1.50	1.50	19.40	20.90	20.97	IW, VAC, IWGM	
								4	1.50	1.50	20.90	22.40	22.47	HS	
								5	1.50	1.50	22.40	23.90	23.97	IW, IWGM	
								6	1.50	1.50	23.90	25.40	25.47		
								7	0.86	0.86	25.40	26.26	26.97		
								CC(w/7)	0.35	0.35	26.26	26.61	27.83	PAL	
								Totals:	10.21	10.21					
4H	14	0125	25.9	35.4	9.5	10.24	107.8								Oriented
								1	1.54	1.54	25.90	27.44	27.25		Liner patch placed at top to accommodate gas expansion.
								2	1.50	1.50	27.44	28.94	28.79		
								3	1.50	1.50	28.94	30.44	30.29	IW, VAC, IWGM	
								4	1.50	1.50	30.44	31.94	31.79	HS	
								5	1.50	1.50	31.94	33.44	33.29	IW, IWGM	
								6	1.50	1.50	33.44	34.94	34.79		
								7	0.95	0.95	34.94	35.89	36.29		Liner patch placed at bottom to accommodate gas expansion
								CC(w/7)	0.25	0.25	35.89	36.14	37.24	PAL	
								Totals:	10.24	10.24					

Notes: UTC = Universal Time Coordinated. The notation "CC(w/x)" refers to the D-tube in which the core catcher is stored, where x is the section number (1–9 or CC). NS = no section, IW = interstitial waters, IWGM = interstitial waters glass Matsumoto, HS = headspace, PAL = paleontology, VAC = vacutainer, SOLH = Solheid. Only a portion of this table appears here. The complete table is available in **ASCII format.**

Table T3. Site 1144 composite depths.

Core	Depth (mbsf)	Cumulative offset (m)	Depth (mcd)
184-1144A-			
1H	0	0.46	0.46
2H	6.9	1.79	8.69
3H	16.4	1.57	17.97
4H	25.9	1.35	27.25
5H	35.4	1.49	36.89
6H	44.9	3.43	48.33
7H	54.4	5.26	59.66
8H	63.9	6.73	70.63
9H	73.4	6.39	79.79
10H	82.9	8.27	91.17
11H	92.4	8.33	100.73
12H	101.9	11.80	113.70
13H	111.4	11.63	123.03
14H	120.9	11.52	132.42
15H	130.4	11.66	142.06
16H	139.9	11.80	151.70
17H	149.4	12.12	161.52
18H	158.9	14.17	173.07
19H	168.4	16.67	185.07
20H	177.9	16.81	194.71
21H	187.4	18.12	205.52
22H	196.9	18.87	215.77
23H	206.4	19.32	225.72
24H	215.9	23.00	238.90
25H	225.4	25.91	251.31
26X	234.9	25.25	260.15
27X	241.3	27.29	268.59
28X	250.9	28.27	279.17
29X	260.5	28.45	288.95
30X	270.1	30.39	300.49
31X	279.7	31.13	310.83
32X	289.3	32.78	322.08
33X	299.0	34.22	333.22
34X	308.6	33.54	342.14
35X	318.2	37.54	355.74
36X	327.9	42.49	370.39
37X	337.5	40.55	378.05
38X	347.1	44.15	391.25
39X	356.7	44.75	401.45
40X	366.4	46.45	412.85
41X	376.0	49.97	425.97
42X	385.6	51.16	436.76
43X	395.2	53.00	448.20
44X	404.8	55.74	460.54
45X	414.4	57.18	471.58
46X	424.0	59.21	483.21
47X	433.6	61.93	495.53
48X	443.2	65.40	508.60
184-1144B-			
2H	0.1	3.38	3.48
3H	9.6	3.44	13.04
4H	19.1	1.86	20.96
5H	28.6	3.30	31.90
6H	38.1	4.70	42.80
7H	47.6	5.50	53.10
8H	57.1	7.69	64.79
9H	66.6	7.62	74.22
10H	76.1	8.75	84.85
11H	85.6	9.53	95.13
12H	95.1	10.67	105.77
13H	104.6	14.65	119.25
14H	114.1	14.64	128.74
15H	123.6	14.22	137.82
16H	133.1	13.70	146.80
17H	142.6	13.32	155.92
18H	152.1	14.84	166.94
19H	161.6	16.29	177.89
20H	171.1	15.55	186.65
21H	180.6	16.17	196.77
22H	190.1	20.08	210.18
23X	199.6	19.94	219.54
24X	209.2	21.40	230.60
25X	218.8	27.29	246.09
26X	228.5	28.65	257.15
27X	234.1	28.81	262.91
28X	243.8	29.77	273.57
29X	253.5	29.93	283.43
30X	263.2	32.79	295.99
31X	272.8	31.15	303.95
32X	282.5	32.75	315.25
33X	292.2	34.86	327.06
34X	301.9	35.98	337.88
35X	311.5	35.46	346.96
36X	321.1	39.75	360.85
37X	330.7	40.87	371.57
38X	340.3	41.71	382.01
39X	350.0	44.89	394.89
40X	359.7	44.37	404.07
41X	369.3	47.89	417.19
42X	378.9	52.59	431.49
43X	388.5	52.28	440.78
44X	398.1	53.58	451.68
45X	407.8	56.52	464.32
46X	417.5	58.45	475.95
47X	426.9	59.31	486.21
48X	436.5	63.74	500.24
49X	446.1	67.19	513.29
184-1144C-			
1H	0	0.00	0.00
2H	8.7	–0.24	8.46
3H	18.2	–0.24	17.96
4H	27.7	4.04	31.74
5H	42.2	3.60	45.80
6H	51.7	4.40	56.10
7H	61.2	6.67	67.87
8H	70.7	7.85	78.55
9H	80.2	8.69	88.89
10H	89.7	8.65	98.35
11H	99.2	11.77	110.97
12H	108.7	13.79	122.49
13H	118.2	14.46	132.66
14H	127.7	11.50	139.20
15H	137.2	13.08	150.28
16H	146.7	12.58	159.28
17H	156.2	14.41	170.61
18H	165.7	15.96	181.66
19H	175.2	16.84	192.04
20H	184.7	17.07	201.77
21H	194.2	19.56	213.76

Note: This table is also available in **ASCII format.**

Table T4. Site 1144 splice tie points.

Hole, core, section, interval (cm)	Depth (mbsf)	Depth (mcd)		Hole, core, section, interval (cm)	Depth (mbsf)	Depth (mcd)
1144C-1H-1, 0	0	0				
1144C-1H-5, 7	6.07	6.07	Tie to	1144B-2H-2, 108	2.69	6.07
1144B-2H-5, 87	6.97	10.35	Tie to	1144A-2H-2, 15	8.56	10.35
1144A-2H-7, 46	16.36	18.15	Tie to	1144A-3H-1, 18	16.58	18.15
1144A-3H-3, 54	19.94	21.51	Tie to	1144B-4H-1, 55	19.65	21.51
1144B-4H-6, 79	27.39	29.25	Tie to	1144A-4H-2, 46	27.90	29.25
1144A-4H-4, 80	31.24	32.59	Tie to	1144B-5H-1, 68	29.29	32.59
1144B-5H-6, 24	36.34	39.64	Tie to	1144A-5H-2, 123.5	38.15	39.64
1144A-5H-5, 104	42.44	43.93	Tie to	1144B-6H-1, 111.5	39.23	43.93
1144B-6H-6, 135	46.95	51.65	Tie to	1144A-6H-3, 32	48.22	51.65
1144A-6H-7, 28	54.18	57.61	Tie to	1144C-6H-1, 151	53.21	57.61
1144C-6H-4, 120	57.40	61.80	Tie to	1144A-7H-2, 64	56.54	61.80
1144A-7H-6, 95	62.54	67.80	Tie to	1144B-8H-2, 151	60.11	67.80
1144B-8H-6, 24	64.84	72.53	Tie to	1144C-7H-4, 16	65.86	72.53
1144C-7H-6, 15	68.80	75.47	Tie to	1144B-9H-2, 100.5	67.85	75.47
1144B-9H-6, 119	74.00	81.62	Tie to	1144A-9H-2, 30	75.23	81.62
1144A-9H-7, 55	82.95	89.34	Tie to	1144C-9H-1, 44	80.65	89.34
1144C-9H-6, 8	87.67	96.36	Tie to	1144B-11H-1, 122.5	86.83	96.36
1144B-11H-6, 7	93.17	102.70	Tie to	1144C-10H-3, 135	94.05	102.70
1144C-10H-6, 31	97.51	106.16	Tie to	1144B-12H-1, 39	95.49	106.16
1144B-12H-6, 143	104.03	114.70	Tie to	1144A-12H-1, 98.5	102.90	114.70
1144A-12H-7, 7	110.05	121.85	Tie to	1144B-13H-2, 109.5	107.20	121.85
1144B-13H-7, 39	113.99	128.64	Append to	1144B-14H-1, 0	114.10	128.74
1144B-14H-7, 39	123.09	137.73	Append to	1144B-15H-1, 0	123.60	137.82
1144B-15H-6, 71	131.04	145.26	Tie to	1144A-15H-3, 15	133.60	145.26
1144A-15H-8, 55	140.18	151.84	Tie to	1144A-16H-1, 13.5	140.04	151.84
1144A-16H-5, 23	146.05	157.85	Tie to	1144B-17H-2, 132	144.53	157.85
1144B-17H-7, 31	151.01	164.33	Tie to	1144A-17H-2, 135	152.21	164.33
1144A-17H-6, 119	158.08	170.20	Tie to	1144B-18H-3, 105	155.36	170.20
1144B-18H-6, 111	159.90	174.74	Tie to	1144A-18H-2, 14	160.57	174.74
1144A-18H-6, 104	167.44	181.61	Tie to	1144B-19H-3, 72	165.32	181.61
1144B-19H-5, 55	168.15	184.44	Tie to	1144C-18H-3, 111	168.48	184.44
1144C-18H-7, 80	174.17	190.13	Tie to	1144B-20H-3, 48	174.58	190.13
1144B-20H-6, 119	179.71	195.26	Tie to	1144A-20H-1, 51	178.45	195.26
1144A-20H-6, 80	186.13	202.94	Tie to	1144C-20H-2, 80	185.87	202.94
1144C-20H-7, 127	193.82	210.89	Tie to	1144B-22H-1, 67	190.81	210.89
1144B-22H-6, 119	198.70	218.78	Tie to	1144A-22H-2, 151	199.91	218.78
1144A-22H-6, 95	205.35	224.22	Tie to	1144B-23X-4, 15.5	204.28	224.22
1144B-23X-6, 23	207.33	227.27	Tie to	1144A-23H-2, 31	207.95	227.27
1144A-23H-7, 95	216.09	235.41				

Note: This table is also available in **ASCII format.**

Table T5. Volcanic ash layers recovered at Site 1144.

Core, section, interval (cm)	Top (mbsf)	Top (mcd)	Bottom (mbsf)	Bottom (mcd)	Thickness (cm)	Description
184-1144A-						
5H-3, 80-82	39.20	40.69	39.22	40.71	1.5	Light gray bioturbated volcanic ash
11H-5, 139-139	99.79	108.12	99.79	108.12	0.5	Thin, discontinuous light gray ash with sharp basal contact
18H-3, 0-6	161.90	176.07	161.96	176.13	6.0	Graded ash with sharp basal contact
18H-5, 0-5	164.90	179.07	164.95	179.12	5.0	Graded ash with sharp basal contact
21H-4, 79-81	192.69	210.81	192.71	210.83	2.0	Quartz sandy silt (altered volcanic ash?)
22H-4, 103-104	202.43	221.30	202.44	221.31	1.0	Light gray silt-size volcanic ash
38X-4, 86-90	352.46	396.61	352.50	396.65	4.0	Dispersed and bioturbated greenish gray volcanic ash
48X-5, 2-5	449.25	514.65	449.28	514.68	3.0	Volcanic ash, spherules, and pyrite lenticular bed
184-1144B-						
18H-7, 92-98	161.21	176.05	161.27	176.11	6.0	Graded ash
25X-3, 6-8	221.86	249.15	221.88	249.17	2.0	Dispersed light gray volcanic ash
30X-2, 11-13	264.82	297.60	264.83	297.62	2.0	Light gray, strongly bioturbated ash
30X-6, 138-143	272.07	304.86	272.13	304.92	6.0	Light gray, strongly bioturbated ash
39X-1, 136-136	351.36	396.25	351.36	396.26	1.0	Dispersed and bioturbated volcanic ash
40X-6, 118-119	368.38	412.75	368.39	412.76	1.0	Dispersed and bioturbated volcanic ash
184-1144C-						
4H-4, 4-6	32.24	36.28	32.26	36.30	2.0	Light colored volcanic ash, with sharp base and normal grading
17H-4, 93-96	161.60	176.01	161.66	176.07	6.0	Light gray volcanic ash, with sharp base and normal grading upward

Table T6. Summary of biohorizons at Site 1144.

Code	Events	Top			Bottom			Age (Ma)	Average depth (mcd)	Average sedimentation rate (m/m.y.)
		Core, section, interval (cm)	Depth (mbsf)	Depth (mcd)	Core, section, interval (cm)	Depth (mbsf)	Depth (mcd)			
		184-1144A-			184-1144A-					
CN	FO *E. huxleyi* acme	7H-CC, 31-37	64.30	**69.56**	8H-CC, 25-31	73.74	80.47	0.09	75.02	
PF	LO pink *G. ruber*	10H-CC, 21-27	92.54	100.81	11H-CC, 10-16	102.30	**110.63**	0.12	101.72	**930**
CN	FO *E. huxleyi**	23H-CC, 14-20	216.38	**235.70**	24H-CC, 15-21	225.26	248.26	0.26	241.98	———
PF	FO pink *G. ruber*	24H-CC, 15-21	225.26	**248.26**	25H-CC, 21-27	235.39	261.30	0.40	254.78	
CN	LO *P. lacunosa*	27X-CC, 35-41	250.78	278.07	28X-CC, 39-45	260.42	**288.69**	0.46	283.38	**310**
BF	LO *Stilostomella*	34X-CC, 30-36	318.47	352.01	35X-CC, 25-31	328.00	**365.54**	0.75	358.78	
CN	LO *R. asanoi**	39X-CC, 31-37	366.56	411.31	40X-CC, 31-37	376.23	**422.68**	0.83	417.00	———
CN	LO small *Gephyrocapsa* acme*	46X-CC, 43-49	433.84	493.05	47X-CC, 24-30	443.19	**505.32**	1.01	499.19	**460**

Notes: FO = first occurrence, LO = last occurrence. CN = calcareous nannofossils, PF = planktonic foraminifers, BF = benthic foraminifers, * = events used in calculating average sedimentation rate. Depth for the top and bottom of biostratigraphic events = the mean of the sample interval. Sources of reference age for all biostratigraphic events are listed in Tables T2, p. 42, and T3, p. 43, both in the "Explanatory Notes" chapter. Bars in average sedimentation rate column indicate the range of samples to which the average sedimentation rate applies. Depth in boldface indicates where the marker species was observed highest or lowest in the studied samples.

Table T7. Calcareous nannofossil checklist for Site 1144.

Epoch	Zone	Core, section, interval (cm)	Depth (mbsf)	Depth (mcd)	Abundance	Preservation	*Calcidiscus leptoporus*	*Ceratolithus cristatus*	*Coccolithus pelagicus*	*Florisphaera profunda*	*Gephyrocapsa* spp. (small)	*Helicosphaera carteri*	*Pontosphaera* spp.	*Pseudoemiliania lacunosa*	*Reticulofenestra asanoi*	*Reticulofenestra* (small-medium sized)	*Rhabdosphaera clavigera*	*Syracosphaera pulchra*	*Umbilicosphaera sibogae*	*Gephyrocapsa caribbeanica*	*Gephyrocapsa margarelii*	*Gephyrocapsa oceanica*	*Helicosphaera hyalina*	*Helicosphaera pavimentum*	*Oolithotus antillarum*	*Scapholithus fossilis*	*Syracosphaera* spp.	*Thorosphaera flabellata*	*Discosphaera tubifera*	*Umbellosphaera irregularis*	*Discoaster pentaradiatus*	*Reticulofenestra pseudoumbilicus*	*Sphenolithus abies/neoabies*	*Discoaster brouweri*	*Discoaster variabilis*	*Emiliania huxleyi*	*Helicosphaera wallichii*	*Umbellosphaera tenuis*
		184-1144A-																																			
		1H-CC, 10-13	6.80	7.26	A	VG	C			A	R	C	F	R			F	F	C		C	A			F	F		R	F						A	
		2H-CC, 15-19	16.61	18.41	A	VG	R	R	R	C	C	C	F	F		F	R	R	C	F	C	A			R	R		R	R	F	F	F	F	A	
		3H-CC, 28-35	26.54	28.15	A	VG	F			A	F	F					F	C	C	R	R	A	R	R	R	R	R		R	F				A	R	R
	NN21B	4H-CC, 18-25	36.07	37.46	A	VG	F		R	A	F	F					F	F	R			A			R	R	R		R					A	R	
		5H-CC, 20-27	45.32	46.85	A	VG	F			A	F	F	R				C	F	C			A	R		R	F	R	F	R					A	R	
		6H-CC, 33-40	55.10	58.57	A	VG	F			A	F	F					C	F	C			A	R	R	R	R	R							A	R	R
		7H-CC, 30-37	64.26	69.56	A	VG	C	R	R	A	C	C					F	F	C	R	F	A	R			R			R					A	R	
		8H-CC, 24-31	73.70	80.47	A	VG	F			A	F	F					F	R	F	R	R	C	R		R		R		R	R				A		R
		9H-CC, 27-33	83.46	89.88	A	VG	F	R		A	C	F					C	F	F	F		C			R		R			R				A		
		10H-CC, 20-27	92.50	100.81	A	G	F			A	D	F	R				F	F	C			C	R		R	F				R				C		
		11H-CC, 9-16	102.26	110.63	A	G	F		R	A	A	F					F	C	C	R		A	R		R	R	R	R		R				C		
		12H-CC, 26-31	111.64	123.46	A	G	F	R		A	A	F					R	C	C			C				R	R			R				C		
		13H-CC, 14-21	121.16	132.83	A	G	F	R	R	A	A	R	R				F	C	C	R		A	R		R	R	R		R	R				C		
		14H-CC, 33-40	130.93	142.49	A	G	R			A	C	R					R	F	F		F	C	R		R	F	R							C	R	
	NN21A	15H-CC, 29-36	140.62	152.32	A	G	F			A	A	F					F	F	C		R	C	R		R	R	R			R				C		
		16H-CC, 44-51	150.09	161.93	A	G	F	R	R	A	C	F	R				F	R	F			A	R		R		R							C		
		17H-CC, 20-27	159.40	171.56	A	G	F	R		A	A	F					F	F	F	R		A	R		R	R	R			R				C		
		18H-CC, 11-18	168.89	183.10	A	G	F	R	R	D	A	F	R				R	F	F			A	R	F	R									C	R	
		19H-CC, 0-7	177.98	194.69	A	G	F			C	A	F	F			R	R	R	F	C	C	A					R			R		R		F		
		20H-CC, 0-7	187.14	203.99	A	G	F			C	A	F	F				R		F	A	C	C								R	F			R		
		21H-CC, 22-26	197.41	215.54	A	G	F			F	A	R	R	R		F	R	R	R	A	C	C					R		R	R	R	R			R		
		22H-CC, 0-5	206.49	225.38	A	G	R		R	F	A	R	R	R		F	R	R		A	C	C													R		
		23H-CC, 16-20	216.37	235.70	A	G	R	R		F	A	R	R	R		R	R	R	R	A	C	C				R			R	R	R	R	R		R		
		24H-CC, 17-21	225.25	248.26	A	M	R	R		F	A	R	R	R		R	R	R	R	D	C	F				R				R							
Pleistocene	NN20	25H-CC, 22-27	235.37	261.30	A	M	R	R	R	F	A	R	R	R		F	R	R	R	A	C	F				R			R	R	F	R	R	R	R	R	
		26X-CC, 28-33	242.49	267.76	A	G																															
		27X-CC, 37-41	250.77	278.07	A	G	R		R	F	A	R	R	R		R	R	R	R	A	C	F				R			R	R	R	R				
		28X-CC, 39-45	260.39	288.69	A	G	R	R		F	A	R	R	C		R	R	R	R	A	C	F							R	R	R	R				
		29X-CC, 35-40	270.27	298.74	A	G	R			F	A	R	R	C		R	R	R	R	C	C	F				R			R	R	R	R	R			
		30X-CC, 31-36	279.79	310.20	A	G	R	R		F	A	R	R	C		R	R	R	R	C	C	C							R	R	R	R	R			
		31X-CC, 21-26	289.31	320.46	A	G	R	R		F	A	R	R	C		R	R	R	R	C	C	C				R				R	R	R				
		32X-CC, 37-42	299.17	331.97	A	G	R	R		F	A	R	R	C		R	R	R	R	C	C	C							R	R		R	R			
		33X-CC, 40-45	308.88	343.12	A	G	R			F	A	R	R	C		R	R	R	R	C	C	C								R	R	R				
		34X-CC, 32-36	318.46	352.01	A	G	R	R		F	A	R	R	C		R	R	R	R	C	C	C				R			R	R	R	R	R			
		35X-CC, 23-31	327.95	365.54	A	M	R	R		F	A	R	R	C		R	R	R	R	C	C	C				R				R	R	R				
		36X-CC, 22-30	337.52	380.06	A	M	F			A	A	F	R	F		R	F	F	F	F	F	A	R			R		R	R								
		37X-CC, 27-34	347.22	387.81	A	M	F			A	A	F		C	R	F		F	C			C	R		R	R											
	NN19b	38X-CC, 31-38	356.87	401.06	A	M	C			A	A	F	R	C	R	C		F	F			C	R		R	R											
		39X-CC, 30-37	366.52	411.31	A	M	C	R		A	A	F	R	C	R	F	F	R	F		F	A	R	F		R											
		40X-CC, 30-37	376.19	422.68	A	M	F	R		A	C	R	R	C	F	F	R	R	R			A				R											
		41X-CC, 33-40	385.87	435.88	A	M	F	R		A	A	F	R	C	C	R	F	F	C		F	A		R													
		42X-CC, 31-38	395.41	446.61	A	M	F	R	R	D	A	R		C	F	R	C	C	C			R	R	F	R	R	R	C									
		43X-CC, 36-43	405.02	458.06	A	M	R	R		A	D	F		C	R	F	C	R	F	F		C		R													
		44X-CC, 26-33	414.51	470.29	A	M	R		R	A	A	F	R	C	R	F	R	R	F	F		C															
		45X-CC, 32-39	424.28	481.50	A	M	R		R	A	C	F		C		C	R	R	R	R	F	C															
		46X-CC, 42-49	433.80	493.05	A	M	F	R	R	A	A	F		C		C	R	R	F	F	F	C	R	R													
		47X-CC, 23-30	443.35	505.32	A	M	F	R		D	C	F		A	R	C	C	R	F																		
		48X-CC, 31-38	453.02	518.46	A	M	F	R	R	D	C	R	R	A	R	C	C	R	F																		

Notes: D = dominant, A = abundant, C = common, F = few/frequent, R = rare, VG = very good, G = good, M = moderate, P = poor. See "Biostratigraphy," p. 9, in the "Explanatory Notes" chapter.

Table T8. Planktonic foraminifer checklist for Site 1144.

Epoch	Zone	Core, section, interval (cm)	Depth (mbsf)	Depth (mcd)	Abundance	Preservation	*Globigerinoides ruber*	*Globorotalia inflata*	*Globorotalia menardii*	*Globorotalia truncatulinoides*	*Pulleniatina obliquiloculata*	*Neogloboquadrina dutertrei*	*Globorotalia crassaformis*	*Globorotalia tumida*	*Globigerinoides ruber* (pink)	*Sphaeroidinella dehiscens*
		184-1144A-														
		1H-CC, 10-13	6.80	7.26	A	VG	A	F								
		2H-CC, 15-19	16.61	18.41	A	VG	A	F					R			
		3H-CC, 28-35	26.54	28.15	A	VG	A	F		P	R	F				
		4H-CC, 18-25	36.07	37.46	A	VG	A	R		P	R	F	P			
		5H-CC, 20-27	45.32	46.85	A	VG	A	F			R	F	R			
		6H-CC, 33-40	55.10	58.57	A	VG	A	F			F	F	F			
		7H-CC, 30-37	64.26	69.56	A	VG	A	F			F	F	F			
		8H-CC, 24-31	73.70	80.47	A	VG	A	F		P	F	F	F			P
		9H-CC, 27-33	83.46	89.88	A	VG	A	F		P	F	F	R			P
		10H-CC, 20-27	92.50	100.81	A	VG	A	F		R	F	F				P
		11H-CC, 9-16	102.26	110.63	A	VG	A	F			F	F	R		R	P
		12H-CC, 26-31	111.64	123.46	A	VG	A	F		P	F	F			R	
		13H-CC, 14-21	121.16	132.83	A	VG	A	F			F	F	F		R	
		14H-CC, 33-40	130.93	142.49	A	VG	F	A			F	A	P		F	
		15H-CC, 29-36	140.62	152.32	A	VG		F	F	R		A			R	
		16H-CC, 44-51	150.09	161.93	A	VG	F		F	P	A	A			P	
		17H-CC, 20-27	159.40	171.56	A	VG	A		F			A	R		R	
		18H-CC, 11-18	168.89	183.10	A	VG	F	F	F	R	A	A			R	
		19H-CC, 0-7	177.98	194.69	A	VG		F		P	F	A			F	
		20H-CC, 0-7	187.14	203.99	A	VG	A	R	R	P	F	A			R	
		21H-CC, 22-26	197.41	215.54	A	VG			F	R	A		R		R	
		22H-CC, 0-5	206.49	225.38	A	VG	A	A		P	F		P		F	
		23H-CC, 16-20	216.37	235.70	A	VG	A	A		P	F	A	P		R	
Pleistocene	N22	24H-CC, 17-21	225.25	248.26	A	VG	A		R		F	A			P	
		25H-CC, 22-27	235.37	261.30	A	VG	F	F				F	R			
		26X-CC, 28-33	242.49	267.76	A	VG	A	A		R	R	F				
		27X-CC, 37-41	250.77	278.07	A	VG	A	A		P	R	A				
		28X-CC, 39-45	260.39	288.69	A	VG	A	F			R	F		R		
		29X-CC, 35-40	270.27	298.74	A	VG	R	F	F	P	A		P			
		30X-CC, 31-36	279.79	310.20	A	VG	R	A		P	F	F	P			
		31X-CC, 21-26	289.31	320.46	A	VG	R	F		P	A		P			
		32X-CC, 37-42	299.17	331.97	A	VG	F	A			F	A				
		33X-CC, 40-45	308.88	343.12	A	VG	R	A			A		P			
		34X-CC, 32-36	318.46	352.01	A	VG				R			P			
		35X-CC, 23-31	327.95	365.54	A	VG		F	R		F	A	P			
		36X-CC, 22-30	337.52	380.06	A	VG	R	A		P	A		P			
		37X-CC, 27-34	347.22	387.81	A	VG	A	A	F	P	F		P			
		38X-CC, 31-38	356.87	401.06	A	VG	A	A	F		R		P			
		39X-CC, 30-37	366.52	411.31	A	VG	A	F		P	F					
		40X-CC, 30-37	376.19	422.68	A	VG	F		F		F		P			
		41X-CC, 33-40	385.87	435.88	A	VG	F		F	P	F		P			
		42X-CC, 31-38	395.41	446.61	A	VG	F		F	R	A		P			
		43X-CC, 36-43	405.02	458.06	A	VG	F			R	A					
		44X-CC, 26-33	414.51	470.29	A	VG	F	F	R	R	A		P			
		45X-CC, 32-39	424.28	481.50	A	VG	A		F	R	A		P			
		46X-CC, 42-49	433.80	493.05	A	VG	F	R	R	R	F		P			
		47X-CC, 23-30	443.35	505.32	A	VG	A			P	F	A				
		48X-CC, 31-38	453.02	518.46	A	VG	A	F	F	P	F					

Notes: D = dominant, A = abundant, C = common, F = few/frequent, R = rare, VG = very good, G = good, M = moderate, P = poor. See **"Biostratigraphy,"** p. 9, in the "Explanatory Notes" chapter.

Table T9. Sedimentation and accumulation rates for selected intervals, based on age-depth model and rates presented in Figure F17, p. 51.

	Bottom of interval					
	Age (Ma)	Depth (mcd)	LSR total (m/m.y.)	LSR carbonate (m/m.y.)	MAR total ($g/cm^2/k.y.$)	MAR carbonate ($g/cm^2/k.y.$)
NN21/NN20	0.26	241.9	937.0	123.5	91.3	12.12
Brunhes/Matuyama	0.78	396.4	324.0	47.1	37.0	5.36
Bottom of hole	1.05	518.6	457.0	67.8	60.6	9.01

Notes: LSR = linear sedimentation rate for total sediment and inorganic carbonate; MAR = mass accumulation rate for total sediment and inorganic carbonate. Brunhes/Matuyama was not observed at this site and was instead interpolated using the LO of the *Reticulofenestra asanoi* datum at 0.83 Ma.

Table T10. Methane concentrations at Site 1144 as obtained by headspace and void-space analysis.

Core, section, interval (cm)	Depth (mbsf)	Depth (mcd)	HS CH_4 concentration (ppmv)	HS CH_4 concentration (ppmv) [normalized]	VS CH_4 concentration (ppmv)
184-1144A-					
1H-3, 0-5	3.00	3.46	2.7	2	
2H-5, 0-5	12.90	14.69	4,847.0	5,043	
3H-4, 0-5	20.90	22.47	64,982.0	81,532	
4H-4, 0-5	30.44	31.79	37,684.0	53,586	380,821
5H-4, 0-5	39.90	41.39	48,919.0	43,028	328,217
6H-4, 0-5	49.40	52.83	48,248.0	50,821	
7H-4, 0-5	58.59	63.85	33,680.0	43,539	460,847
8H-4, 0-5	68.40	75.13	32,675.0	31,324	381,037
9H-4, 0-5	77.90	84.29	35,151.0	29,694	237,306
10H-4, 0-5	87.40	95.67	42,972.0	35,253	345,306
11H-3, 0-5	95.40	103.73	18,813.0	20,064	427,502
12H-3, 0-5	104.90	116.70	25,773.0	24,707	315,557
13H-3, 0-5	114.40	126.03	19,244.0	21,050	361,280
14H-3, 0-5	123.41	134.93	11,531.0	9,938	370,530
15H-3, 0-5	133.45	145.11	24,834.0	23,542	281,964
16H-3, 0-5	142.82	154.62	13,537.0	11,785	260,501
17H-3, 0-5	152.36	164.48	12,742.0	14,119	451,468
18H-3, 0-5	161.90	176.07	7,759.0	7,118	391,125
19H-3, 0-5	171.40	188.07	9,963.0	16,347	559,544
20H-3, 0-5	180.90	197.71	3,862.0	5,884	759,284
21H-3, 0-5	190.40	208.52	12,125.0	16,164	
22H-3, 0-5	199.90	218.77	6,193.0	7,770	693,133
23H-4, 10-15	210.74	230.06	14,613.0	15,585	57,014
24H-4, 0-5	220.40	243.40	11,492.0	12,570	664,711
25H-4, 0-5	229.90	255.81	11,028.0	16,507	711,319
26X-4, 0-5	239.40	264.65	14,438.0	12,196	715,168
27X-4, 0-5	245.80	273.09	11,624.0	16,258	
28X-4, 0-5	255.40	283.67	11,794.0	15,019	588,091
29X-3, 0-5	263.50	291.95	25,198.0	26,542	284,481
31X-4, 0-5	284.20	315.33	22,170.0	19,106	301,996
32X-4, 0-5	293.80	326.58	19,789.0	23,780	363,408
33X-4, 0-5	303.50	337.72	21,819.0	25,501	320,896
34X-4, 0-5	313.10	346.64	23,760.0	23,849	580,584
35X-4, 0-5	322.70	360.24	17,484.0	21,310	367,427
36X-4, 0-5	332.40	374.89	21,003.0	22,974	
37X-3, 0-5	340.50	381.05	54,131.0	40,512	
38X-3, 0-5	350.10	394.25	37,515.0	29,637	
39X-3, 0-5	359.70	404.45	46,061.0	35,088	
40X-3, 0-5	369.40	415.85	60,589.0	43,440	
41X-3, 0-5	379.00	428.97	31,812.0	29,502	
42X-3, 0-5	388.60	439.76	26,980.0	25,577	
43X-3, 0-5	398.20	451.20	36,020.0	28,456	
44X-3, 0-5	407.80	463.54	17,095.0	22,790	
45X-3, 0-5	417.41	474.59	22,700.0	17,607	
46X-3, 0-5	427.00	486.21	8,225.0	8,256	
47X-3, 0-5	436.40	498.53	5,783.0	4,790	
48X-3, 0-5	446.01	511.61	2,925.0	2,290	

Notes: Headspace normalized to weight of sample is also listed. HS = headspace, VS = void space.

Table T11. Inorganic carbon, carbonate, total carbon, total organic carbon, total nitrogen, and total sulfur contents at Site 1144. (See table note. Continued on next two pages.)

Core, section, interval (cm)	Depth (mbsf)	Depth (mcd)	IC (wt%)	$CaCO_3$ (wt%)	TC (wt%)	TOC (wt%)	TN (wt%)	TS (wt%)	C/N
184-1144A-									
1H-1, 107-108	1.07	1.53	1.47	12.23	2.20	0.73	0.21	0.14	3.47
1H-3, 107-108	4.07	4.53	1.31	10.94	1.95	0.64	0.16	0.15	3.93
2H-1, 107-108	7.97	9.76	1.62	13.46	2.77	1.15	0.23	0.59	4.98
2H-3, 107-108	10.97	12.76	1.33	11.05	2.53	1.21	0.22	0.64	5.58
2H-5, 107-108	13.97	15.76	1.21	10.09	2.56	1.35	0.16	0.75	8.59
3H-1, 107-108	17.47	19.04	1.33	11.04	2.45	1.12	0.19	0.41	6.03
3H-3, 107-108	20.47	22.04	1.31	10.91	2.39	1.08	0.21	0.28	5.15
3H-5, 107-108	23.47	25.04	1.27	10.62	2.32	1.04	0.19	0.31	5.48
4H-1, 107-108	26.97	28.32	1.26	10.53	2.26	1.00	0.17	0.23	5.86
4H-3, 107-108	30.01	31.36	1.46	12.14	2.56	1.10	0.20	0.32	5.36
4H-5, 107-108	33.01	34.36	1.25	10.38	2.28	1.03	0.19	0.35	5.33
5H-1, 107-108	36.47	37.96	1.30	10.87	2.43	1.12	0.15	0.34	7.47
5H-3, 107-108	39.47	40.96	1.39	11.56	2.39	1.00	0.15	0.20	6.76
5H-5, 107-108	42.47	43.96	1.42	11.81	2.47	1.05	0.19	0.39	5.63
6H-1, 107-108	45.97	49.40	1.57	13.07	2.67	1.10	0.15	0.27	7.34
6H-3, 107-108	48.97	52.40	1.51	12.54	2.54	1.03	0.15	0.30	7.06
6H-5, 107-108	51.97	55.40	1.58	13.20	2.46	0.88	0.14	0.22	6.35
7H-1, 107-108	55.47	60.73	1.58	13.13	2.56	0.98	0.19	0.24	5.07
7H-3, 107-108	58.29	63.55	1.53	12.71	2.39	0.87	0.18	0.26	4.73
7H-5, 107-108	61.16	66.42	1.52	12.69	2.48	0.96	0.20	0.26	4.90
8H-1, 107-108	64.97	71.70	1.59	13.21	2.46	0.88	0.14	0.21	6.33
8H-3, 107-108	67.97	74.70	1.19	9.93	1.96	0.77	0.17	0.19	4.42
8H-5, 107-108	70.97	77.70	1.04	8.65	1.69	0.65	0.14	0.07	4.60
9H-1, 107-108	74.47	80.86	1.40	11.68	2.12	0.72	0.13	0.12	5.58
9H-3, 107-108	77.47	83.86	1.51	12.57	2.28	0.77	0.15	0.75	5.27
9H-5, 107-108	80.47	86.86	1.40	11.70	2.16	0.76	0.13		5.85
10H-1, 107-108	83.97	92.24	1.20	10.02	1.89	0.69	0.16	0.13	4.37
10H-3, 107-108	86.97	95.24	1.42	11.87	2.21	0.79	0.12		6.30
10H-5, 107-108	89.92	98.19	1.59	13.25	2.35	0.76	0.12		6.32
11H-1, 107-108	93.47	101.80	1.80	14.96	2.77	0.97	0.15	0.60	6.65
11H-3, 107-108	96.47	104.80	1.26	10.51	1.95	0.69	0.12		5.74
11H-5, 107-108	99.47	107.80	1.42	11.83	2.14	0.72	0.18	0.17	4.06
12H-1, 107-108	102.97	114.77	1.77	14.77	2.58	0.81	0.13		6.16
12H-3, 107-108	105.97	117.77	1.53	12.72	2.57	1.04	0.14		7.39
12H-5, 107-108	108.97	120.77	1.62	13.50	2.60	0.98	0.20	0.60	5.00
13H-1, 107-108	112.47	124.10	1.37	11.38					
13H-3, 107-108	115.47	127.10	1.49	12.39					
13H-5, 107-108	118.47	130.10	1.57	13.08	2.44	0.87	0.14	0.32	6.10
14H-1, 97-98	121.87	133.39	1.41	11.78					
14H-3, 107-108	124.48	136.00	1.48	12.31					
14H-5, 107-108	127.43	138.95	1.42	11.81	2.24	0.83	0.12	0.19	7.06
15H-1, 107-108	131.47	143.13	1.67	13.88					
15H-3, 107-108	134.52	146.18	1.80	14.97	2.67	0.87	0.17	0.26	5.13
15H-5, 107-108	137.52	149.18	1.57	13.11					
15H-7, 107-108	139.2	150.86	1.43	11.87	2.16	0.74	0.12	0.27	6.07
16H-1, 107-108	140.97	152.77	1.47	12.26					
16H-3, 107-108	143.89	155.69	1.47	12.26	2.44	0.97	0.13		7.29
16H-5, 107-108	146.89	158.69	1.44	12.03					
17H-1, 107-108	150.47	162.59	1.17	9.71	1.83	0.67	0.12		5.77
17H-3, 107-108	153.43	165.55	1.22	10.12	2.17	0.95	0.14		6.83
17H-5, 107-108	156.46	168.58	1.37	11.42	2.11	0.74	0.20	0.15	3.73
18H-1, 107-108	159.97	174.14	1.30	10.82	2.12	0.82	0.13		6.34
18H-3, 107-108	162.97	177.14	1.70	14.19	2.74	1.04	0.14		7.33
18H-5, 107-108	165.97	180.14	2.10	17.47	2.95	0.85	0.14	0.20	5.89
19H-1, 107-108	169.47	186.14	1.78	14.87	2.64	0.86	0.12		7.02
19H-3, 107-108	172.47	189.14	1.62	13.46					
19H-5, 107-108	175.47	192.14	1.39	11.61	2.08	0.68	0.17	0.25	4.02
20H-1, 107-108	178.97	195.78	1.87	15.57					
20H-3, 107-108	181.97	198.78	1.84	15.29					
20H-5, 107-108	184.97	201.78	2.57	21.39	3.13	0.56	0.19	0.15	2.97
21H-1, 107-108	188.47	206.59	2.25	18.76					
21H-3, 107-108	191.47	209.59	2.09	17.39					
21H-5, 107-108	194.47	212.59	1.60	13.34	2.28	0.68	0.16	0.31	4.15
22H-3, 107-108	200.97	219.84	1.88	15.66					
22H-5, 107-108	203.97	222.84	2.39	19.88	3.10	0.71	0.20	0.13	3.64

Table T11 (continued).

Core, section, interval (cm)	Depth (mbsf)	Depth (mcd)	IC (wt%)	$CaCO_3$ (wt%)	TC (wt%)	TOC (wt%)	TN (wt%)	TS (wt%)	C/N
23H-1, 107-108	207.47	226.79	1.68	14.00					
23H-3, 107-108	210.21	229.53	1.64	13.62					
23H-5, 107-108	213.21	232.53	1.91	15.90	2.56	0.65	0.12	0.12	5.43
24H-1, 107-108	216.97	239.97	1.38	11.46					
24H-3, 107-108	219.97	242.97	1.27	10.55					
24H-5, 107-108	222.97	245.97	1.91	15.91	2.51	0.60	0.12		4.84
25H-1, 107-108	226.47	252.38	2.11	17.54					
25H-3, 107-108	229.47	255.38	1.82	15.14					
25H-5, 107-108	232.47	258.38	1.63	13.59	2.37	0.74	0.15	0.11	4.83
26X-1, 107-108	235.97	261.22	1.59	13.24					
26X-3, 107-108	238.97	264.22	1.58	13.17					
26X-5, 107-108	241.97	267.22	1.67	13.93	2.43	0.76	0.11	0.10	6.71
27X-1, 107-108	242.37	269.66	1.93	16.06					
27X-3, 107-108	245.37	272.66	2.08	17.29					
27X-5, 107-108	248.37	275.66	2.16	18.01	2.87	0.71	0.18		3.92
28X-1, 107-108	251.97	280.24	1.88	15.62					
28X-3, 107-108	254.97	283.24	1.58	13.15					
28X-5, 107-108	257.97	286.24	1.48	12.36	2.02	0.54	0.11	0.48	4.76
29X-1, 107-108	261.57	290.02	2.82	23.45					
29X-3, 107-108	264.57	293.02	2.21	18.40					
29X-5, 107-108	267.57	296.02	1.52	12.65	2.18	0.66	0.12		5.29
30X-1, 107-108	271.17	301.56	1.29	10.78					
30X-3, 107-108	274.17	304.56	1.70	14.20					
30X-5, 107-108	277.17	307.56	1.44	12.03	2.10	0.66	0.21	0.26	3.16
31X-1, 107-108	280.77	311.90	1.66	13.85					
31X-3, 107-108	283.77	314.90	1.31	10.91					
31X-5, 107-108	286.77	317.90	2.02	16.86	2.68	0.66	0.17	0.09	3.91
32X-1, 107-108	290.37	323.15	1.69	14.06					
32X-3, 107-108	293.37	326.15	1.79	14.95					
32X-5, 107-108	296.37	329.15	1.97	16.43	2.83	0.86	0.15	0.12	5.72
33X-1, 107-108	300.07	334.29	1.86	15.45					
33X-3, 107-108	303.07	337.29	1.96	16.36					
33X-5, 107-108	306.07	340.29	2.05	17.09	2.83	0.77	0.12	0.12	6.23
34X-1, 107-108	309.67	343.21	1.90	15.82					
34X-3, 107-108	312.67	346.21	1.80	15.03					
34X-5, 107-108	315.67	349.21	1.66	13.86	2.24	0.58	0.13		4.29
34X-5, 107-108 (R)	315.67	349.21	1.66	13.86	2.30	0.64	0.10	0.20	6.40
35X-1, 107-108	319.27	356.81	2.23	18.60					
35X-3, 107-108	322.27	359.81	1.70	14.13					
35X-5, 107-108	325.27	362.81	1.53	12.71	2.09	0.56	0.12	0.15	4.79
36X-1, 107-108	328.97	371.46	1.37	11.39					
36X-3, 107-108	331.97	374.46	1.42	11.86					
36X-5, 107-108	334.97	377.46	1.70	14.15	2.36	0.66	0.16	0.24	4.07
37X-1, 107-108	338.57	379.12	1.35	11.28	1.95	0.60	0.11	0.07	5.45
37X-3, 107-108	341.57	382.12	1.80	14.99					
37X-5, 107-108	344.57	385.12	1.85	15.37	2.25	0.40	0.08		4.80
38X-1, 107-108	348.17	392.32	1.84	15.31	2.58	0.74	0.09		8.20
38X-3, 107-108	351.17	395.32	1.45	12.09					
38X-5, 107-108	354.17	398.32	1.40	11.65	1.93	0.53	0.12	0.17	4.49
39X-1, 107-108	357.77	402.52	1.84	15.31					
39X-3, 107-108 (R)	360.77	405.52	1.47	12.22	2.05	0.59	0.11		5.46
39X-3, 107-108	360.77	405.52	1.47	12.22	2.03	0.57	0.09	0.21	6.33
39X-5, 107-108	363.77	408.52	1.76	14.68					
40X-1, 107-108	367.47	413.92	1.78	14.80	2.51	0.73	0.10		7.37
40X-3, 107-108	370.47	416.92	1.61	13.45					
40X-5, 107-108	373.47	419.92	1.95	16.22	2.36	0.42	0.15		2.87
41X-1, 107-108	377.07	427.04	1.27	10.58					
41X-3, 107-108	380.07	430.04	1.27	10.58					
41X-5, 107-108	383.07	433.04	1.74	14.45	2.17	0.43	0.12		3.48
41X-5, 107-108 (R)	383.07	433.04	1.74	14.45	2.12	0.38	0.08	0.06	4.75
42X-1, 107-108	386.67	437.83	1.54	12.87					
42X-3, 107-108	389.67	440.83	2.05	17.09					
42X-5, 107-108	392.67	443.83	1.78	14.85	2.26	0.48	0.10		4.95
43X-1, 107-108	396.27	449.27	1.81	15.05					
43X-3, 107-108	399.27	452.27	1.24	10.35					
43X-5, 107-108	402.27	455.27	1.41	11.78	1.86	0.45	0.11		4.15
43X-5, 107-108 (R)	402.27	455.27	1.41	11.78	1.91	0.50	0.08	0.26	6.25
44X-1, 107-108	405.87	461.61	1.79	14.92					
44X-3, 107-108	408.87	464.61	1.40	11.62					
44X-5, 107-108	411.87	467.61	1.48	12.33	1.78	0.30	0.08		3.62
45X-1, 107-108	415.47	472.65	1.74	14.51					

Table T11 (continued).

Core, section, interval (cm)	Depth (mbsf)	Depth (mcd)	IC (wt%)	$CaCO_3$ (wt%)	TC (wt%)	TOC (wt%)	TN (wt%)	TS (wt%)	C/N
45X-3, 107-108	418.48	475.66	1.44	12.02					
45X-5, 107-108	421.50	478.68	1.39	11.57	1.80	0.41	0.10		4.25
45X-5, 107-108 (R)	421.50	478.68	1.39	11.57	1.80	0.41	0.07	0.05	5.86
46X-1, 107-108	425.07	484.28	1.41	11.73					
46X-3, 107-108	428.07	487.28	2.33	19.43					
46X-5, 107-108	431.07	490.28	1.76	14.64	2.07	0.31	0.10		3.13
47X-1, 107-108	434.67	496.60	1.64	13.66					
47X-3, 107-108	437.67	499.60	1.86	15.47					
47X-5, 107-108	440.67	502.60	2.55	21.21	2.87	0.33	0.08		3.86
47X-5, 107-108 (R)	440.67	502.60	2.55	21.21	2.89	0.35	0.06	0.03	5.83
48X-1, 107-108	444.27	509.67	2.47	20.54					
48X-3, 107-108	447.28	512.68	2.57	21.42					
48X-5, 107-108	450.30	515.70	2.63	21.88	2.92	0.30	0.08		3.61

Note: IC = inorganic carbon, $CaCO_3$= calcium carbonate, TC = total carbon, TOC = total organic carbon, TN = total nitrogen, TS = total sulfur, C/N = carbon/nitrogen ratio, R = replicate.

Table T12. Rock-Eval results for Site 1144, including replicate samples and comparison to TOC by difference data.

Core, section, interval (cm)	Depth (mbsf)	Depth (mcd)	T_{max}	S_1	S_2	S_3	PI	TOC	HI	OI	TOC by difference (wt%)
First Run:											
184-1144A- (except wood)											
2H-5, 107-108	13.97	15.76	409	0.27	1.63	0.45	0.14	1.17	139	38	1.35
6H-1, 107-108	45.97	49.40	409	0.19	1.03	0.40	0.16	0.80	128	50	1.10
12H-5, 107-108	108.97	120.77	412	0.16	1.01	0.34	0.14	0.73	138	46	0.98
18H-5, 107-108	165.97	180.14	408	0.15	0.72	0.34	0.17	0.56	128	60	0.85
24H-5, 107-108	222.97	245.97	389	0.08	0.36	0.34	0.18	0.41	87	82	0.60
28X-5, 107-108	257.97	286.24	388	0.07	0.33	0.32	0.17	0.40	82	80	0.40
32X-5, 107-108	296.37	329.15	404	0.19	0.87	0.38	0.18	0.52	167	73	0.52
39X-3, 107-108	360.77	405.52	387	0.05	0.30	0.30	0.15	0.39	76	76	0.59
43X-5, 107-108	402.27	455.27	371	0.04	0.16	0.23	0.20	0.28	57	82	0.45
48X-5, 107-108	450.30	515.70	382	0.02	0.12	0.32	0.14	0.21	57	152	0.30
184-1144B-											
B24-X wood			329	20.20	54.20	11.40	0.27	39.60	136	28	59.00*
24X-2, 36-37 wood	211.05	232.46									
Second Run:											
184-1144A-											
5H-1, 107-108	36.47	37.96	414	0.15	0.90	1.01	0.14	0.88	102	113	1.12
8H-5, 107-108	70.97	77.70	388	0.11	0.41	0.98	0.21	0.49	83	200	0.65
11H-1, 107-108	93.47	101.80	402	0.13	0.61	1.02	0.18	0.49	124	208	0.97
11H-5, 107-108	99.47	107.80	400	0.11	0.53	0.87	0.17	0.48	110	181	0.72
14H-5, 107-108	127.43	138.95	411	0.12	0.65	0.81	0.16	0.55	118	147	0.83
18H-3, 107-108	162.97	177.14	407	0.10	0.59	0.88	0.15	0.51	115	172	0.85
20H-5, 107-108	184.97	201.78	390	0.08	0.32	0.87	0.20	0.41	78	212	0.56
26X-5, 107-108	241.97	267.22	410	0.08	0.52	0.72	0.13	0.50	104	144	0.76
40X-1, 107-108	367.47	413.92	419	0.02	0.16	0.82	0.11	0.32	50	256	0.73
40X-5, 107-108	373.47	419.92	381	0.05	0.21	0.74	0.19	0.29	72	255	0.42
45X-5, 107-108	421.50	478.68	379	0.02	0.10	0.53	0.17	0.24	41	220	0.41
46X-5, 107-108	431.07	490.28	383	0.03	0.14	0.63	0.19	0.29	48	217	0.31
47X-5, 107-108	440.67	502.60	379	0.01	0.08	0.66	0.12	0.18	44	366	0.33
14H-5 (R), 107-108	127.43	138.95	413	0.11	0.67	0.83	0.14	0.60	111	138	0.83
6H-1 (R), 107-108	45.97	49.40	415	0.15	1.00	1.35	0.13	0.80	125	168	1.10
6H-1 (R), 107-108	45.97	49.40	413	0.18	1.00	1.03	0.15	0.81	123	127	1.10
18H-1 (R), 107-108	159.97	174.14	406	0.15	0.68	0.97	0.18	0.60	113	161	0.85

Notes: T_{max} = temperature (°C) of maximum release of pyrolysis HC, S_1 = mg/g volatile HC, S_2 = pyrolysis HC mg/g, S_3 = pyrolysis CO_2 mg/g, PI = production index, TOC = total organic carbon, HI = hydrogen index, OI = oxygen index. * = total carbon. (R) = replicate. See "Organic Geochemistry," p. 14, in the "Explanatory Notes" chapter for more information.

Table T13. Chlorin concentration per gram dry weight (arbitrary absorbance units) at Site 1144. (Continued on next two pages.)

Core, section, interval (cm)	Depth (mbsf)	Depth (mcd)	Chlorins
184-1144A-			
1H-1, 35-36	0.35	0.81	1.36
1H-1, 107-108	1.07	1.53	1.51
1H-2, 35-36	1.85	2.31	1.68
1H-2, 107-108	2.57	3.03	1.95
1H-3, 35-36	3.35	3.81	1.25
1H-3, 107-108	4.07	4.53	1.05
1H-4, 35-36	4.85	5.31	2.72
1H-4, 107-108	5.57	6.03	1.57
1H-5, 35-36	6.35	6.81	1.86
2H-1, 35-36	7.25	9.04	3.47
2H-1, 107-108	7.97	9.76	4.27
2H-2, 35-36	8.75	10.54	3.16
2H-2, 107-108	9.47	11.26	2.85
2H-3, 35-36	10.25	12.04	3.04
2H-3, 107-108	10.97	12.76	2.96
2H-4, 35-36	11.75	13.54	2.67
2H-4, 107-108	12.47	14.26	2.50
2H-5, 35-36	13.25	15.04	2.31
2H-5, 107-108	13.97	15.76	2.89
2H-6, 35-36	14.75	16.54	2.79
2H-6, 107-108	15.47	17.26	3.32
2H-7, 35-36	16.25	18.04	3.16
3H-1, 35-36	16.75	18.32	2.60
3H-1, 107-108	17.47	19.04	1.91
3H-2, 35-36	18.25	19.82	3.24
3H-2, 107-108	18.97	20.54	2.61
3H-3, 35-36	19.75	21.32	2.28
3H-3, 107-108	20.47	22.04	2.10
3H-4, 35-36	21.25	22.82	2.54
3H-4, 107-108	21.97	23.54	2.13
3H-5, 35-36	22.75	24.32	1.88
3H-5, 107-108	23.47	25.04	2.36
3H-6, 35-36	24.25	25.82	2.12
3H-6, 107-108	24.97	26.54	2.35
3H-7, 35-36	25.75	27.32	3.22
4H-1, 35-36	26.25	27.60	2.11
4H-1, 107-108	26.97	28.32	1.39
4H-2, 35-36	27.79	29.14	2.72
4H-2, 107-108	28.51	29.86	1.86
4H-3, 35-36	29.29	30.64	2.57
4H-3, 107-108	30.01	31.36	2.19
4H-4, 35-36	30.79	32.14	3.09
4H-4, 107-108	31.51	32.86	3.62
4H-5, 35-36	32.29	33.64	1.74
4H-5, 107-108	33.01	34.36	2.83
4H-6, 35-36	33.79	35.14	2.22
4H-6, 107-108	34.51	35.86	1.97
4H-7, 35-36	35.29	36.64	2.56
5H-1, 35-36	35.75	37.24	3.13
5H-1, 107-108	36.47	37.96	2.35
5H-2, 35-36	37.25	38.74	2.97
5H-2, 107-108	37.97	39.46	2.37
5H-3, 35-36	38.75	40.24	1.82
5H-3, 107-108	39.47	40.96	1.90
5H-4, 35-36	40.25	41.74	2.13
5H-4, 107-108	40.97	42.46	2.08
5H-5, 35-36	41.75	43.24	1.89
5H-5, 107-108	42.47	43.96	2.23
5H-6, 35-36	43.25	44.74	1.95
5H-6, 107-108	43.97	45.46	1.77
5H-7, 35-36	44.68	46.17	1.98
6H-1, 35-36	45.25	48.68	1.42
6H-1, 107-108	45.97	49.40	1.65
6H-2, 35-36	46.75	50.18	2.03
6H-2, 107-108	47.47	50.90	1.80
6H-3, 35-36	48.25	51.68	1.88
6H-3, 107-108	48.97	52.40	2.15
6H-4, 35-36	49.75	53.18	1.55
6H-4, 107-108	50.47	53.90	1.97
6H-5, 35-36	51.25	54.68	2.32
6H-5, 107-108	51.97	55.40	1.43
6H-6, 35-36	52.75	56.18	1.86
6H-6, 107-108	53.47	56.90	2.22
6H-7, 35-36	54.25	57.68	1.99
7H-1, 35-36	54.75	60.01	2.08
7H-1, 107-108	55.47	60.73	2.11
7H-2, 35-36	56.25	61.51	2.53
7H-2, 107-108	56.97	62.23	2.01
7H-3, 35-36	57.57	62.83	1.74
7H-3, 107-108	58.29	63.55	1.55
7H-4, 35-36	58.94	64.20	1.81
7H-4, 107-108	59.66	64.92	2.21
7H-5, 35-36	60.44	65.70	1.45
7H-5, 107-108	61.16	66.42	2.46
7H-6, 35-36	61.94	67.20	2.80
7H-6, 107-108	62.66	67.92	2.15
7H-7, 35-36	63.44	68.70	2.42
8H-1, 35-36	64.25	70.98	1.39
8H-1, 107-108	64.97	71.70	1.22
8H-2, 35-36	65.75	72.48	1.24
8H-2, 107-108	66.47	73.20	1.24
8H-3, 35-36	67.25	73.98	1.29
8H-3, 107-108	67.97	74.70	0.84
8H-4, 35-36	68.75	75.48	0.59
8H-4, 107-108	69.47	76.20	0.63
8H-5, 35-36	70.25	76.98	0.64
8H-5, 107-108	70.97	77.70	0.84
8H-6, 35-36	71.75	78.48	0.70
8H-6, 107-108	72.47	79.20	0.85
8H-7, 35-36	73.25	79.98	1.09
9H-1, 35-36	73.75	80.14	0.71
9H-1, 107-108	74.47	80.86	0.91
9H-2, 35-36	75.25	81.64	1.09
9H-2, 107-108	75.97	82.36	0.99
9H-3, 35-36	76.75	83.14	1.05
9H-3, 107-108	77.47	83.86	1.42
9H-4, 35-36	78.25	84.64	1.29
9H-4, 107-108	78.97	85.36	1.41
9H-5, 35-36	79.75	86.14	1.26
9H-5, 107-108	80.47	86.86	1.45
9H-6, 35-36	81.25	87.64	1.14
9H-6, 107-108	81.97	88.36	1.29
9H-7, 35-36	82.75	89.14	1.34
10H-1, 35-36	83.25	91.52	0.86
10H-1, 107-108	83.97	92.24	0.83
10H-2, 35-36	84.75	93.02	0.82
10H-2, 107-108	85.47	93.74	1.19
10H-3, 35-36	86.25	94.52	1.41
10H-3, 107-108	86.97	95.24	1.02
10H-4, 35-36	87.75	96.02	1.22
10H-4, 107-108	88.47	96.74	1.03
10H-5, 35-36	89.20	97.47	1.57
10H-5, 107-108	89.92	98.19	0.85
10H-6, 35-36	90.70	98.97	1.17
10H-6, 107-108	91.42	99.69	1.10
10H-7, 33-35	92.18	100.45	1.06
11H-1, 35-36	92.75	101.08	1.63
11H-1, 107-108	93.47	101.80	1.14
11H-2, 35-36	94.25	102.58	0.82
11H-2, 107-108	94.97	103.30	0.79
11H-3, 35-36	95.75	104.08	1.14
11H-3, 107-108	96.47	104.80	0.86
11H-4, 35-36	97.25	105.58	0.92

Table T13 (continued).

Core, section, interval (cm)	Depth (mbsf)	Depth (mcd)	Chlorins
11H-4, 107-108	97.97	106.30	1.22
11H-5, 35-36	98.75	107.08	0.75
11H-5, 107-108	99.47	107.80	0.73
11H-6, 35-36	100.25	108.58	0.73
11H-6, 107-108	100.97	109.30	0.78
11H-7, 35-36	101.75	110.08	1.39
12H-1, 35-36	102.25	114.05	1.66
12H-1, 107-108	102.97	114.77	1.64
12H-2, 35-36	103.75	115.55	2.09
12H-2, 107-108	104.47	116.27	2.80
12H-3, 35-36	105.25	117.05	2.99
12H-3, 107-108	105.97	117.77	2.84
12H-4, 35-36	106.75	118.55	1.88
12H-4, 107-108	107.47	119.27	2.48
12H-5, 35-36	108.25	120.05	2.17
12H-5, 107-108	108.97	120.77	2.16
12H-6, 35-36	109.75	121.55	1.77
12H-7, 35-36	110.33	122.13	1.43
12H-7, 108-109	111.06	122.86	1.91
13H-1, 35-36	111.75	123.38	1.14
13H-1, 107-108	112.47	124.10	1.13
13H-2, 35-36	113.25	124.88	1.31
13H-2, 107-108	113.97	125.60	1.26
13H-3, 35-36	114.75	126.38	1.28
13H-3, 107-108	115.47	127.10	1.39
13H-4, 35-36	116.25	127.88	1.37
13H-4, 107-108	116.97	128.60	1.49
13H-5, 35-36	117.75	129.38	1.60
13H-5, 107-108	118.47	130.10	1.65
13H-6, 35-36	119.25	130.88	2.07
13H-6, 107-108	119.97	131.60	1.42
13H-7, 35-36	120.64	132.27	1.44
14H-1, 35-36	121.25	132.77	1.39
14H-1, 97-98	121.87	133.39	1.35
14H-2, 38-39	122.29	133.81	1.42
14H-2, 107-108	122.98	134.50	1.48
14H-3, 35-36	123.76	135.28	1.88
14H-3, 107-108	124.48	136.00	1.58
14H-4, 35-36	125.26	136.78	1.47
14H-4, 107-108	125.98	137.50	1.23
14H-5, 35-36	126.71	138.23	1.27
14H-5, 107-108	127.43	138.95	1.23
14H-6, 35-36	128.21	139.73	1.45
14H-6, 107-108	128.93	140.45	1.20
14H-7, 38-39	129.64	141.16	1.40
15H-1, 35-36	130.75	142.41	1.22
15H-1, 107-108	131.47	143.13	1.33
15H-2, 35-36	132.25	143.91	1.65
15H-2, 107-108	132.97	144.63	1.41
15H-3, 35-36	133.80	145.46	1.83
15H-3, 107-108	134.52	146.18	1.28
15H-4, 35-36	135.30	146.96	1.27
15H-4, 107-108	136.02	147.68	1.16
15H-5, 33-34	136.78	148.44	1.10
15H-5, 107-108	137.52	149.18	0.81
15H-7, 35-36	138.48	150.14	1.08
15H-7, 107-108	139.20	150.86	0.68
15H-8, 33-34	139.96	151.62	0.73
16H-1, 35-36	140.25	152.05	1.10
16H-1, 107-108	140.97	152.77	0.79
16H-2, 35-36	141.67	153.47	1.08
16H-3, 35-36	143.17	154.97	1.09
16H-3, 107-108	143.89	155.69	0.74
16H-4, 35-36	144.67	156.47	0.78
16H-4, 107-108	145.39	157.19	1.03
16H-5, 35-36	146.17	157.97	1.14
16H-5, 107-108	146.89	158.69	1.01
16H-6, 35-36	147.67	159.47	1.07
16H-6, 107-108	148.39	160.19	1.13
16H-7, 38-39	149.20	161.00	0.99
17H-1, 35-36	149.75	161.87	0.93
17H-1, 107-108	150.47	162.59	0.70
17H-2, 35-36	151.21	163.33	0.85
17H-2, 107-108	151.93	164.05	0.91
17H-3, 35-36	152.71	164.83	0.85
17H-3, 107-108	153.43	165.55	0.82
17H-4, 35-36	154.22	166.34	0.97
17H-4, 107-108	154.94	167.06	1.32
17H-5, 35-36	155.74	167.86	1.16
17H-5, 107-108	156.46	168.58	1.17
17H-6, 35-36	157.24	169.36	1.13
17H-6, 107-108	157.96	170.08	0.82
17H-7, 35-36	158.74	170.86	0.97
18H-1, 35-36	159.25	173.42	0.57
18H-1, 107-108	159.97	174.14	0.42
18H-2, 35-36	160.75	174.92	0.60
18H-2, 107-108	161.47	175.64	0.97
18H-3, 35-36	162.25	176.42	0.57
18H-3, 107-108	162.97	177.14	0.67
18H-4, 35-36	163.75	177.92	1.04
18H-4, 107-108	164.47	178.64	0.58
18H-5, 35-36	165.25	179.42	0.84
18H-5, 107-108	165.97	180.14	1.33
18H-6, 35-36	166.75	180.92	1.16
18H-6, 107-108	167.47	181.64	1.15
18H-7, 35-36	168.25	182.42	0.98
19H-1, 35-36	168.75	185.42	0.66
19H-1, 107-108	169.47	186.14	0.73
19H-2, 35-36	170.25	186.92	0.91
19H-2, 107-108	170.97	187.64	1.19
19H-3, 35-36	171.75	188.42	1.22
19H-3, 107-108	172.47	189.14	0.91
19H-4, 35-36	173.25	189.92	0.80
19H-4, 107-108	173.97	190.64	1.08
19H-5, 35-36	174.75	191.42	0.95
19H-5, 107-108	175.47	192.14	1.49
19H-6, 35-36	176.25	192.92	1.07
19H-6, 107-108	176.97	193.64	0.99
19H-7, 35-36	177.66	194.33	0.79
20H-1, 35-36	178.25	195.06	0.71
20H-1, 107-108	178.97	195.78	0.94
20H-2, 35-36	179.75	196.56	0.98
20H-2, 107-108	180.47	197.28	1.17
20H-3, 35-36	181.25	198.06	0.69
20H-3, 107-108	181.97	198.78	0.87
20H-4, 35-36	182.75	199.56	0.95
20H-4, 107-108	183.47	200.28	0.76
20H-5, 35-36	184.25	201.06	0.70
20H-5, 107-108	184.97	201.78	0.52
20H-6, 35-36	185.68	202.49	0.65
20H-6, 107-108	186.40	203.21	1.00
21H-1, 35-36	187.75	205.87	0.53
21H-1, 107-108	188.47	206.59	0.50
21H-2, 35-36	189.25	207.37	0.31
21H-2, 107-108	189.97	208.09	1.04
21H-3, 35-36	190.75	208.87	2.09
21H-3, 107-108	191.47	209.59	1.46
21H-4, 35-36	192.25	210.37	1.70
21H-4, 107-108	192.97	211.09	1.19
21H-5, 35-36	193.75	211.87	1.41
21H-5, 107-108	194.47	212.59	1.28
21H-6, 35-36	195.25	213.37	1.22

Table T13 (continued).

Core, section, interval (cm)	Depth (mbsf)	Depth (mcd)	Chlorins
21H-6, 107-108	195.97	214.09	0.98
21H-7, 35-36	196.75	214.87	1.11
22H-1, 35-36	197.25	216.12	0.96
22H-2, 35-36	198.75	217.62	0.95
22H-2, 107-108	199.47	218.34	1.11
22H-3, 35-36	200.25	219.12	0.93
22H-3, 107-108	200.97	219.84	1.22
22H-4, 35-36	201.75	220.62	1.25
22H-4, 107-108	202.47	221.34	1.16
22H-5, 35-36	203.25	222.12	1.00
22H-5, 107-108	203.97	222.84	0.86
22H-6, 35-36	204.75	223.62	1.02
22H-6, 107-108	205.47	224.34	1.03
22H-7, 35-36	206.25	225.12	0.90
23H-1, 35-36	206.75	226.07	0.99
23H-1, 107-108	207.47	226.79	0.78
23H-2, 35-36	207.99	227.31	0.94
23H-2, 107-108	208.71	228.03	0.79
23H-3, 35-36	209.49	228.81	0.65
23H-3, 107-108	210.21	229.53	0.78
23H-4, 35-36	210.99	230.31	0.55
23H-4, 107-108	211.71	231.03	0.76
23H-5, 35-36	212.49	231.81	0.65
23H-5, 107-108	213.21	232.53	0.65
23H-6, 35-36	213.99	233.31	0.64
23H-6, 107-108	214.71	234.03	0.65
23H-7, 35-36	215.49	234.81	0.84
24H-1, 35-36	216.25	239.25	0.82
24H-1, 107-108	216.97	239.97	0.89
24H-2, 35-36	217.75	240.75	0.77
24H-2, 107-108	218.47	241.47	0.66
24H-3, 35-36	219.25	242.25	0.47
24H-3, 107-108	219.97	242.97	0.55
24H-4, 35-36	220.75	243.75	0.81
24H-4, 107-108	221.47	244.47	0.71
24H-5, 35-36	222.25	245.25	0.58
24H-5, 107-108	222.97	245.97	0.44
24H-6, 35-36	223.75	246.75	0.49
24H-6, 107-108	224.47	247.47	0.58
24H-7, 35-36	224.95	247.95	0.44
25H-1, 35-36	225.75	251.66	1.46
25H-1, 107-108	226.47	252.38	1.19
25H-2, 35-36	227.25	253.16	1.33
25H-2, 107-108	227.97	253.88	1.29
25H-3, 35-36	228.75	254.66	1.02
25H-3, 107-108	229.47	255.38	1.03
25H-4, 35-36	230.25	256.16	0.94
25H-4, 107-108	230.97	256.88	1.16
25H-5, 35-36	231.75	257.66	1.35
25H-5, 107-108	232.47	258.38	0.77
25H-6, 35-36	233.25	259.16	0.99
25H-6, 107-108	233.97	259.88	0.90
25H-7, 35-36	234.75	260.66	0.87
26X-1, 35-36	235.25	260.50	0.73
26X-1, 107-108	235.97	261.22	0.79
26X-2, 35-36	236.75	262.00	0.78
26X-2, 107-108	237.47	262.72	0.86
26X-3, 35-36	238.25	263.50	0.73
26X-3, 107-108	238.97	264.22	0.74
26X-4, 35-36	239.75	265.00	0.79
26X-4, 107-108	240.47	265.72	0.82
26X-5, 35-36	241.25	266.50	0.83
26X-5, 107-108	241.97	267.22	0.79
27X-1, 35-36	241.65	268.94	0.98
27X-1, 107-108	242.37	269.66	0.83
27X-2, 35-36	243.15	270.44	1.07
27X-2, 107-108	243.87	271.16	0.98
27X-3, 35-36	244.65	271.94	0.80
27X-3, 107-108	245.37	272.66	0.75
27X-4, 35-36	246.15	273.44	1.09
27X-4, 107-108	246.87	274.16	0.98
27X-5, 35-36	247.65	274.94	0.70
27X-5, 107-108	248.37	275.66	0.96
27X-6, 35-36	249.15	276.44	0.82
27X-6, 107-108	249.87	277.16	0.91
27X-7, 35-36	250.35	277.64	0.73
28X-1, 35-36	251.25	279.52	0.70
28X-1, 107-108	251.97	280.24	0.66
28X-2, 35-36	252.75	281.02	0.69
28X-2, 107-108	253.47	281.74	0.82
28X-3, 35-36	254.25	282.52	0.70
28X-3, 107-108	254.97	283.24	0.66
28X-4, 35-36	255.75	284.02	0.60
28X-4, 107-108	256.47	284.74	0.57
28X-5, 35-36	257.25	285.52	0.47
28X-5, 107-108	257.97	286.24	0.45
28X-6, 35-36	258.75	287.02	0.60
28X-6, 107-108	259.47	287.74	0.54
28X-7, 35-36	259.95	288.22	0.58
29X-1, 35-36	260.85	289.30	0.40
29X-1, 107-108	261.57	290.02	0.48
29X-2, 35-36	262.35	290.80	0.45
29X-2, 107-108	263.07	291.52	0.46
29X-3, 35-36	263.85	292.30	0.34
29X-3, 107-108	264.57	293.02	0.42
29X-4, 35-36	265.35	293.80	0.42
29X-4, 107-108	266.07	294.52	0.42
29X-5, 35-36	266.85	295.30	0.59
29X-5, 107-108	267.57	296.02	0.56
29X-6, 35-36	268.35	296.80	0.57
29X-6, 107-108	269.07	297.52	0.66
29X-7, 35-36	269.85	298.30	0.55
30X-1, 35-36	270.45	300.84	0.41
30X-1, 107-108	271.17	301.56	0.48
30X-2, 35-36	271.95	302.34	0.71
30X-2, 107-108	272.67	303.06	0.67
30X-3, 35-36	273.45	303.84	0.74
30X-3, 107-108	274.17	304.56	0.83
30X-4, 35-36	274.95	305.34	1.12
30X-4, 107-108	275.67	306.06	0.85
30X-5, 35-36	276.45	306.84	0.86
30X-5, 107-108	277.17	307.56	0.93
30X-6, 35-36	277.95	308.34	0.80
30X-6, 107-108	278.67	309.06	0.91
30X-7, 35-36	279.45	309.84	0.83
31X-1, 35-36	280.05	311.18	0.74
31X-1, 107-108	280.77	311.90	0.55
31X-2, 35-36	281.55	312.68	0.59
31X-2, 107-108	282.27	313.40	0.59
31X-3, 35-36	283.05	314.18	0.41
31X-3, 107-108	283.77	314.90	0.34
31X-4, 35-36	284.55	315.68	0.50
31X-4, 107-108	285.27	316.40	0.53

Table T14. Composition of interstitial waters in Holes 1144A and 1144B. (Continued on next page.)

Core, section, interval (cm)	Depth (mbsf)	Depth (mcd)	pH	Alkalinity (mM)	Salinity	Cl^- (mM)	Cl^- (mM)	Na^+ (mM)	K^+ (mM)	Ca^{2+} (mM)	Mg^{2+} (mM)	SO_4^{2-} (mM)	HPO_4^{2-} (µM)	NH_4^+ (mM)	H_4SiO_4 (µM)	Li^+ (µM)	Sr^{2+} (µM)
184-1144A-																	
1H-2, 145-150	2.98	3.44	7.44	3.88	34.0												
1H-4, 145-150	5.98	6.44	7.73	5.68	34.5	552		472	12.50	9.40	51.5	25.18	21.7	0.8	628.6	24	92
2H-3, 145-150	11.38	13.17	8.20	34.94	34.0	555		452	11.20	4.80	47.3	0.00	191.1	3.7	717.4	11	75
2H-5, 145-150	14.38	16.17	7.64	33.28	33.5												
3H-3, 145-150	20.88	22.45	7.86	32.29	33.5	555		457	11.40	3.40	44.9	0.00	260.7	7.1	814.9	13	68
3H-5, 145-150	23.88	25.45			33.5												
4H-3, 145-150	30.42	31.77	7.87	31.95	34.0	557		457	11.40	3.20	44.2	0.00	254.3	7.8	793.2	12	72
4H-5, 145-150	33.42	34.77	7.87	31.76	34.0												
5H-3, 145-150	39.88	41.37	7.84	30.36	34.0	559		455	11.30	3.30	44.0		219.2	8.0	804.1	15	74
5H-5, 145-150	42.88	44.37			33.0												
6H-3, 145-150	49.38	52.81	7.84	29.3	33.0	558		458	11.20	3.20	43.4	0.00	175.1	7.3	780.2	15	71
6H-5, 145-150	52.38	55.81	7.87	27.99	33.0												
7H-3, 132-137	58.57	63.83	7.79		33.0	556		452	11.20	4.10	40.5	0.00	192.7	7.7	799.7	15	71
7H-5, 145-150	61.57	66.83			32.5												
8H-3, 145-150	68.38	75.11	7.87	22.88	32.0	556		454	10.80	3.40	38.7	0.00	197.4	7.7	754.3	12	70
8H-5, 145-150	71.38	78.11			32.0												
9H-3, 145-150	77.88	84.27	7.89	21.75	32.0	556		454	10.80	3.40	38.8		165.5	7.6	767.3	13	69
9H-5, 145-150	80.88	87.27			32.0												
10H-3, 145-150	87.38	95.65	7.89	23.74	32.0			455	10.90	3.40	39.6	0.00					
10H-5, 145-150	90.33	98.60			32.0												
11H-2, 145-150	95.38	103.71	7.70	25.36	32.0			453	10.80	3.50	40.4	0.26					
11H-5, 145-150	99.88	108.21			32.0												
12H-2, 145-150	104.88	116.68	7.84	27.3	32.0	552		452	10.50	3.80	40.9		228.8	8.0	771.6	17	73
12H-5, 145-150	109.38	121.18			32.0												
13H-2, 145-150	114.38	126.01	7.49	25.34	32.0			453	10.20	3.80	38.1						
13H-5, 145-150	118.88	130.51			32.0												
14H-2, 145-150	123.39	134.91	7.47	23.69	32.0			458	9.90	3.80	37.2	0.00					
14H-5, 145-150	127.84	139.36			32.0												
15H-2, 145-150	133.38	145.04				556		452	10.00	3.90	36.9	0.00	176.7	8.3	804.1	15	74
15H-2, 150-155	133.43	145.09	7.52	21.94	32.0												
15H-5, 145-150	137.93	149.59			32.0												
16H-2, 145-150	142.80	154.60	7.62	20.96	32.0			453	9.90	3.60	35.6						
16H-5, 145-150	147.30	159.10			32.0												
17H-2, 145-150	152.34	164.46	7.60	21.3	32.0			452	9.80	4.30	35.7	0.00					
17H-5, 145-150	156.87	168.99	7.64	20.79	32.0												
18H-2, 145-150	161.88	176.05	7.68	21.44	32.0	554		457	9.70	3.90	36.7	0.00	157.5	8.4	743.4	17	77
18H-5, 145-150	166.38	180.55	7.56	20.85	32.0												
19H-2, 145-150	171.38	188.05	7.56	21.64	32.0			453	10.30	4.00	35.7	0.00					
19H-5, 145-150	175.88	192.55	7.43	21.13	32.0												
20H-2, 145-150	180.88	197.69	7.54	22.82	32.0	550		456	10.20	3.90	36.0	0.00	108	7.8		19	82
20H-5, 138-143	185.31	202.12	7.74	20.71	33.0												
23H-4, 0-10	210.69	230.01	7.64	19.93	32.0	550		456	10.20	3.90	34.1	0.00	90.4	8.0		20	83
26X-2, 145-150	237.88	263.13	7.87		32.0	550		453	9.50	4.30	34.8		66.5	7.5		19	90
26X-4, 145-150	240.88	266.13			32.0												
27X-2, 145-150	244.28	271.57	7.91		32.0	553		449	9.20	5.10	34.2	0.00	61.7	7.8	825.7	20	92
27X-5, 145-150	248.78	276.07			32.0												
28X-2, 145-150	253.88	282.15	7.87		31.0			449	9.10	4.40	33.8	0.00					
28X-5, 145-150	258.38	286.65			32.0												
29X-2, 140-150	263.45	291.90	7.84	17.22	32.0			454	9.30	4.70	34.1	0.00					
29X-5, 140-150	267.95	296.40			32.0												
30X-2, 140-150	273.05	303.44	7.84	17.16	32.0	552		451	9.20	4.90	34.2	0.16	61.7		767.3	21	95
30X-5, 140-150	277.55	307.94			32.0												
31X-2, 140-150	282.65	313.78	7.84	17.22	32.0			453	9.00	5.40	33.8	0.13					
31X-5, 140-150	287.15	318.28			32.0												
32X-2, 140-150	292.25	325.03	7.84	16.82	32.0			45	8.90	5.10	34.8	0.00					
32X-5, 140-150	296.75	329.53			32.0												
33X-2, 140-150	301.95	336.17	7.87	17.12	32.0	549		449	8.90	5.00	34.9	0.00	36.1	7.4	810.6	27	104
33X-5, 140-150	306.45	340.67			32.0												
34X-2, 140-150	311.55	345.09	7.84		32.0			451	8.80	5.40	34.5	0.66					
34X-5, 140-150	316.05	349.59			32.0												
35X-2, 140-150	321.15	358.69	7.89	13.98	32.0			456	8.90	5.10	33.1	0.00					
35X-5, 140-150	325.65	363.19			32.0												
36X-2, 140-150	330.85	373.34	7.84	14.46	32.0	553		450	8.60	5.50	33.8	0.00	28.1	6.9	836.6	26	109
36X-5, 140-150	335.35	377.84			32.0												
37X-2, 140-150	340.45	381.00	7.84	13.34	32.0			449	8.30	6.10	33.9	0.00					
37X-5, 140-150	344.95	385.50			32.0					5.38							
38X-2, 140-150	350.05	394.20	7.87	12.7	32.0			453	8.30	6.05	33.5	0.00					
38X-5, 140-150	354.55	398.70			31.0					5.44							

Table T14 (continued).

Core, section, interval (cm)	Depth (mbsf)	Depth (mcd)	pH	Alkalinity (mM)	Salinity	Cl^- (mM)	Cl^- (mM)	Na^+ (mM)	K^+ (mM)	Ca^{2+} (mM)	Mg^{2+} (mM)	SO_4^{2-} (mM)	HPO_4^{2-} (µM)	NH_4^+ (mM)	H_4SiO_4 (µM)	Li^+ (µM)	Sr^{2+} (µM)
39X-2, 140-150	359.65	404.40	7.77	12.47	31.0	555		452	8.20	5.71	33.8	0.00	16.2		851.7	28	114
39X-5, 140-150	364.15	408.90			32.0		550			5.48							
40X-2, 140-150	369.35	415.80	7.90		32.0		553	473	7.70	5.41	33.4	0.37					
40X-5, 140-150	373.85	420.30			31.0		549			5.31							
41X-2, 140-150	378.95	428.92	7.74	10.68	31.0		551	470	7.50	5.66	33.0	0.00					
41X-5, 140-150	383.45	433.42			31.0		552			5.72							
42X-2, 140-150	388.55	439.71	7.84	9.73	31.0	556	555	472	7.50	5.90	33.2	0.00	6.5	4.1	433.7	29	118
42X-5, 140-150	393.05	444.21			31.0		553			5.88							
43X-2, 140-150	398.15	451.15	7.52	9.9	31.0		554	473	7.40	6.64	33.2	0.00					
43X-5, 140-150	402.65	455.65			31.0		549			6.01							
44X-2, 140-150	407.75	463.49	7.43	9.11	31.0		547	474	7.20	6.70	33.5	0.00					
44X-5, 140-150	412.25	467.99			31.0												
45X-2, 140-150	417.35	474.53	7.48	8.53	31.0	553	554	473	6.90	6.10	33.7	0.00	6.6	3.1	414.2	27	143
45X-5, 140-150	421.88	479.06			31.0		552										
46X-2, 140-150	426.95	486.16	7.49	8.19	31.0		551	472	6.80	6.20	34.2	0.00					
46X-5, 140-150	431.45	490.66			31.5		553										
47X-2, 140-150	436.55	498.48	7.62	7.11	32.0		549	470	7.00	5.90	35.4	1.43					
47X-5, 140-150	441.05	502.98			32.5		555										
48X-2, 140-150	446.15	511.55	7.52		31.0	556		474	8.40	5.30	35.6	0.00	7.1	2.4	284.3	30	202
48X-5, 140-150	450.68	516.08			31.5		560										
184-1144B-																	
22H-2, 138-150	193.04	213.12	7.81	22.05	32.5												
23X-2, 140-150	202.55	222.49	7.86	20.75	32.0												
24X-2, 140-150	212.15	233.55	7.86	20.2	32.0												
25X-2, 140-150	221.75	249.04	7.81	20.35	32.0												
26X-2, 140-150	231.45	260.10	7.84	19.56	33.0												

Table T15. Thermal conductivity measurements at Site 1144. (**See table note.** Continued on next two pages.)

Leg	Site	Hole	Core	Type	Section	Top interval (cm)	Depth (mbsf)	Depth (mcd)	Thermal conductivity (W/[m·K])	Thermal conductivity (3-pt mean)
184	1144	A	1	H	2	75	2.25	2.71	0.851	
184	1144	A	1	H	2	75	2.25	2.71	0.873	
184	1144	A	1	H	2	75	2.25	2.71	0.855	0.86
184	1144	A	1	H	5	35	6.35	6.81	0.933	
184	1144	A	1	H	5	35	6.35	6.81	0.933	
184	1144	A	1	H	5	35	6.35	6.81	0.915	0.93
184	1144	A	2	H	2	75	9.15	10.94	0.934	
184	1144	A	2	H	2	75	9.15	10.94	0.918	
184	1144	A	2	H	2	75	9.15	10.94	0.960	0.94
184	1144	A	2	H	5	75	13.65	15.44	0.894	
184	1144	A	2	H	5	75	13.65	15.44	0.891	
184	1144	A	2	H	5	75	13.65	15.44	0.864	0.88
184	1144	A	3	H	2	73	18.63	20.20	0.836	
184	1144	A	3	H	2	73	18.63	20.20	0.837	
184	1144	A	3	H	2	73	18.63	20.20	0.817	0.83
184	1144	A	3	H	5	75	23.15	24.72	0.921	
184	1144	A	3	H	5	75	23.15	24.72	0.862	
184	1144	A	3	H	5	75	23.15	24.72	0.882	0.89
184	1144	A	4	H	2	75	28.19	29.54	0.753	
184	1144	A	4	H	2	75	28.19	29.54	0.735	
184	1144	A	4	H	2	75	28.19	29.54	0.755	0.75
184	1144	A	4	H	5	74	32.68	34.03	0.847	
184	1144	A	4	H	5	74	32.68	34.03	0.862	
184	1144	A	4	H	5	74	32.68	34.03	0.848	0.85
184	1144	A	5	H	2	74	37.64	39.13	0.862	
184	1144	A	5	H	2	74	37.64	39.13	0.848	
184	1144	A	5	H	2	74	37.64	39.13	0.872	0.86
184	1144	A	5	H	5	74	42.14	43.63	0.850	
184	1144	A	5	H	5	74	42.14	43.63	0.826	
184	1144	A	5	H	5	74	42.14	43.63	0.831	0.84
184	1144	A	6	H	2	75	47.15	50.58	0.879	
184	1144	A	6	H	2	75	47.15	50.58	0.864	
184	1144	A	6	H	2	75	47.15	50.58	0.887	0.88
184	1144	A	6	H	5	78	51.68	55.11	0.915	
184	1144	A	6	H	5	78	51.68	55.11	0.916	
184	1144	A	6	H	5	78	51.68	55.11	0.918	0.92
184	1144	A	7	H	2	75	56.65	61.91	0.863	
184	1144	A	7	H	2	75	56.65	61.91	0.925	
184	1144	A	7	H	2	75	56.65	61.91	0.906	0.90
184	1144	A	7	H	5	75	60.84	66.10	0.810	
184	1144	A	7	H	5	75	60.84	66.10	0.812	
184	1144	A	7	H	5	75	60.84	66.10	0.812	0.81
184	1144	A	8	H	2	75	66.15	72.88	0.904	
184	1144	A	8	H	2	75	66.15	72.88	0.899	
184	1144	A	8	H	2	75	66.15	72.88	0.914	0.91
184	1144	A	8	H	5	78	70.68	77.41	0.757	
184	1144	A	8	H	5	78	70.68	77.41	0.734	
184	1144	A	8	H	5	78	70.68	77.41	0.737	0.74
184	1144	A	9	H	2	81	75.71	82.10	0.895	
184	1144	A	9	H	2	81	75.71	82.10	0.881	
184	1144	A	9	H	2	81	75.71	82.10	0.895	0.89
184	1144	A	9	H	5	73	80.13	86.52	0.943	
184	1144	A	9	H	5	73	80.13	86.52	0.937	
184	1144	A	9	H	5	73	80.13	86.52	0.954	0.94
184	1144	A	10	H	2	77	85.17	93.44	1.018	
184	1144	A	10	H	2	77	85.17	93.44	1.040	
184	1144	A	10	H	2	77	85.17	93.44	1.023	1.03
184	1144	A	10	H	5	72	89.57	97.84	0.897	
184	1144	A	10	H	5	72	89.57	97.84	0.903	
184	1144	A	10	H	5	72	89.57	97.84	0.915	0.91
184	1144	A	11	H	2	75	94.65	102.98	0.857	
184	1144	A	11	H	2	75	94.65	102.98	0.854	
184	1144	A	11	H	2	75	94.65	102.98	0.855	0.86
184	1144	A	11	H	5	72	99.12	107.45	0.857	
184	1144	A	11	H	5	72	99.12	107.45	0.848	
184	1144	A	11	H	5	72	99.12	107.45	0.850	0.85
184	1144	A	12	H	2	72	104.12	115.92	0.858	

Table T15 (continued).

Leg	Site	Hole	Core	Type	Section	Top interval (cm)	Depth (mbsf)	Depth (mcd)	Thermal conductivity (W/[m·K])	Thermal conductivity (3-pt mean)
184	1144	A	12	H	2	72	104.12	115.92	0.855	
184	1144	A	12	H	2	72	104.12	115.92	0.853	0.86
184	1144	A	12	H	5	72	108.62	120.42	0.912	
184	1144	A	12	H	5	72	108.62	120.42	0.895	
184	1144	A	12	H	5	72	108.62	120.42	0.899	0.90
184	1144	A	14	H	5	72	127.08	138.60	0.842	
184	1144	A	14	H	5	72	127.08	138.60	0.832	
184	1144	A	14	H	5	72	127.08	138.60	0.803	0.83
184	1144	A	15	H	5	72	137.17	148.83	0.829	
184	1144	A	15	H	5	72	137.17	148.83	0.834	
184	1144	A	15	H	5	72	137.17	148.83	0.835	0.83
184	1144	A	16	H	5	73	146.55	158.35	0.948	
184	1144	A	16	H	5	73	146.55	158.35	0.924	
184	1144	A	16	H	5	73	146.55	158.35	0.925	0.93
184	1144	A	17	H	5	72	156.11	168.23	1.030	
184	1144	A	17	H	5	72	156.11	168.23	1.010	
184	1144	A	17	H	5	72	156.11	168.23	1.018	1.02
184	1144	A	18	H	5	72	165.62	179.79	0.949	
184	1144	A	18	H	5	72	165.62	179.79	0.953	
184	1144	A	18	H	5	72	165.62	179.79	0.953	0.95
184	1144	A	19	H	5	72	175.12	191.79	1.008	
184	1144	A	19	H	5	72	175.12	191.79	0.992	
184	1144	A	19	H	5	72	175.12	191.79	0.997	1.00
184	1144	A	20	H	5	67	184.57	201.38	0.927	
184	1144	A	20	H	5	67	184.57	201.38	0.937	
184	1144	A	20	H	5	67	184.57	201.38	0.923	0.93
184	1144	A	21	H	5	78	194.18	212.30	0.980	
184	1144	A	21	H	5	78	194.18	212.30	1.015	
184	1144	A	21	H	5	78	194.18	212.30	1.015	1.00
184	1144	A	22	H	5	75	203.65	222.52	0.911	
184	1144	A	22	H	5	75	203.65	222.52	0.914	
184	1144	A	22	H	5	75	203.65	222.52	0.912	0.91
184	1144	A	23	H	5	73	212.87	232.19	0.981	
184	1144	A	23	H	5	73	212.87	232.19	0.993	
184	1144	A	23	H	5	73	212.87	232.19	0.926	0.97
184	1144	A	24	H	5	67	222.57	245.57	1.003	
184	1144	A	24	H	5	67	222.57	245.57	1.014	
184	1144	A	24	H	5	67	222.57	245.57	1.017	1.01
184	1144	A	25	H	5	74	232.14	258.05	1.123	
184	1144	A	25	H	5	74	232.14	258.05	1.132	
184	1144	A	25	H	5	74	232.14	258.05	1.117	1.12
184	1144	A	26	X	5	75	241.65	266.90	0.860	
184	1144	A	26	X	5	75	241.65	266.90	0.860	
184	1144	A	26	X	5	75	241.65	266.90	0.848	0.86
184	1144	A	27	X	5	75	248.05	275.34	0.949	
184	1144	A	27	X	5	75	248.05	275.34	0.934	
184	1144	A	27	X	5	75	248.05	275.34	0.926	0.94
184	1144	A	28	X	5	74	257.64	285.91	0.984	
184	1144	A	28	X	5	74	257.64	285.91	0.970	
184	1144	A	28	X	5	74	257.64	285.91	0.975	0.98
184	1144	A	29	X	5	75	267.25	295.70	1.003	
184	1144	A	29	X	5	75	267.25	295.70	0.990	
184	1144	A	29	X	5	75	267.25	295.70	0.993	1.00
184	1144	A	30	X	5	75	276.85	307.24	1.060	
184	1144	A	30	X	5	75	276.85	307.24	1.044	
184	1144	A	30	X	5	75	276.85	307.24	1.002	1.04
184	1144	A	31	X	5	75	286.45	317.58	0.994	
184	1144	A	31	X	5	75	286.45	317.58	0.973	
184	1144	A	31	X	5	75	286.45	317.58	0.976	0.98
184	1144	A	32	X	5	75	296.05	328.83	1.016	
184	1144	A	32	X	5	75	296.05	328.83	1.009	
184	1144	A	32	X	5	75	296.05	328.83	1.032	1.02
184	1144	A	33	X	5	75	305.75	339.97	0.975	
184	1144	A	33	X	5	75	305.75	339.97	0.969	
184	1144	A	33	X	5	75	305.75	339.97	0.962	0.97
184	1144	A	34	X	5	75	315.35	348.89	0.855	
184	1144	A	34	X	5	75	315.35	348.89	0.853	
184	1144	A	34	X	5	75	315.35	348.89	0.849	0.85
184	1144	A	35	X	5	78	324.98	362.52	0.936	
184	1144	A	35	X	5	78	324.98	362.52	0.969	

Table T15 (continued).

Leg	Site	Hole	Core	Type	Section	Top interval (cm)	Depth (mbsf)	Depth (mcd)	Thermal conductivity (W/[m·K])	Thermal conductivity (3-pt mean)
184	1144	A	35	X	5	78	324.98	362.52	0.959	0.95
184	1144	A	36	X	5	75	334.65	377.14	0.920	
184	1144	A	36	X	5	75	334.65	377.14	0.983	
184	1144	A	36	X	5	75	334.65	377.14	0.977	0.96
184	1144	A	37	X	5	70	344.20	384.75	0.989	
184	1144	A	37	X	5	70	344.20	384.75	0.997	
184	1144	A	37	X	5	70	344.20	384.75	0.980	0.99
184	1144	A	38	X	5	75	353.85	398.00	0.917	
184	1144	A	38	X	5	75	353.85	398.00	0.916	
184	1144	A	38	X	5	75	353.85	398.00	0.917	0.92
184	1144	A	39	X	5	75	363.45	408.20	0.883	
184	1144	A	39	X	5	75	363.45	408.20	0.877	
184	1144	A	39	X	5	75	363.45	408.20	0.885	0.88
184	1144	A	40	X	5	70	373.10	419.55	1.109	
184	1144	A	40	X	5	70	373.10	419.55	1.083	
184	1144	A	40	X	5	70	373.10	419.55	1.090	1.09
184	1144	A	41	X	5	70	382.70	432.67	1.010	
184	1144	A	41	X	5	70	382.70	432.67	0.994	
184	1144	A	41	X	5	70	382.70	432.67	1.014	1.01
184	1144	A	42	X	5	75	392.35	443.51	1.084	
184	1144	A	42	X	5	75	392.35	443.51	1.081	
184	1144	A	42	X	5	75	392.35	443.51	1.081	1.08
184	1144	A	43	X	5	75	401.95	454.95	0.902	
184	1144	A	43	X	5	75	401.95	454.95	0.825	
184	1144	A	43	X	5	75	401.95	454.95	0.876	0.87
184	1144	A	44	X	5	75	411.55	467.29	1.082	
184	1144	A	44	X	5	75	411.55	467.29	1.086	
184	1144	A	44	X	5	75	411.55	467.29	1.086	1.08
184	1144	A	45	X	5	75	421.18	478.36	1.160	
184	1144	A	45	X	5	75	421.18	478.36	1.138	
184	1144	A	45	X	5	75	421.18	478.36	1.140	1.15
184	1144	A	46	X	5	75	430.75	489.96	1.205	
184	1144	A	46	X	5	75	430.75	489.96	1.201	
184	1144	A	46	X	5	75	430.75	489.96	1.221	1.21
184	1144	A	47	X	5	75	440.35	502.28	1.115	
184	1144	A	47	X	5	75	440.35	502.28	1.104	
184	1144	A	47	X	5	75	440.35	502.28	1.107	1.11
184	1144	A	48	X	5	75	449.98	515.38	1.107	
184	1144	A	48	X	5	75	449.98	515.38	1.080	
184	1144	A	48	X	5	75	449.98	515.38	1.074	1.09

Note: This table is also available in **ASCII format.**

Table T16. Summary of logging operations at Site 1144.

Date (March 1999)	Time (local)	
15	1145	Hole preparation complete. Rig up wireline.
15	1310	Rig into hole with HNGS-APS-HLDS-DIT.
15	1443	Uplog at 275 m/hr from 443 to 370 mbsf. Rig into hole to total depth.
15	1505	Uplog at 275 m/hr from 443 mbsf to EOP. Pull out of hole.
15	1830	Rig into hole with NGT-FMS-LSS.
15	2014	Uplog at 275 m/hr from 447 mbsf to EOP. Rig into hole to total depth.
15	2135	Uplog at 275 m/hr from 447 mbsf to EOP. Pull out of hole.
16	0035	Rig into hole with NGT-GHMT-GPIT.
16	0310	Uplog at 275 m/hr from 445 mbsf to EOP. Rig into hole to total depth.
16	0400	Uplog at 275 m/hr from 450 mbsf to EOP. Pull out of hole.
16	0530	End of logging operations.

Note: HNGS = hostile environment natural gamma-ray sonde, APS = accelerator porosity sonde, HLDS = hostile environment lithodensity sonde, DIT = dual-induction tool, EOP = end of pipe, NGT = natural gamma-ray tool, FMS = Formation MicroScanner, LSS = long-spaced sonic logging tool, GHMT = geological high-resolution magnetic tool, GPIT = general-purpose inclinometer tool.